Satellite Passive Microwave Sea-Ice Concentration Data Set Intercomparison: Closed Ice and Ship-Based Observations

Stefan Kern[1], Thomas Lavergne[2], Dirk Notz[3], Leif Toudal Pedersen[4], Rasmus Tage Tonboe[5], Roberto Saldo[4], and Atle Macdonald Sørensen[2]

[1]Integrated Climate Data Center (ICDC), Center for Earth System Research and Sustainability (CEN), University of Hamburg, Hamburg, Germany
[2]Research and Development Department, Norwegian Meteorological Institute, Oslo, Norway
[3]~~M~~Institute for Marine Research, University of Hamburg and Max-Planck Institute for Meteorology, Hamburg, Germany
[4]Danish Technical University, Lyngby, Denmark
[5]Danish Meteorological Institute, Copenhagen, Denmark

Correspondence to: Stefan Kern (stefan.kern@uni-hamburg.de)

Abstract. ~~Accurate sea-ice concentration (SIC) data are a pre-requisite to reliably monitor the polar sea-ice covers. Over the last four decades, many algorithms have been developed to retrieve the SIC from satellite microwave radiometry, some of them applied to generate long-term data products.~~ We report on results of a systematic inter-comparison of ten global sea-ice concentration (SIC) data products at 12.5 to 50.0 km grid resolution for both the Arctic and the Antarctic. The products are compared with each other with respect to differences in SIC, sea-ice area (SIA), and sea-ice extent (SIE), and they are compared against a global winter-time near-100% reference SIC data set for closed pack ice conditions and against global year-round ship-based visual observations of the sea-ice cover. We can group the products based on the concept of their SIC retrieval algorithms~~observed inter-product consistency and differences of the inter-comparison results~~. Group I consists of data sets using the self-optimizing EUMETSAT-OSISAF /~~–~~ ESA-CCI algorithms. Group II includes data using the ~~NASA-Team 2 and~~ Comiso-Bootstrap algorithm~~s~~, and the NOAA-NSIDC sea-ice concentration climate data record (CDR). The standard NASA-Team and the ARTIST Sea Ice (ASI) algorithms are put into ~~a separate~~ group III, and NASA-Team 2 is the only element of group IV~~because of their often quite diverse results~~. ~~Within group I and II evaluation results and intra-product differences are mostly very similar. For instance, among group I products, SIA agrees within ±100 000 km² in both hemispheres during maximum and minimum sea-ice cover. Among group II products, satellite- minus ship-based SIC differences agree within ±0.7%. Standing out with large negative differences to other products and evaluation data is the standard NASA-Team algorithm, in both hemispheres.~~ The three CDRs of group I (SICCI-25km, SICCI-50km, and OSI-450) are biased low compared to ~~the~~a 100% reference SIC data set with biases of -0.4% to -1.0% (Arctic) and -0.3% to -1.1% (Antarctic). Products of group II appear to be mostly biased high in the Arctic by between +1.0% and +3.5%, while their biases in the Antarctic ~~only~~ range from -0.2% to +0.9%. Group III product biases are different for the Arctic: +0.9% (NASA-Team), -3.7% (ASI) but similar for the Antarctic: -5.4% and -5.6%, respectively. The standard deviation is smaller in the Arctic for the quoted group I products: 1.9% to 2.9% and Antarctic: 2.5% to 3.1%, than for group II and III products: Arctic: 3.6% to 5.0%, Antarctic: 4.0~~5~~% to 6~~5~~.45%. We refer to the paper to understand why we could not give values for group IV here. ~~Products of group I exhibit larger overall satellite- minus ship-based SIC differences than group II in both hemispheres. However, compared to group II, group I products' standard deviations are smaller, correlations higher and evaluation results are less sensitive to seasonal changes.~~ We discuss the impact of truncating the SIC distribution, as naturally retrieved by the algorithms around the 100% sea-ice concentration end. We show that evaluation studies of such truncated SIC products can result in misleading statistics and favour data sets that systematically overestimate SIC. We describe a method to re-construct the un-truncated distribution of SIC before the evaluation is performed. On the basis of this evaluation, we open a discussion about the overestimation of SIC in data products, with far-reaching consequences for, e.g., surface heat-flux estimations in winter. We

also document inconsistencies in the behaviour of the weather filters used in products of group II, and suggest advancing studies about the influence of these weather filters on SIA and SIE time-series and their trends.

1 Introduction

For more than 40 years, the fraction of the polar oceans covered ~~with~~by sea ice, or sea-ice concentration, has been monitored by means of satellite microwave radiometry. This enabled a better understanding of ocean–sea-ice–atmosphere interactions for~~in~~ the polar regions where observations with other means than satellites are challenging due to remoteness, harsh environment and limited daylight. Based on the long-term satellite record, a substantial negative trend in the Arctic sea-ice area and extent has been found (e.g. Meier et al., 2014; Comiso et al., 2012, 2017a). In the Antarctic, sea-ice area and extent are highly variable with a period of positive trend (Turner et al., 2013; Comiso et al., 2017b) and sea-ice extent maxima (Reid et al., 2015) being followed recently by record minima (Schlosser et al., 2018; Turner et al., 2017; Stuecker et al., 2017).

In this contribution, we evaluate a number of satellite estimates of the~~spatially and temporally resolved~~ sea-ice concentration from which sea-ice area and extent are derived. Such detailed evaluation allows one to better estimate the uncertainties of these products, knowledge of which is required for all their applications. These applications range from estimates of the future evolution of the Arctic sea-ice cover, whose confidence is directly affected by observational uncertainty of sea-ice concentration (e.g., Niederdrenk and Notz, 2018), and short-term forecasts for ship routing (e.g., Wayand et al., 2019; Melia et al., 2017) to detailed climate-model evaluation (e.g., Ivanova et al., 2017).

The sea-ice concentration~~, from which sea-ice area and extent are derived,~~ is computed from satellite observations of the microwave brightness temperature (TB), which is a measure of the Earth-leaving thermal microwave radiation received by the satellite sensor. A number of different satellite sensors has been in place for sea-ice monitoring, summarized in Table 1 (see also Lavergne et al., 2019, Table 2). With these sensors the polar regions are covered almost completely daily since October 1978 (every other day with Scanning Multichannel Microwave Radiometer (SMMR) before July 1987).

A considerable number of different algorithms to compute the sea-ice concentration from microwave satellite TB measurements has been developed during the past decades. All exploit the fact that under typical viewing angles (50-55 degrees) the difference in microwave brightness temperature, measured at horizontal (h) and vertical (v) polarization, between open water and sea ice is sufficiently large to estimate sea-ice concentration. Whether or not a given algorithm is accepted by the scientific community as a~~n~~ candidate for~~algorithm to~~ comput~~ing~~e a climate data record (CDR) depends, among other things, on the length of the available satellite raw data record, spatial and temporal resolution, quantification of uncertainties, and sensitivity to noise ~~reduction and mitigation of~~which might introduce artificial trends (e.g., Tonboe et al., 2016; Lavergne et al., 2019).

Several inter-comparison studies were carried out to assess the quality of the sea-ice concentration obtained with different algorithms (e.g., Andersen et al., 2007; Ivanova et al., 2014, 2015; Beitsch et al., 2015; Comiso et al., 2017a). Two different kinds of such inter-comparisons exist. One kind deals with an inter-comparison of sea-ice cover products of a certain number of algorithms without incorporating independent information of the sea-ice cover. Such inter-comparisons provide very valuable information about inter-product consistencies in, e.g. the overall sea-ice concentration distribution, and in sea-ice area and extent time series and trends. They also reveal differences, for instance, with respect to the representation of the seasonal cycle or with respect to regional differences between sea-ice concentration estimates. Inter-comparisons of this kind are, e.g., Ivanova et al. (2014) and Comiso et al. (2017a). These studies, however, do not provide information about how~~the absolute~~ accurate~~cy of~~ a sea-ice concentration product is. The other kind of algorithm inter-comparison studies deals with the comparison of the satellite sea-ice concentration with independent data. These can be ship-based observations, or sea-ice concentration estimates derived from independent satellite observations, for instance, in the optical frequency range or with active microwave sensors such as Synthetic Aperture Radar (SAR). Inter-comparisons of this second kind seldom involve

more than one to two algorithms (e.g., Wiebe et al., 2009; Meier, 2005; Comiso et al., 1997; Comiso and Steffen, 2001; Markus and Dokken, 2002; Kern et al., 2003; Cavalieri et al., 2010; Spreen et al., 2008). Exceptions to this are Andersen et al. (2007), who compared seven different algorithms with ship-based sea-ice cover observations and SAR imagery for the high Arctic, and Beitsch et al. (2015), who compared six different algorithms with ship-based sea-ice cover observations in the Antarctic. Both these studies each focused on one hemisphere only. The work of Andersen et al. (2007) is relatively old and is based on comparably old versions of the algorithms and products. In the present paper, we inter-compare the newest available versions of the sea-ice concentration algorithm and products used in both studies, including three CDRs. We perform our evaluation for both hemispheres. Additionally, we take advantage of a recently published new calibration / validation data package (see Section 2.2).

This paper is the first of a series of papers in which we are going to present and discuss results of a systematic evaluation of ten sea-ice concentration products (see Sect. 2). We want to provide users and algorithm developers with new information about the accuracy and precision of this suite of products, some of which are widely used in the climate research community~~,~~ ~~in less than a handful of papers, and in a form allowing a comparison of product skills at a glance~~. In this paper~~contribution~~, we present the sea-ice concentration products used. We focus on differences in sea-ice concentration, area and extent, and on inter-comparisons with near-100% reference sea-ice concentrations and with a large suite of ship-based manual visual observations of the sea-ice conditions. The second paper is going to focus on an inter-comparison with sea-ice parameters derived from MODerate resolution Imaging Spectroradiometer (MODIS) satellite observations in the Arctic.~~winter time near-100% reference sea ice concentrations, and with a large suite of ship based manual visual observations of the sea ice conditions. The second contribution is going to focus on Arctic summer conditions, presenting and discussing results of an inter-comparison with sea ice parameters derived from MODerate resolution Imaging Spectroradiometer (MODIS) satellite observations.~~ The third ~~contribution~~paper is going to focus on presenting and discussing results of an inter-comparison with sea-ice concentrations computed from Landsat satellite visible imagery.

In the following Sect. 2, we introduce the sea-ice concentration data sets and ancillary data used as input. This section~~It~~ further describes the preparation of the ancillary data and inter-comparison steps. Section 3 illustrates how the sea-ice concentration products compare with each other in terms of multi-annual monthly average sea-ice concentration as well as sea-ice area and extent. In Sect. 4 and Sect. 5, we show the results of the inter-comparison against a near-100% reference data set and against ship-based sea-ice observations, respectively. Section 6 covers a discussion, an outlook, and conclusions.

2 Data & Methodologies

2.1 Sea-ice concentration data sets

For this study, we consider 10 different sea-ice concentration products (Table 2, with more details in Appendices A to F). There are many more algorithms and products available than we are using here, see e.g. Ivanova et al. (2015). The main criteria for our choice of algorithms and products are 1) length of the product time series, 2) grid resolution, 3) accessibility and sustained production~~continuation~~. We exclude~~avoid~~ products with less than ten years coverage and/or with a ~~considerably~~ finer grid resolution than 12.5 km. ~~After~~Following Table 2 we comment on several specific issues that are important for the correct interpretation of sea-ice concentration products, namely the grid resolution, the land spill-over correction, the weather / open water filter, and the sea-ice concentration distributions around 0% and 100%.

We group the products according to their concept for sea-ice concentration retrieval (Table 2, column “Group”). Group I contains the four EUMETSAT-OSISAF – ESA-CCI products. Group II contains the CBT-like algorithms, which are CBT-SSMI; CBT-AMSRE and NOAA-CDR (the latter is a combination of CBT-SSMI and NT1-SSMI but is clearly dominated by CBT-SSMI). NT1-SSMI and ASI-SSMI are assigned to group III. These algorithms follow a different concept to retrieve the sea-ice concentration where the sea-ice concentration is mainly based on a brightness temperature polarization difference.

Finally, NT2-AMSRE is assigned to group IV; its concept to derive sea-ice concentrations via a look-up table and model atmospheres is fundamentally different from the other nine algorithms.

2.1.1 Grid resolution

Given grid resolutions apply to every grid cell for group I products~~OSI-450 and SICCI-12km, SICCI-25km, and SICCI-50km~~ since their EASE grid has equal area of all grid cells (App. A). For all other products which are provided on polar-stereographic grid (App. B through F), the grid resolution is true at 70 degrees latitude (see also Peng et al., 2013). For the computation of sea-ice area and extent (Sect. 3), we take this difference in grid-cell area into account and use the respective files of the grid-cell areas provided by NSIDC (ftp://sidads.colorado.edu/pub/DATASETS/brightness-temperatures/polar-stereo/tools/geo-coord/grid, last access date: 26/9/2018).

2.1.2 Land spill-over correction

The difference in brightness temperatures observed over open water (low) and land (high) combined with the size of the field-of-view of several kilometres to a few tens of kilometres can cause spurious sea-ice concentrations to appear along coasts (e.g., Lavergne et al., 2019). Various methods to reduce this so-called land spill-over effect are applied in all products (Cavalieri et al., 1999; Cho et al., 1996; Maass and Kaleschke, 2010). For ASI-SSMI (App. B), reduction of land spill-over effects is carried out for both the ASI algorithm as well as the NASA-Team algorithm product used over~~for~~ open water. For NOAA-CDR (App. F), the reduction of land spill-over effects is applied separately to both input data sets before merging (Meier and Windnagel, 2018). In this paper, we do not further correct potential differences between the ten products caused by this effect.

2.1.3 Weather / open water filter

The two standard weather filters based on brightness temperature gradient ratios at 19 GHz, 22 GHz, and 37 GHz, which mitigate noise due to atmospheric moisture and wind-induced roughening of the ocean surface (Cavalieri et al., 1995, 1999) are applied in the products NT1-SSMI and NT2-AMSRE. In the products CBT-SSMI and CBT-AMSRE, spurious sea-ice concentrations caused by weather effects are filtered using the same frequencies as mentioned above but applying a bootstrap technique (Comiso and Nishio, 2008). For NOAA-CDR (App. F), the above-mentioned weather filters are applied before the merging (Meier and Windnagel, 2018). In the two NASA GSFC (App. C, D) sea-ice concentration products, i.e., NT1-SSMI~~,~~ version 1~~,~~ and CBT-SSMI~~,~~ version 3~~,~~ weather effects are reduced by screening of input brightness temperatures, application of the above-mentioned weather filters, and some additional manual correction (Meier and Windnagel, 2018; Peng et al., 2013, https://nsidc.org/data/g02202/versions/3, https://nsidc.org/data/nsidc-0051, and https://nsidc.org/data/nsidc-0079). In the ASI-SSMI product no specific weather filter is applied to the ASI algorithm itself. However, ASI algorithm sea-ice concentrations are set to 0% where NASA-Team algorithm sea-ice concentration values are < 30% (see App. B). Because the above-mentioned two weather filters are applied to the NASA-Team sea-ice concentration, the ASI-SSMI product implicitly contains a weather filter as well (Ezraty et al., 2007). Note that the 5-day median filter used for the ASI-SSMI product used here (Kern et al., 2010) not only removes remaining spurious sea ice over open ocean but also reduces weather-induced elevated sea-ice concentrations along the ice edge. In the group I~~EUMETSAT OSISAF ESA CCI~~ products a dynamic open water filter is applied. It is based~~roots~~ on the quoted standard weather filters but takes into account changes in filter efficiency due to changes in the frequencies between the different sensors, for instance between SMMR and SSM/I. Also, it does not use the channels close to 22 GHz. ~~Still, that filter uses a global sea-ice concentration cut-off at about 10% SIC (Lavergne et al., 2019).~~ All weather filters may in addition to the spurious ice also remove real ice along the ice edge. ~~Finally,~~ ~~a~~All ten products apply a monthly varying climatological sea-ice cover mask to erase spurious sea ice at low latitudes.

We investigate the temporal consistency of the weather filters. For this we focus on the sea-ice concentration interval]0.0%, 30.0%], i.e. exclude grid cells set to exactly 0.0% by the weather filter. Then, for each day of the month, we identify the 5% percentile of all gridded sea-ice concentrations falling into the above-mentioned interval. Subsequently, we average over the month.~~the weather filters by computing time series of the monthly mean 5% percentile of sea ice concentrations of the range]0.0% to 30.0%], i.e. excluding the grid cells set by the open water filter to exactly 0.0%.~~ We look at two aspects. First, it is desirable that these time-series are mostly stable across the time-period covered by a given data record, indicating that the weather filter cuts the sea-ice edge evenly across inter-annual variability and changes of frequencies. Second, it is also desirable that the weather filter cuts "well below" the 15% SIC threshold that is commonly used in the computation of the sea-ice extent (SIE) (e.g. Gloersen et al., 1992; Meier et al., 2014, Comiso et al., 2017) but also of the sea-ice area (SIA) (e.g. Gloersen et al., 1992; Cavalieri and Parkinson, 2012; Ivanova et al., 2014).~~value so that it does not interfere with the computation of sea ice area (SIA) and extent (SIE) that use this threshold to define the sea ice edge (e.g., Gloersen et al., 1992).~~ We choose the 5% percentile (and not a minimum value) to obtain less noisy time-series. We plot examples of these time-series for all ten products in Fig. 1 and Fig. 2 for the Arctic and Antarctic, respectively. For the Arctic we use March (Fig. 1 a) and September (Fig. 1 g); for the Antarctic September (Fig. 2 a) and February (Fig. 2 g). In addition to the time-series, we also plot the cumulative distribution of the daily sea-ice concentrations of the range]0.0% to 30.0%] for the respective month for the year 2004 as an example for CBT-SSMI, OSI-450, NT1-SSMI, ASI-SSMI, and NT2-AMSRE.

We find~~confirm the finding from Lavergne et al. (2019, their Fig. 9), with~~ little inter-annual variation of the monthly mean percentile sea-ice concentration over time particularly for OSI-450 and SICCI-25km (see also Lavergne et al., 2019). Changes as caused, e.g., due to a switch in sensor remain below 1%. On average, the 5% percentile sea-ice concentration is < 12%, which ensures that the enhanced open water filter applied in these two products barely influences computation of SIA and SIE. For group II products~~CBT-AMSRE, CBT-SSMI and NOAA-CDR~~, these monthly mean 5% percentile sea-ice concentrations are considerably larger and sometimes exceed 15%. Additionally, the time-series for CBT-SSMI and NOAA-CDR reveal larger inter-annual variations than OSI-450, inter-sensor transitions (e.g. in 1987-1988 changing from SMMR to SSM/I, Fig. 1 g), and in 2007-2008 changing from SSM/I to SSMIS, Fig. 1 a) leading to trends in the percentile time-series. Compared to OSI-450 and SICCI-25km we find for NOAA-CDR: 1) The sea-ice concentration at which the weather filter applies varies seasonally. For instance, in the year 1996, the mean 5% percentile of sea-ice concentrations within the interval]0%, 30%] is for the Arctic 14% in March but 17% in September, and for the Antarctic 16% in September but 18% in February. OSI-450 cuts at 10%, SICCI-25km at 11% in these months, and for both hemispheres. 2) The inter-annual variation of the sea-ice concentration at which the filter applies is larger for NOAA-CDR than for OSI-450 and SICCI-25km. The time-series for NT1-SSMI, ASI-SSMI, and NT2-AMSRE, in contrast, have very low (~~partly~~ ~1%) monthly mean 5% percentile sea-ice concentration values with little or no inter-annual variation.

In the plots of the sample daily cumulative fraction for year 2004, we find~~CBT-SSMI and OSI-450 reveal~~ a ~~hockey-stick shaped~~ cumulative distribution with a first increasing, later merely constant slope with no sea-ice concentrations below ~10% and ~8% for CBT-SSMI and OSI-450, respectively (Fig. 1 b, c, h and i; Fig. 2 b, c, h and i). This agrees with the application of the open water filter presented in Lavergne et al. (2019). For NT1-SSMI and NT2-AMSRE, in contrast, we find~~reveal~~ a substantial amount of near-0% sea-ice concentrations (Fig. 1 d, f, j and l; Fig. 2 d, f, j and l). This suggests that while a weather filter is applied (according to the documentations) there are still concentrations near 0% left. We checked this by looking at the respective daily sea-ice concentration maps. Both products reveal a considerable number of grid cells with < 5% sea-ice concentration along the ice edge. ~~Note that the fact that except~~ All but the group I~~EUMETSAT-OSISAF—ESA-CCI~~ products (see Table 2), ~~all products~~ only provide integer sea-ice concentration values. At the near-0% end of the sea-ice concentration distribution these products have sea-ice concentrations 0%, 1%, 2%, and so forth. The number of NT2-AMSRE sea-ice concentration values of 1% exceeds the 5% percentile most of the time which is the explanation why most NT2-AMSRE values are missing in the ~~, paired with this large number of near 0% sea ice concentration values for, e.g. NT2-~~

~~AMSRE, results in a no show of this product in the~~ time series in plots a) and g) of Fig. 1 and Fig. 2. We take the results~~information from~~ shown in these two figures into account when discussing the results presented in Sect. 3.

2.1.4 Distribution around ~~0% and~~ 100%

A considerable fraction of this paper focuses on the evaluation near 100% sea-ice concentration. Sea-ice concentrations are retrieved from satellite microwave brightness temperatures using a geophysical algorithm, usually involving tie points. Tie points are typical signatures, e.g. brightness temperatures, or parameters derived from these, of ice (SIC: 100%) and open water (Sic: 0%). Because of the natural variability of the surface properties of 100% sea ice relevant for its microwave remote sensing, one fixed tie point value for 100% sea ice, even if retrieved daily, can only be an average representation of these properties. In other words, ten different kinds of 100% sea ice can cause ten different brightness temperatures. As a result, a retrieved sea-ice concentration naturally varies *around* 100%. This means even though the actual sea-ice concentration is exactly 100% the retrieved one could be, for example, 97% or 100% or 103%. While the group I~~EUMETSAT OSISAF – ESA CCI~~ products ~~allow using~~retain the naturally retrieved sea-ice concentration ~~on either side of 100%~~ the others do not; in all group II to group IV~~those other~~ products (see Table 2) sea-ice concentrations are truncated at 0% and 100%, i.e. values < 0% are set to 0% and values > 100% are set to 100%. ~~.~~Figure 3 illustrates the sea-ice concentration distribution at the locations of the near-100% sea-ice concentration reference data set (see Sect. 2.2) for SICCI-25km, SICCI-50km and NOAA-CDR for the Arctic (plots a) to c)) and the Antarctic (plots d) to f)).

We use a Gaussian fit to ~~simulate~~reconstruct the true distribution of the sea-ice concentration retrieval around 100% for type II and III product types. The methodology is tested on the group I products. This is done by finding that Gaussian curve which provides the lowest root-mean-squared difference (RMSD) to the sea-ice concentration distribution for values ≤ 99%, i.e., basically the left hand side of the histograms shown in Fig. 3. For the fitting process, we also take into account the fraction of sea-ice concentrations ≤ 99% relative to the entire count of valid sea-ice concentrations: F_{99}. The difference between original F_{99} and F_{99} resulting from the Gaussian fit, ΔF_{99}, has to be < 0.1. We allow a maximum RMSD value of 0.0125. We first binned SICCI-25km and SICCI-50km sea-ice concentration values to integer values to be consistent~~comply~~ with the other products. Figure 3 a, b and d, e) illustrate that the fits (red) agree well with the originally retrieved SICCI-25km and SICCI-50km sea-ice concentrations (blue) with modal values slightly below 100%. Figure 3 c, f) illustrate how well the Gaussian fit matches the original sea-ice concentration distribution for sea-ice concentrations ≤ 99% for NOAA-CDR as an example. Here the modal sea-ice concentrations of the Gaussian fit are larger than 100%: 103.5% for NH (Fig. 3 c) and 100.9% for SH (Fig. 3 f). In addition, the Gaussian curve is broader than for SICCI-25km and SICCI-50km, resulting in larger values for the standard deviation. We also note that F_{99} is ~0.6 and ~0.5 for SICCI-25km and SICCI-50km, respectively, but only ~0.2 and ~0.4 for NOAA-CDR. We take the information from Fig. 3 into account when interpreting the results presented in Sect. 4 and Sect. 5. We refer to Appendix H for the full set of sea-ice concentrations and Gaussian fits obtained for all ten products in both hemispheres.

2.2 The near-100% sea-ice concentration reference data set

For the evaluation of the ten products at 100% sea-ice concentration (see Sect. 4), we use the Round Robin Data Package version 2 (RRDP2) near-100% reference sea-ice concentration data set developed within the ESA Sea_Ice_cci and EU-SPICES projects (Pedersen et al., 2019). In short, for this reference data set, areas of ~100% sea-ice concentration are found by identifying areas of interest (AOI) of approximately 100 km x 100 km size with net convergence in the ice drift pattern on two consecutive 1-day periods. Information about convergence is derived from the PolarView / MyOcean / CMEMS ice drift data set derived from Envisat ASAR, RADARSAT-2 SAR and Sentinel-1 SAR imagery. By choosing AOIs for~~in~~ regions with high ~~-~~concentrations ~~regions~~, near 100% sea-ice concentration can be assured (e.g., Kwok, 2002; Andersen et al., 2007) in winter. Each AOI contains up to hundred 10 km x 10 km cells for which the SAR ice drift is computed. The number of cells depends

on SAR image coverage. Convergence in the ice drift pattern results in a decrease in the total area of these cells. A cell is included in the dataset of ~100% sea-ice concentration if the area reduction between day 1 and day 2 is between 0.4% and 1.52% and if more than 40% of the AOI contains cells with such an area reduction. The RRDP2 near-100% sea-ice concentration reference data set contains the AOI centre geographic latitude and longitude, time, total sea-ice concentration (100%) and AOI average area reduction due to net ice convergence. It is available for years 2007 through 2015 for both hemispheres.

~~We only use AOIs for winter months, i.e., November through March (Arctic) and May through September (Antarctic). By doing so we ensure that small scale openings, which may remain in an area of high ice concentration and net ice convergence, are frozen and thus sea ice concentrations are close to 100%. We use only AOIs for which the average area reduction between day 1 and day 2 is between 0.4 and 1.5%.~~We cannot provide a definite uncertainty for this reference data set but for its production, we combine a suite of measures to ensure high precision and close-to-zero bias (high accuracy). The drift/convergence selection is based on convergence on two consecutive days of 1-day drift. During winter, i.e., November through March (Arctic) and May through September (Antarctic), this is assumed to ensure that all openings existing on day 0 (prior to the two convergence days) are closed by convergence or refrozen. The refreezing assumption is the reason for the product quality to be higher during winter when openings rapidly refreeze than during summer when openings may not freeze up. There is no prior assumption of the initial ice concentration (on day 0), but the ice-drift product requires quite high concentrations for the 2-D cross correlation to work. Andersen et al. (2007) reported an accuracy of 2% for ice-water SAR image classification from ice analysts without additional drift / convergence information and a sea-ice concentration standard deviation of ~1% for own cold-season high-resolution high-quality SAR image classification. Based on our above-mentioned measures and the results of Andersen et al. (2007) we can state estimated values for precision: ~1% and accuracy: <0.5% for our reference data set.

We co-locate the sea-ice concentrations of the ten products with the selected AOI grid cells by computing the minimum distance between AOI grid cell centre and grid cell centre of the respective sea-ice concentration product. For this step, we convert the geographic coordinates of all data sets into ~~e~~Cartesian coordinates taking into account the different projections. Figure 4 illustrates the spatial distribution of selected AOIs for both hemispheres for two different years by showing the co-located OSI-450 sea-ice concentration. We give an example of~~or~~ a typical "good distribution" (Fig. 4 a, c) and for a typical "poor distribution" (Fig. 4 b, d). The RRDP2 near-100% sea-ice concentration reference data set contains basically no AOIs in the Eastern Antarctic because of the lack of ~~sufficiently frequent~~ SAR image coverage~~acquisitions~~ required for the ice drift product used to generate this RRDP2 data set.

We evaluate the products at their native grid resolution without applying any spatial averaging. For each product, we compute the mean difference "product minus 100%" and its standard deviation as well as the cumulative distribution function of the differences.

2.3 Ship-based visual sea-ice cover observations

According to the Antarctic Sea Ice Processes & Climate (ASPeCt) protocol http://www.aspect.aq (Worby and Allison, 1999; Worby and Dirita, 1999, see also Worby et al., 2008) and the IceWatch/ASSIST (Arctic Ship-based Sea-Ice Standardization) protocol (http://icewatch.gina.alaska.edu), ship-based observations of the sea-ice conditions shall be carried out every hour, at least every second hour, during daylight conditions while the ship is traversing the sea ice. Observations shall be carried out from the ship's bridge for an area of about one kilometre around the ship and shall report ice conditions as follows: total ice concentration, type of openings, and concentration, thickness, ridge fraction and height, and snow depth and type for up to three ice types. ~~Such a protocol was not implemented in the Arctic in the same rigorous way as in the Antarctic. Nevertheless, ship based visual observations were carried out as well during numerous cruises into the Arctic Ocean and its peripheral seas, using a slightly different protocol, established in the late 2000s. The need for a slightly different protocol can~~

be explained by various forms of melt on Arctic sea ice, which are largely lacking for Antarctic sea ice. All ship-based visual observations used here result from manual, non-automated observations.

For our evaluation of the ten products with respect to ship-based visual observations of the sea-ice conditions (see Sect. 5), we use about 15 000 individual observations. About ~7000 of these were carried out in the Antarctic (ASPeCt) and ~8000 in the Arctic (IceWatch/ASSIST). About ~7000 of these were carried out in the Antarctic under the framework of the ASPeCt protocol. A substantial fraction of the Antarctic observations (until 2005) is available via http://www.aspect.aq (Worby et al., 2008). The more recent observations were collected from various sources (e.g. PANGAEA, ACE-CRC, AWI, see also Beitsch et al., 2015) and merged with the existing ASPeCt data. The majority of the ASSIST data is taken from the data portal http://icewatch.gina.alaska.edu. Additional sources for ASSIST data are PANGAEA (for Polarstern cruises before IceWatch/ASSIST), the Arctic Data Center of the NSF: https://arcticdata.io/catalog/#data, and the data archive of the Bering Sea Ecosystem Study (BEST): https://www.eol.ucar.edu/projects/best/ice.shtml. All data are standardized, i.e. the ascii format data files containing the observations use similar formats for all variables and missing data. Beitsch et al., 2015), merged with the existing ASPeCt data and standardized. Standardization means that the resulting ascii format data file containing all observations uses similar formats for all variables and missing data. The data are also manually quality checked for outliers. For the comparison presented in this manuscript, we use all ASPeCt and IceWatch/ASSIST observations from the period June 2002 through December 2015. This data set is available via http://icdc.cen.uni.hamburg.de/1/daten/cryosphere/seaiceparameters-shipobs, last access date: 28/3/2019.

In the Arctic, ship-based sea-ice observations have been collected under the IceWatch/ASSIST (Arctic Ship-based Sea-Ice Standardization) initiative and are available via http://icewatch.gina.alaska.edu. The majority of the data used in this manuscript for the Arctic is taken from that portal. Additional sources for ship-based sea-ice observations are again PANGAEA (for Polarstern cruises before IceWatch/ASSIST), the Arctic Data Center of the NSF: https://arcticdata.io/catalog/#data, and the data archive of the Bering Sea Ecosystem Study (BEST): https://www.eol.ucar.edu/projects/best/ice.shtml. In total ~8000 observations are available for the Arctic. We prepare these data in the same way as the ASPeCt observations for the Antarctic and use all observations from the period June 2002 through December 2015. This data set is available via http://icdc.cen.uni.hamburg.de/1/daten/cryosphere/seaiceparameters-shipobs, last access date: 28/3/2019.

Figure 5 summarizes the locations of the ship-based observations used in this manuscript, separately for the Arctic (Fig. 5 a, b) and the Antarctic (Fig. 5 c, d). InFor both hemispheres, just comparably small regions contain such observations. Figure 5 a, c) illustrates that some regions are visited during several years while others just once or twice during the 13-year period considered. The seasonal distribution (Fig. 5 b, d) illustrates that the more central (Arctic) or southern (Antarctic) regions were only visited during summer months due to harsh winter conditions and missingpaired with lack of daylight forin these regions.

We co-locate the sea-ice concentrations of the ten products with the selected ship-based observations by computing the minimum distance between geographic location of the ship-based observation and the grid cell centre of the respective sea-ice concentration product. For this step, we convert the geographic coordinates of all data sets into cartesian coordinates taking into account the different projections of the sea-ice concentration products. AfterFollowing the co-location, we average over all ship-based and all satellite-based sea-ice concentration values, including reports of open water, i.e. 0% concentration, of one day following the approach of Beitsch et al. (2015). This results in a comparison of along ship-track daily average sea-ice conditions. Data pairs with less than three ship-based observations per day are discarded. The results of the comparison between ship-based and satellite-based sea-ice concentration are solely based on these daily average sea-ice concentrations. Note that all satellite-based data are used at their native grid resolution.

The ship-based and satellite-based sea-ice concentration data sets are inter-compared (Sect. 5) by means of histograms, scatterplots and linear regression analysis and statistics separately for summer data, winter data, and data of the entire year. Summer comprises months May through September for the Arctic and months November through March for the Antarctic; winter comprises the respective remaining months. For the histograms, sea-ice concentrations are put into bins 0 … 5%, 5%

~~… 15%, 15% … 25%, … , 85% … 95%, 95% … 100%. By doing so we get an impression about the distribution of both sea-ice concentration data sets at the precision of the ship-based observations, which is ~ 10%.~~ In the scatterplots, we compare the daily average sea-ice concentrations and additionally compute averages of the satellite-based sea-ice concentration for each of the above-mentioned bins applied to the ship-based data and vice versa. We compute the overall average sea-ice concentration difference and its standard deviation, and perform a linear regression analysis based on the daily average and the binned data. ~~All these results are presented in Sect. 5.~~

3 Inter-comparison of sea-ice area~~, and~~ extent, and distribution

We follow Ivanova et al. (2014) and begin our inter-comparison with time-series of the sea-ice area (SIA) and sea-ice extent (SIE) (Subsection 3.1 and 3.2) derived from monthly mean sea-ice concentration. The monthly mean sea-ice concentration is derived for every product at the native grid and grid resolution using data of all days of a month of the entire sea-ice concentration range including 0%. SIE is computed by summing over the grid-cell area of grid cells with > 15% sea-ice concentration. SIA is computed by summing over the ice-covered portion of the grid-cell area of grid cells with > 15% sea-ice concentration. By using this threshold, we follow Gloersen et al. (1992) and numerous SIA and SIE inter-comparison studies. We compare SIA and SIE time-series for the entire period for which we have data from the respective products at the time of the analysis. We exclude sea-ice concentrations estimated for lakes and other inland waters. We fill the circular area with missing data around the pole caused by the satellite orbit inclination and swath width with a constant sea-ice concentration value of 98%. Andersen et al. (2007) found a mean sea-ice concentration of ~98% from a comparison of cold season passive microwave and synthetic aperture radar observations in the high Arctic. They noted a smaller value of ~95% in summer. Both values are confirmed by own work (Kern, 2018, http://icdc.cen.uni-hamburg.de/fileadmin/user_upload/ESA_Sea-Ice-ECV_Phase2/SICCI_Phase2_SIV-Retrieval_Report_v02.pdf, last accessed September 6, 2019). Using 98% instead of 95% during summer results in an overestimation of the SIA of about 10 000 km², a small value compared to other sources of biases for the SIA during summer. This filling is applied~~of 98%; this applies~~ to the Arctic and only to the products at polar-stereographic projection. This area is already interpolated spatially in the four group I~~EUMETSAT OSISAF – ESA CCI~~ products~~ already~~. As described in Lavergne et al. (2019), these products contain a fully filtered and truncated to the range [0.0% … 100.0%] version and a non-filtered, non-truncated version of the sea-ice concentration. The latter contains the naturally retrieved sea-ice concentrations, i.e., also values < 0% and > 100% (see Sect. 2.1.3) and no weather filters are applied (see Sect. 2.1.3). We use the fully filtered and truncated version~~Note that we use the fully filtered and truncated versions of these products, i.e. the variables, which are the main entry point to this product files~~. ~~The two most relevant filters applied are the open-water filter, and a statistical land spill-over removal filter (Lavergne et al., 2019). In addition, these filtered sea ice concentrations are truncated to values between 0% and 100%, even though the retrieval naturally provides a sea ice concentration distribution around these two values (see Fig. 3 and Lavergne et al. (2019)).~~ Without th~~e~~is~~ truncation the SIA of the group I~~EUMETSAT OSISAF – ESA CCI~~ products increases slightly, while the SIE does not change because the number of grid cells covered with > 15% sea ice is not influenced by the truncation (not shown). ~~In Fig. 6, we present the SIA and SIE time series of months March and September for the Arctic; in Fig. 8 we show the SIA and SIE extent time series of months February and September for the Antarctic. The months chosen reflect the time of the typical minimum and maximum SIA and SIE.~~

We complement these SIA and SIE time series with maps of the multi-annual average sea-ice concentration difference for selected months~~ in the Arctic (Fig. 7) and Antarctic (Fig. 9 and Fig. 10)~~ for the AMSR-E measurement period: June 2002 to September 2011 (Subsection 3.3 and 3.4). We choose this period to be able to compare all ten products for a similarly long time-period. For these maps, we first re-grid the monthly mean sea-ice concentrations of all products, except SICCI-50km, onto the EASE grid version 2.0 with 50 km grid resolution using bilinear interpolation. Then we compute the multi-annual

average sea-ice concentration for each month from which we subsequently calculate an ensemble median ~~(see map k) in Fig. 7 and Fig. 9 and 10)~~ and the difference product minus ensemble median ~~(all other maps in Fig. 7 and Fig. 9 and 10)~~.

~~Finally, we summarize differences between the mean sea-ice concentrations of all products and differences between the mean SIA and SIE values of all products in Fig. 11 and in Appendix G, Fig. G1 through Fig. G6. Similarly to the sea ice concentration maps mentioned above, we re-grid the monthly mean sea-ice concentration onto the EASE grid version 2.0 with 50 km grid resolution using bilinear interpolation and apply a common land mask (the one of SICCI-50km) to all products. The differences between SIA and SIE values shown in Fig. 11 are computed from these gridded 50 km resolution, common land mask products.~~

3.1 Arctic sea-ice area and extent time-series

The SIA and SIE time-series ~~shown in Fig. 6~~ for the Arctic reveal a very similar overall development for the products extending back into the 1980~~ties~~s and 1990~~ties~~s (Fig. 6). This applies to: i) the overall negative trend in both quantities; ii) the inter-annual variability as, for instance, during 1991-1997 and around 2007 and 2012 for ~~the September~~ SIA and SIE in September (Fig. 6 b, d), or in 2011 for the relative minimum in March SIA and SIE (Fig. 6 a, c); iii) to the ranking between the products. NOAA-CDR and CBT-SSMI provide largest SIA and SIE in~~for~~ both March and September~~, exceeding the next largest one, OSI-450, by ~600 000 km² (SIA) and ~200 000 km² (SIE)~~. NT1-SSMI provides lowest SIA and SIE in~~for~~ September, while in~~for~~ March we find SIA and SIE from ASI-SSMI to be even lower. It is obvious that differences between products are smaller for SIE than for SIA as was shown also by Ivanova et al., (2014).

For the AMSR-E period, when SIA and SIE of all ten products are available, the inter-annual variation is similar for all ten products. We find ~~that the products not discussed in the previous paragraph, i.e. the~~ ESA-CCI products, CBT-AMSRE and NT2-AMSRE, fall into the ranges of SIA and SIE given by the other products. An exception to this is SICCI-50km, providing clearly the lowest SIE of all products in March (Fig. 6 c). We will discuss this finding in Sect. 3.3~~the context of Fig. 7~~.

3.2 Antarctic sea-ice area and extent time-series

The SIA and SIE time-series ~~shown in Fig. 8~~ for the Antarctic reveal a similar overall development for products extending back into the 1980~~ties~~s and 1990~~ties~~s (Fig. 7). This applies to i): the overall positive trend until 2015 in both quantities; ii) the inter-annual variability, for instance, during 2000-2003 for ~~the February~~ SIA and SIE in February (Fig. 7~~8~~ b, d), or in 2008 for the relative minimum in ~~September~~ SIA and SIE in September (Fig. 7~~8~~ a, c); iii) the ranking between products. NOAA-CDR and CBT-SSMI provide largest SIA while NT1-SSMI provides smallest SIA, being ~1.8 million km² and 300 000 km² below the SIA of NOAA-CDR and CBT-SSMI in~~for~~ September and February, respectively. ~~OSI-450 and ASI-SSMI SIA mostly fall into the range given by the other products.~~ OSI-450 and CBT-SSMI provide the largest SIE, exceeding the smallest SIE: NT1-SSMI by ~500 000 km² and ~300 000 km² in September and February, respectively (Fig. 7~~8~~ c, d). Inter-product differences are larger for SIA than SIE in~~for~~ September but not in~~for~~ February.

For the AMSR-E period, the inter-annual variation is similar for all ten products. In~~For~~ September, SIA and SIE of the ESA-CCI products mostly fall between ASI-SSMI and OSI-450 (Fig. ~~8~~7 a, c). ~~For~~In February (Fig. ~~8~~7 b, d), SICCI-50km provides smallest overall SIA and SIE while the SICCI-12km and SICCI-25km products agree closely with OSI-450. In contrast to the Arctic (compare Fig. 6), NT2-AMSRE clearly provides largest SIA in~~for both~~ September and February~~, exceeding the second largest SIA: CBT-AMSRE for September and ASI-SSMI for February by ~ 500 000 km²~~ (Fig. ~~8~~7 a, b). NT2-AMSRE provides largest SIE in~~for~~ February as well (Fig. 7~~8~~ d).

Figure 7 c) contains an example of discontinuities caused by the application of weather filters not adapted to sensor changes. Wintertime Antarctic OSI-450 and CBT-SSMI SIE agree with each other for the SMMR period. After 1987 the CBT-SSMI SIE is below the OSI-450 SIE by ~150 000 km². This corresponds to the area of one quarter of all 25 km grid cells at a

latitude of 60°S, the approximate average location of the Antarctic sea-ice edge in September. This change in SIE is concomitant with a jump in the weather-filter sea-ice concentration from 11% to 14% (Fig. 2 a). It is noteworthy that the 23.0 GHz channels of the SMMR instrument have been highly unstable since launch, and eventually ceased to function on 11 March 1985 (Njoku et al., 1998). Thus, the water-vapour part of the "classic" weather filter is un-reliable in the early decade of the satellite data record. This is solved in the OSI-450 product by relying on explicit atmospheric correction of the brightness temperatures using -among others- water vapour fields from atmosphere re-analysis (see Lavergne et al., 2019). Another example of this kind (not shown), is a shift between OSI-450 SIE and NOAA-CDR SIE by 50 000 km² to 100 000 km² between 2007 and 2008. This shift is concomitant with a discontinuity in the weather-filter sea-ice concentration for NOAA-CDR in March (Arctic, Fig. 1 a) and September (Antarctic, Fig. 2 a) during the transition from 2007 to 2008. This corresponds to when SSMIS (F17) is processed instead of SSM/I (F15). OSI-450 exhibits no discontinuity here.

~~3.2~~3.3 Arctic sea-ice concentration distribution differences

~~For~~In March, the difference between the sea-ice concentration of an individual product and the ensemble median of all ten products (Fig. ~~7~~8) remains within ±5% over most of the Arctic Ocean, except for ASI-SSMI (Fig. ~~8~~7 d) and SICCI-12km (Fig. ~~8~~7 f). ~~While the former exhibits less sea ice than the ensemble mean over almost the entire Arctic Ocean, the latter exhibits less sea ice particularly north of Greenland and the Canadian Arctic Archipelago with differences < 5%.~~ The largest differences between individual products and the ensemble median are located in the peripheral seas~~, i.e. Sea of Okthosk, Bering Sea, Baffin Bay, Labrador Sea, Irminger Sea, Greenland and Barents Seas~~. Group II and IV (see Table 2) products have more sea ice than the ensemble median ~~CBT-SSMI, NOAA-CDR, CBT-AMSRE and NT2-AMSRE~~ (Fig. ~~7~~8 b, c, i, j) ~~show more sea ice than the ensemble mean – especially in the Irminger Sea (the two SSM/I products), the Labrador Sea (the two AMSR-E products), and Sea of Okthosk and Bering Sea (all four products);~~ differences can exceed 20%. ~~Note the similarity in the distribution of differences for CBT-SSMI and NOAA-CDR (Fig. 7 b, c).~~ NT1-SSMI (Fig. ~~8~~7 a) ~~show~~has less sea ice than the ensemble median with negative differences greater than~~of <~~ -10% or even ~~<~~ 15% in magnitude in all peripheral seas. Differences of OSI-450 or SICCI-25km and the ensemble median are within ±5% almost everywhere~~overall~~ (Fig. ~~8~~8 e, g). SICCI-50km exhibits ~~shows ~ 2% more sea ice than the ensemble mean for most of the sea-ice cover. However, we find areas of considerably less sea ice than the ensemble mean, i.e.~~ negative differences greater than~~≤~~ -20% in magnitude~~,~~ along some of the coastlines, e.g., ~~in~~ the Labrador Sea, the Irminger Sea or the coastlines of~~in~~ the Pechora Sea and Barents Sea~~s~~ (Fig. ~~8~~7 h). A careful check of these areas in daily and monthly mean maps of the SICCI-50km sea-ice concentration reveals that for~~in~~ regions with~~of~~ a relatively narrow sea-ice cover stretching along coastlines, the coarse resolution of the 6.9 GHz frequency channel entering the algorithm (see Table 2), in ~~the~~ combination with~~of~~ land spill-over filter and open water filter can result in an unwanted complete removal of sea ice from the grid cells of the~~SICCI-50km~~ product ~~grid cells with ice~~. We are confident that this explains the particularly low SICCI-50km SIA and SIE shown in Fig. 6 a) and c) for~~in~~ Arctic SIE in~~for~~ March.

For the matrices shown in Fig. 9 (and Fig. 12, Appendices G1 to G6), we re-grid the monthly mean sea-ice concentration onto the EASE grid version 2.0 with 50 km grid resolution using bilinear interpolation and apply a common land mask (the one of SICCI-50km) to all products. The differences between SIA and SIE values are computed from these gridded 50 km resolution, common land mask products. Figure ~~1~~9~~1~~ a) agrees with the results shown in Fig. ~~8~~7. In~~For~~ winter (March), ~~small, i.e. < 1%, overall~~ sea-ice concentration differences between members of groups I to III are < 1%. ~~are found within three groups of products: I) EUMETSAT-OSISAF – ESA-CCI, II) NT2-AMSRE, CBT-AMSRE, CBT-SSMI, and NOAA-CDR, and III) ASI-SSMI and NT1-SSMI. Note we assign the two products of group III to a separate group only for simplicity; they often differ considerably.~~ Group III members NT1-SSMI and ASI-SSMI (see Table 2) exhibit~~s~~ less sea ice than the other groups~~: ~ 2% compared to group I and ~ 5% compared to group II~~. Group II and IV members exhibit higher sea-ice concentrations than the other two groups in winter and summer (September). ~~For~~In summer~~September~~ (Fig. 9~~11~~ d~~b~~), ~~we find small overall~~ sea-ice concentration differences remain < 2% between members of~~within~~ groups I and II ~~of < 2%~~ but not within group III~~;~~ where

differences exceed 10% ~~between ASI-SSMI and NT1-SSMI. Of the ten products, NT1-SSMI exhibits the smallest overall mean September sea-ice concentration, which is 7-8% below the products of group I, and more than 10% below the products of group II. Group II September sea-ice concentrations exceed those of group I by 5-8%.~~ We refer to App. G for the respective results ~~for~~of the other months.

~~3.3 Antarctic sea-ice area and extent~~

~~1.1 The SIA and SIE time-series shown in Fig. 8 for the Antarctic reveal a similar overall development for products extending back into the 1980ties and 1990ties. This applies to i): the overall positive trend until 2015 in both quantities; ii) the inter-annual variability, for instance, during 2000-2003 for the February SIA and SIE (Fig. 8 b, d), or in 2008 for the relative minimum in September SIA and SIE (Fig. 8 a, c); iii) the ranking between products. NOAA-CDR and CBT-SSMI provide largest SIA while NT1-SSMI provides smallest SIA, being ~ 1.8 million km² and 300 000 km² below the SIA of NOAA-CDR and CBT-SSMI for September and February, respectively. OSI-450 and ASI-SSMI SIA mostly fall into the range given by the other products. OSI-450 and CBT-SSMI provide largest SIE, exceeding the smallest SIE: NT1-SSMI by ~ 500 000 km² and ~ 300 000 km² in September and February, respectively (Fig. 8 c, d). Inter-product differences are larger for SIA than SIE for September but not for February.~~

~~For the AMSR-E period, the inter-annual variation is similar for all ten products. For September, SIA and SIE of the ESA-CCI products mostly fall between ASI-SSMI and OSI-450 (Fig. 8 a, c). For February (Fig. 8 b, d), SICCI-50km provides smallest overall SIA and SIE while the SICCI-12km and SICCI-25km products agree closely with OSI-450. In contrast to the Arctic (compare Fig. 6), NT2-AMSRE clearly provides largest SIA for both September and February, exceeding the second largest SIA: CBT-AMSRE for September and ASI-SSMI for February by ~ 500 000 km² (Fig. 8 a, b). NT2-AMSRE provides largest SIE for February as well (Fig. 8 d).~~

3.4 Antarctic sea-ice concentration distribution differences

In September (Fig. 10~~9~~), most products show more sea ice than the ensemble median over high-concentration ice and less sea ice along the marginal ice zone. ~~Exceptions are NT1-SSMI, ASI-SSMI, and NT2-AMSRE / CBT-AMSRE.~~ NT1-SSMI (Fig. ~~9~~10 a) exhibits considerably less sea ice than the ensemble median almost everywhere ~~with differences even < -20%~~ (see also Fig. 12 a). ASI-SSMI (Fig. 10~~9~~ d) exhibits a ~~difference~~ distribution of sea-ice concentration differences that is reversed compared to most other products~~, exhibiting less sea ice than the ensemble mean over high-concentration ice and more sea ice along the marginal ice zone~~. CBT-AMSRE and especially NT2-AMSRE (Fig. 10~~9~~ i, j) show more sea ice than the ensemble median for~~in~~ most regions. This is evident in Fig. 12 a) as well. ~~– except the marginal ice zone in the Pacific ocean; differences exceed 15% for NT2-AMSRE in the northern Weddell Sea.~~

~~Figure 11 g) agrees with these findings. NT1-SSMI and NT2-AMSRE stand out by providing the smallest and the largest September mean sea-ice concentration, respectively. The overall mean NT1-SSMI September sea-ice concentration is smaller than EUMETSAT-OSISAF – ESA-CCI (group I, compare Sect. 3.2) by 7-9%, and group II (CBT-SSMI, NOAA-CDR, CBT-AMSRE, and NT2-AMSRE) by 9-14%; 14% is for NT2-AMSRE. The overall mean NT2-AMSRE September sea-ice concentration exceeds those from group I by 5-6%, and the other products within group II by 3-4%. Between the EUMETSAT-OSISAF – ESA-CCI products (group I), sea-ice concentration differences are within ±1.1%, consistent to the Arctic where these differences are within ±0.7% (Fig. 11 a).~~

In January (Fig. 11~~0~~), the few, comparably small, high-concentration areas exhibit sea-ice concentration differences mostly below ±5%. Over the lower concentration areas, i.e. mainly in the Weddell Sea and the Ross Sea~~s~~, most products show less sea ice than the ensemble median ~~but~~with differences ~~are small, staying~~ between 0 and -6%. NT1-SSMI has less sea ice while ASI-SSMI and particularly NT2-AMSRE have more sea ice (see also Fig. 12 d). ~~Exceptions to this are NT1-SSMI, ASI-SSMI, and NT2-AMSRE. NT1-SSMI shows even less sea ice (Fig. 10 a), differences reach -10%. ASI-SSMI (Fig. 10 d) and NT2-AMSRE (Fig. 10 j) show more sea ice than the ensemble mean; differences are < 6% for ASI-SSMI but exceed 10% for NT2-AMSRE.~~ Important to note are ~~is~~ the ~~fringe of large, ~ 10%,~~ negative differences of ~ -10% along most of the Antarctic

coast for SICCI-50km (Fig. 110 h). ~~Careful check of these regions in the daily and monthly SICCI-50km sea-ice concentration maps reveals that~~ Like~~as~~ for~~in~~ the Arctic, the coarse resolution of the 6.9 GHz frequency channels combined with~~application of~~ land-spill over ~~filter~~ and open water filters can result in the unwanted removal of ~~grid cells with~~sea ice from grid cells (compare Fig. 87 h) and discussion of it) with the same influence on SICCI-50km SIA and SIE values~~. We are therefore confident that the comparably small February SICCI-50km SIA and SIE values~~ (Fig. 87 b, d) ~~are, like in the Arctic, caused by a too aggressive filtering~~. This is also evident in Fig. 12 d) where SICCI-50km exhibits the largest inter-product differences within group I.

~~Figure 11 g) agrees with these findings. NT1-SSMI and NT2-AMSRE stand out by providing the smallest and the largest September mean sea-ice concentration, respectively. The overall mean NT1-SSMI September sea-ice concentration is smaller than EUMETSAT-OSISAF – ESA-CCI (group I, compare Sect. 3.2) by 7-9%, and group II (CBT-SSMI, NOAA-CDR, CBT-AMSRE, and NT2-AMSRE) by 9-14%; 14% is for NT2-AMSRE. The overall mean NT2-AMSRE September sea-ice concentration exceeds those from group I by 5-6%, and the other products within group II by 3-4%. Between the EUMETSAT-OSISAF – ESA-CCI products (group I), sea-ice concentration differences are within ±1.1%, consistent to the Arctic where these differences are within ±0.7% (Fig. 11 a).~~

~~The sea-ice concentration differences shown in Fig. 11 j) confirm the observations from Fig. 10. As for September (compare Fig. 11 g), NT2-AMSRE stands out as the product with a substantially larger mean sea-ice concentration than all other products in February; differences range from 6.5% for ASI-SSMI to 12% for NT1-SSMI. Compared to September, NT1-SSMI stands out less in February. Sea-ice concentration differences within group II (excluding NT2-AMSRE) are smaller for CBT-AMSRE but larger for the other two products. Differences within group I are as small as for September, i.e. within ±1.1%, but not for SICCI-50km (as can be expected from Fig. 10 h). Note that we show February (Fig. 11 j) instead of January (Fig. 10) to be consistent with the SIA and SIE differences shown in Figure 11 k), l) and refer the reader to Fig. G2 a, b) in App. G for comparison of the sea-ice concentration difference matrices of months January and February.~~

For the results shown in Fig. 6 through Fig. 1~~1~~2 we used the truncated sea-ice concentration values as far as it concerns ~~the~~ group I~~EUMETSAT-OSISAF – ESA-CCI~~ products. Repeating these computations with the non-truncated values, e.g. in~~for~~ September and March, does not change the results with respect to SIE~~, because only the 15% sea-ice concentration threshold counts which is not changed by this action. With respect to~~ SIA ~~we find an~~ increase by ~50 000 km² in ~~the respective~~ winter months and there is almost no impact in~~for the~~ summer ~~months~~.

3.5 Summary and discussion of sea-ice area and extent findings

The partly substantial inter-product mean sea-ice concentration differences (Figures 8 through 12) are associated with a notable impact on SIA and SIE (Fig. 9 and Fig. 12). For summer SIE, inter-product differences are below ~200 000 km² (Arctic, Fig. 9 f) and below ~300 000 km² (Antarctic, Fig. 12 f) for most products. NT1-SSMI (Arctic) and SICCI-50km, NT1-SSMI, NT2-AMSRE (Antarctic) show the largest differences here. For winter SIE, most inter-product differences are below ~200 000 km² for the Antarctic (Fig. 12 c); larger differences are mostly found for NT1-SSMI (see also Fig. 7 c). For the Arctic (Fig. 9 c), inter-product differences range between 100 000 km² and 600 000 km² and seem to be associated with the type of algorithm and partly also the sensor.

For Arctic winter SIA (Fig. 9 b), group III products provide systematically smaller values (by ~400 000 km²) than the other three groups while group II SSMI products provide systematically larger values (by ~300 000km²). Group I and CBT- and NT2-AMSRE exhibit the lowest inter-product SIA differences. For Arctic summer SIA (Fig. 9 e), group II and IV products agree with each other within 100 000 km² but exceed group I SIA by ~400 000 km². This equals to 10% of the summer minimum Arctic SIA. For Antarctic summer SIA (Fig. 12 e), NT2-AMSRE exceeds SIA of all other products by ~400 000 km². This equals 20% of the summer minimum Antarctic SIA. SIA differences between the other products are almost all <

200 000 km². For Antarctic winter SIA (Fig. 12 b), NT2-AMSRE and NT1-SSMI stand out with very large systematic differences to all other products.

We summarize our findings from the matrices in Fig. 9 and Fig. 12 (see also App. G1 to G6) as follows: i) Absolute and relative (to the respective minimum or maximum value) inter-product differences are smaller for SIE than for SIA. ii) SIA and SIE derived from products of different algorithms of the same group (see Table 2) may differ considerably. iii) Inter-product differences for SIA and SIE for the investigated CDRs are, on average, larger for the Arctic than the Antarctic.

We note that the grid resolution of the products is not necessarily compatible with the true spatial resolution because the footprints of the satellite sensor channels used in some of the algorithms is coarser (Table 2). This applies to NT1-SSMI, CBT-SSMI, NOAA-CDR, and OSI-450, i.e. the products at 25 km grid resolution based on SMMR, SSM/I, and SSMIS data. For these products, we expect that gradients in the sea-ice concentration are more smeared than for products with a better match between footprint size and grid resolution as, for instance, CBT-AMSRE or SICCI-25km. This is illustrated for OSI-450 and SICCI-25km in Lavergne et al. (2019, Figure 6). For a typical wintertime Antarctic ice edge at 65°S comprising half a compact and half an open sea-ice cover, this difference in the match of true resolution and grid resolution between SSM/I and AMSR-E products would result in a slightly larger SIE (by ~200 000 km²) derived from the SSM/I product. This is because a compact ice edge is smeared more in the SSM/I product, resulting in more grid cells with a sea-ice concentration > 15%, the threshold used currently to compute SIE. In fact we find that during winter OSI-450 SIE exceeds SICCI-25km SIE by ~100 000 km² in the Arctic (Fig. 9 c) and by ~200 000 km² in the Antarctic (Fig. 12 c). Since the algorithms used for the sea-ice concentration retrieval for these two products are almost identical, the difference in SIE can well be attributed to the above-mentioned impact of differences between true and grid resolution. The second pair of almost identical algorithms is CBT-SSMI and CBT-AMSRE. In the Arctic, in winter, CBT-SSMI SIE exceeds CBT-AMSRE SIE by ~400 000 km² (Fig. 9 c) but in the Antarctic CBT-SSMI SIE is smaller than CBT-AMSRE SIE by ~100 000 km² (Fig. 12 c). Differences in the algorithm itself and/or in the weather filter might be the cause. We refer to the discussion at the end of Sect. 3.2 in this context.

4 Comparison with near-100% SIC reference data set

In this section, we present ~~the~~ results of the evaluation of the ten products at 100% sea-ice concentration using the data described in Sect. 2.2. ~~We note that this is an extension of the analysis shown in Lavergne et al. (2019), where the non-truncated SICCI-25km, SICCI-50km and OSI-450 sea-ice concentrations were used, i.e. including the natural geophysical retrieval noise with a certain fraction of the sea-ice concentration values above 100% (see Sect. 2.1.4). Here, in contrast, we need to focus on the truncated products, i.e. those constrained to the sea-ice concentration range 0% … 100%, because none of the other products provide access to the non-truncated sea-ice concentration values.~~

We note upfront that caution should be exercised when reporting and interpreting evaluation statistics like bias (mean value minus 100%) or root mean square error, near the 100% end of truncated sea-ice concentration products. This applies to the results presented in this section but also to Sect. 5. First, the bias of truncated products will necessarily be negative or zero (mean value lower than or equal to 100%), even if ~~though~~ the bias of the product was exactly 0% before truncation. Second, products whose non-truncated distribution is biased high (modal value larger than 100%) will seemingly achieve better evaluation statistics after truncation, because of the accumulation of values > 100% being folded to exactly 100%. Both bias and RMSE of these products are smaller than those of products that do not overestimate at 100% sea-ice concentration. The larger the fraction of truncated values, the better the statistics. ~~This is also illustrated in Fig. 3, where we infer the distribution of non-truncated values (red) from the distributions of truncated products (black).~~ The values that accumulate at the 100% bin in the truncated product are in majority from the above 100% range of the non-truncated distribution (note the value of F_{99} in Fig. 3), and improve the evaluation statistics (bias and RMSE). In fact, under the hypothesis that the distribution of the retrieved sea-ice concentration is mostly Gaussian around the modal value before truncation, products with overestimation of the non-

truncated distribution can be recognized by their abnormal (with respect to a Gaussian model) accumulation of values exactly at 100%. ~~In the following, we thus start our analysis of the comparison against the near-100% sea-ice concentration reference data with a description of the observed distribution of values, using frequency histograms. We then report bias and RMSE values of the truncated and non-truncated sea-ice concentrations, using Gaussian fits (Sect. 2.1.4).~~ For more discussion and quantification of the error distribution of sea-ice concentration products and algorithms before truncation around 100% (and around 0%), see Ivanova et al. (2015).

4.1 Arctic

The distribution of the sea-ice concentration near 100% is shown for the Arctic for each product in Fig. 1~~3~~2 a) in form of the cumulative fraction of the deviation (bias) from 100% ~~as a colour coded vertical bar~~. As expected the cumulative fraction increases towards 1.0~~00%~~ for all products. ~~Distributions within the pair: SICCI-25km and OSI-450 as well as the pair: CBT-SSMI and CBT-AMSRE are quite similar, as expected; distributions of SICCI-12km and ASI-SSMI are similar particularly at the uppermost five to six bins. Apart from these similarities, c~~Considerable differences between the products are evident. Group I ~~EUMETSAT-OSISAF – ESA-CCI~~ products (see Table 2) exhibit a cumulative fraction between ~0.5 ~~(SICCI-50km)~~ and ~0.7 ~~(SICCI-12km) in the last bin but one, i.e.~~ in bin -1.5% … -0.5%. ~~Both CBT~~ Group II products~~,~~ and NT1-SSMI ~~and NOAA-CDR~~ exhibit ~~a~~ substantially lower ~~cumulative~~ fractions for this bin: between ~0.2 (NOAA-CDR, see also F_{99} in Fig. 3 c) and~~to~~ ~0.4 (NT1-SSMI). Consequently, the change in cumulative fraction to the last bin is between 0.6 and 0.8 for group II and NT1-SSMI but only between 0.3 and 0.5 for group I. The respective F_{99} values in Fig. 3 and App. H suggest that a large portion of the cumulative fraction in the last bin is in fact due to sea-ice concentrations > 100% being set to 100% (i.e. truncated). ~~The distributions for these products look like as if one has taken the distribution of, for instance, OSI-450 but deleted the fractions of (at least) bins -1.5% … -0.5% and -2.5% … -1.5% if not also -3.5% … -2.5%; the distributions look incomplete. ASI-SSMI and NT2-AMSRE exhibit a cumulative fraction of ~0.8 in the last but one bin. However, while the cumulative fraction increases slowly towards a value of 0.8 for ASI-SSMI, f~~For NT2-AMSRE, the cumulative fraction~~it~~ increases abruptly from < 0.1 in bin -2.5% … -1.5% to ~0.8 in bin -1.5% … -0.5%. This behaviour is completely different to all other products and confirms the results of Andersen et al. (2007) and Ivanova et al. (2015). For their inter-comparison of sea-ice concentration algorithms in the high Arctic, Andersen et al. (2007) extended the range within which the NT2 algorithm permits to retrieve the sea-ice concentration to 120%, in order to be able to properly compare all algorithms with respect to their precision close to 100%. The original implementation of the NT2 algorithm is constrained to sea-ice concentrations up to 100%. Ivanova et al. (2015) ~~They~~ also aimed to compare the precision of ~~existing~~several sea-ice concentration algorithms at 100% by means of computing the standard deviation of the sea-ice concentration at 100%. They were, however, unable to obtain standard deviations with a comparable statistics because of large positive biases for the, e.g., NT2 and ASI algorithms and because of the truncation of sea-ice concentrations at 100%. Only by constructing a reference sea-ice concentration of 75%, Ivanova et al. (2015) were able to carry out a comparison of the sea-ice concentration standard deviation based on non-truncated sea-ice concentrations.

These cumulative distributions suggest that an inter-comparison of the mean difference to 100%, i.e. the bias, and its standard deviation, i.e. the precision, should be carried out by means of the Gaussian fit proposed in Subsection 2.1.4 ~~and Fig. 3~~. Consequently, the mean sea-ice concentrations of the ten products shown by the black symbols in Fig. 1~~4~~3 a) for the Arctic near-100% reference sea-ice concentration locations are the modal values of the Gaussian fits. ~~and t~~The error bars denote one standard deviation of this fit around the modal value. The blue symbols and error bars denote the respective mean and one standard deviation computed from the non-truncated ~~EUMETSAT-OSISAF – ESA-CCI~~ group I sea-ice concentration products. All values shown here are summarized together with the results obtained from the truncated sea-ice concentration products in Table 3.

Figure 1~~3~~ a) confirms our hypothesis that those products where the cumulative distributions seem to contain a large fraction of sea-ice concentrations larger than 100% set to 100%~~be incomplete~~ (Fig. 1~~2~~ a), i.e. the group II~~two CBT~~ products, and NT1-SSMI ~~and NOAA CDR~~, are likely to over-estimate the actual sea-ice concentration. ~~These products reveal a modal sea-ice concentration > 100% according to the Gaussian fit applied; t~~The over-estimation is particularly high for NOAA-CDR with a modal sea-ice concentration of ~103% (see also Table 3). ~~Of t~~The group I~~EUMETSAT OSISAF – ESA CCI~~ products ~~SICCI-50km (99.5%), OSI-450 (99.0%), SICCI-25km and SICCI-12km, in this order,~~ exhibit modal sea-ice concentrations that are slightly below and closest to the near-100% reference. ~~Figure 13 a) illustrates that t~~The Gaussian fit almost perfectly matches the actually observed non-truncated sea-ice concentration for SICCI-50km also in terms of the standard deviation (compare blue and black symbols in Fig. 1~~3~~ a) and Table 3). The match is less accurate ~~good~~ for OSI-450 and SICCI-25km~~, where the mean observed sea-ice concentration falls below the fitted one by ~ 1%~~.

In addition, Fig. 1~~3~~ a) and Table 3 confirm our hypothesis that the group II~~two CBT~~ products~~,~~ and NT1-SSMI ~~and NOAA CDR,~~ are likely to have~~xhibit~~ a standard deviation that is lowered ~~considerably~~ by truncating sea-ice concentrations to a maximum of 100%. ~~All four products exhibit a standard deviation around the modal sea-ice concentration from the Gaussian fit of 4–5%, while the standard deviation computed from the truncated SICs is < 2% for the two CBT products and NOAA-CDR (Table 3). For~~ This is illustrated by the~~EUMETSAT OSISAF – ESA CCI products the~~ standard deviations of the non-truncated and the truncated sea-ice concentration for group I products ~~exceeds that of the truncated one systematically, as expected, by 0.4–0.6%~~ (Table 3). Under the assumption that the standard deviation of the Gaussian fit is a better measure of the spread in sea-ice concentrations near (but below) 100%, we state that the CDRs of group I: SICCI-50km, OSI-450, and SICCI-25km allow a better precision than group II products~~of ~ 2%, ~ 3%, and ~ 3%, respectively, while products such as NOAA CDR or the CBT products allow a precision of ~ 5% and ~ 3.5%, respectively~~. We also confirm the findings of Lavergne et al. (2019) that the ~~EUMETSAT OSISAF – ESA CCI~~ group I products are slightly – but significantly – biased low.

For ASI-SSMI and NT2-AMSRE, the application of a Gaussian fit is potentially not justified given the way sea-ice concentrations are retrieved. ASI-SSMI is non-linear near 100% (Kaleschke et al., 2001) while no statement about the functional relationship of the input satellite data and the retrieved sea-ice concentrations can be made for NT2-AMSRE (Markus and Cavalieri, 2000; Brucker et al., 2014). Our analysis, however, results in a reasonable Gaussian fit for ASI-SSMI ~~in terms of RMSD of the fitted histogram (0.0062) as well as values for F_{99}: 0.806 and ΔF_{99} (0.001)~~ (see App. H, Fig. H1 a). We are confident therefore that the values taken from the fit and shown in Fig. 1~~3~~ a) and Table 3 can be used. In contrast, the NT2-AMSRE sea-ice concentration distribution does not allow reasonable application of a Gaussian fit (see App. H, Fig H1 j) and we do not report it along with the others in Fig. 14 a). ~~and the respective values shown in Fig. 13 a) and Table 3 (and also Fig. 13 b) and Table 4) have to be interpreted carefully.~~ We note that Andersen et al. (2007) reported a mean NT2 sea-ice concentration of ~105% with a standard deviation of ~5% at near-100% sea-ice concentrations for their unconstrained version of this algorithm. ~~Note that the standard deviation of 1.7% provided in Table 3 for the Gaussian fit of NT2-AMSRE is actually a weighted mean RMSD obtained from an evaluation of NT2-AMSRE sea-ice concentration data against satellite Landsat and air-borne optical imagery (Cavalieri et al., 2006). The respective standard deviation of 3.2% provided in Table 4 is a weighted mean RMSD obtained from an evaluation of NT2-AMSRE sea-ice concentration data against satellite MODIS optical imagery (Cavalieri et al., 2010).~~

~~Finally, we remark that the results of this comparison are based on data from winter months (see Sect. 2.2). But also during winter temperatures can get close to 0°C which might influence the brightness temperatures used to compute the sea-ice concentration and which also questions the assumption of prevailing freezing conditions applied in the generation of the near-100% reference sea-ice concentration data set. By using the co-located air temperature from ERA-Interim reanalysis data included in the RRDP2 data set (Pedersen et al., 2019), we repeated our analysis for cases with air temperatures below -10°C. We find that biases between satellite and reference sea-ice concentrations change by less than 0.1% for all products except~~

~~NT1-SSMI for which we find a reduction in the bias by 0.3-0.4% when constraining the analysis to cold cases. The same finding applies to the Antarctic (see Sect. 4.2) where the reduction in the bias for NT1-SSMI is even higher: 0.6-0.7%.~~

4.2 Antarctic

The cumulative fraction of the deviation (bias) from 100% f~~F~~or the Antarctic (Fig. 13 b), we find more similarities in the cumulative fractions of the deviation from 100% ~~sea-ice concentration of the ten products is shown in Fig. 12 b). While we again observe considerable differences between the products, we find more similarities between products~~ than for the Arctic. Common to all products, ~~that show a gradual increase of the cumulative fraction, i.e. all products~~ except NT2-AMSRE and ASI-SSMI, is a notable step change in the cumulative fraction between ~~the last but one~~ bin ~~(~~-1.5% … -0.5%~~)~~ and the last bin~~, around 0%.~~ This step change is least pronounced for NT1-SSMI and most pronounced for NOAA-CDR exhibiting cumulative fractions of ~0.8 and ~0.4, respectively, in ~~at~~ the last ~~but one~~ bin ~~(see also F_{99} value in Fig. 3 f)~~. Step changes are~~seem~~ slightly larger for the two CBT products ~~with a cumulative fraction: 0.4-0.5 compared to~~ than for ~~the~~ group I~~EUMETSAT-OSISAF – ESA-CCI~~ products ~~with cumulative fractions of 0.5-0.6~~ (see also F_{99} values in Fig. 3 d), e)). ~~Again, as expected, CBT-SSMI and CBT-AMSRE are very similar as are SICCI-25km, OSI-450 and, this time also, SICCI-12km (compare with Fig. 12 a). The~~ For ASI-SSMI the cumulative fraction~~distribution of ASI-SSMI sea-ice concentration biases seems to~~ level~~s~~ off before the last bins (see~~which is~~ also ~~confirmed by a~~the F_{99} value ~~of the Gaussian fit of 0.93 (see~~ App. H, Fig. H2 a)~~., indicating that~~ 93% of the ASI-SSMI sea-ice concentrations at the near-100% reference sea-ice concentration locations are below 99.5%. ~~Similar to the Arctic, t~~The distribution for NT2-AMSRE is extremely narrow~~.; only the last two bins are occupied with the last but one bin exhibiting a cumulative fraction of ~0.25, suggesting that~~ About 75% of the NT2-AMSRE sea-ice concentrations at the near-100% reference sea-ice concentration locations are above 99.5%. This behaviour is, like ~~in~~for the Arctic, completely different to all other products and agrees with~~echo~~ the findings of Ivanova et al. (2015), see also our discussion in Sect. 4.1.

~~Figure 13 b) and Table 4 illustrate that, when using the Gaussian fit as a measure, all~~ Group I and II products ~~except ASI-SSMI, NT1-SSMI and NT2-AMSRE~~ provide a modal sea-ice concentration which deviates by less than ~1% from 100% (Fig. 14 b), Table 4). While group II ~~the two CBT~~ products ~~and NOAA-CDR~~ tend to exhibit~~have~~ a modal sea-ice concentration > 100%, ~~all EUMETSAT-OSISAF – ESA-CCI~~ group I products ~~have~~exhibit modal sea-ice concentrations < 100%. ~~NT1-SSMI and ASI-SSMI both under-estimate the near-100% reference sea-ice concentration by ~5%. We find that the m~~Modal sea-ice concentration~~s~~ obtained with the Gaussian fit agree~~s~~ within 0.5% to the actually measured mean sea-ice concentration derived from the non-truncated values of group I~~the EUMETSAT-OSISAF – ESA-CCI~~ products (compare black and blue symbols in Fig. 1~~4~~3 b). ~~In addition, the r~~Respective standard deviations match better in the Antarctic than the Arctic and are systematically smaller for the truncated than the non-truncated results (compare black and blue bars Fig. 1~~4~~3 a) and b) as well as Table 3 and 4). ~~Like in the Arctic, using the non-truncated EUMETSAT-OSISAF – ESA-CCI products results in a systematically larger standard deviation, as expected, by 0.5 to 1.0% (Table 4), than obtained with the truncated products. We can confirm the notion from Sect. 4.1 that application of the Gaussian fit results in a larger standard deviation~~ f~~F~~or group II~~the two CBT~~ products ~~and NOAA-CDR. U~~using the the Gaussian fit method suggests~~truncated products results in a~~ standard deviations between ~4.5% and ~5.5% while using the truncated values results in a standard deviation between 2.0% and 2.5% ~~while the Gaussian fit suggests standard deviations of ~4.5% for CBT-SSMI and NOAA-CDR and ~5.5% for CBT-AMSRE~~. Following our assumption in Sect. 4.1, we state ~~Therefore, again under the assumption that the standard deviations obtained from the Gaussian fit of the sea-ice concentration distribution at the near-100% reference sea-ice concentration locations is a reasonable measure for the spread of the concentration values, we find highest~~ a better precision for group I products: SICCI-50km, SICCI-25km, and OSI-450 than group II products ~~with standard deviations of 2.5%, 3.0% and 3.0%, respectively. For CBT-SSMI, NOAA-CDR, and CBT-AMSRE we find a lower precision with standard deviations of ~4.5%, 4.5%, and 5.5%, respectively~~. Similarly

but to a lesser extent than in the Arctic, ~~the EUMETSAT OSISAF – ESA CCI~~ group I products are slightly biased low with respect to the validation data set.

4.3 Summary and discussion of the evaluation near 100%

In near-100% sea-ice concentration conditions, most retrieval algorithms will naturally retrieve some~~bell shaped~~ distribution of values ~~, returning values both below and above~~around 100% sea-ice concentration, i.e. also values > 100%. However, these ~~above 100%~~ values are almost never accessible to the user, and thus generally not accessible for validation. Here, we used the availability of these "off-range" estimates in the group I~~four EUMETSAT OSISAF – ESA CCI~~ products to demonstrate how the entire~~"off range"~~ distribution around 100% can effectively be reconstructed a-posteriori from the products with truncated sea-ice concentration distributions (Fig. 3, App. H). This Gaussian-fit methodology allows us to go deeper in the analysis of near-100% conditions. Indeed, if the analysis had been limited to the truncated distributions only (~~shown in~~ Fig. 13~~2~~), algorithms that over-estimate sea-ice concentration (modal value of the non-truncated distribution larger than 100%) would obtain better validation statistics (smaller bias and RMSE) than products without such ~~no~~ over-estimation ~~(modal value of the non-truncated distribution exactly at 100%)~~. The larger the over-estimation, the better the statistics would be. Using the Gaussian fit, we unveil a possible over-estimation of several sea-ice concentration products, including NT1-SSMI, CBT-SSMI, and NOAA-CDR in the Arctic, and NOAA-CDR (but only slightly) in the Antarctic ~~sea ice conditions~~. This Gaussian-fit methodology also confirms that group I~~the EUMETSAT OSISAF – ESA CCI~~ products are slightly low biased in the Arctic (~~as already documented by~~see Lavergne et al., 2019). The worst of these biases we find in the Arctic for SICCI-12km that was not openly distributed at the end of the ESA CCI Sea Ice Phase 2 project, partly based on these results.

Our results suggest that group I products, i.e., the three CDRs OSI-450, SICCI-25km and SICCI-50km, are more accurate and have a higher precision than the fourth CDR investigated: NOAA-CDR; this applies to both hemispheres. Group I products can be regarded as being superior, in terms of the precision and accuracy, to NT1-SSMI and CBT-SSMI as well. Our results furthermore confirm earlier work (Andersen et al., 2007; Ivanova et al., 2015) that the accuracy of NT2-algorithm products near 100% cannot be quantitatively assessed. We hypothesize that this is merely caused by the fact that sea-ice concentrations are constrained to a maximum of 100% by the algorithm concept. This is fundamentally different to the other nine products investigated. In the iterative retrieval used in the NT2 algorithm, sea-ice concentrations are only allowed to converge at 100% from one side, i.e. < 100% - in contrast to other iterative algorithms such as, e.g., the polynya signature simulation method (PSSM) (Markus and Burns, 1995). Another element of the NT2-algorithm, which complicates quantitative assessment of the accuracy near 100% sea-ice concentration, is the usage of model atmospheres to create look-up tables from which the sea-ice concentration is retrieved. This approach likely reduces the natural variability of the obtained sea-ice concentration. We refer to Brucker et al. [2014] for more details of NT2-algorithm sea-ice concentration uncertainty.

The results of the comparison in Sect. 4.1 and 4.2 are based on winter data (see Sect. 2.2). But also during winter temperatures can get close to 0°C influencing the brightness temperatures used to compute the sea-ice concentration and questioning the assumption of freezing conditions for generation of the near-100% reference sea-ice concentration data set. By using the co-located air temperature from ERA-Interim reanalysis data included in the RRDP2 data set (Pedersen et al., 2019), we repeated the analyses for cold cases, i.e., air temperatures below -10°C. We find that biases between satellite and reference sea-ice concentrations change by less than 0.1% for all products except NT1-SSMI. For NT1-SSMI constraining the analyses to cold cases yields a bias reduction by ~0.4% for the Arctic and ~0.7% for the Antarctic, indicating that this particular algorithm is more sensitive than others to variability of air temerature.

5 Comparison with ship-based visual sea-ice cover observations

In this section, we present the results of the evaluation of the ten products at intermediate sea-ice concentrations by means of an inter-comparison to the visual ship-based observations described in Sect. 2.3. ~~Like in Sect. 4 we show the results separately for the Arctic (Sect. 5.1) and the Antarctic (Sect. 5.2).~~

Upfront we note the limitations of the manual ship-based visual sea-ice cover observations used here. They were collected by a myriad of different observers with different levels of experience for this task. For an untrained observer it is relatively straightforward to estimate the total sea-ice concentration for closed ice conditions, i.e. > 80%, or very open ice conditions, i.e. < 30%. It is more difficult, however, to estimate whether sea ice covers, e.g. 40% or 50% of the 1 km radius area around the ship. Therefore, we can expect a reduced accuracy for ship-observations of the intermediate sea-ice concentration range from ~30% to ~ 80%. At the same time, this is possibly the sea-ice concentration range where the different spatial scales of the two kind of observations compared here have the largest impact on the results. Note that Worby and Comiso [2004] reported an uncertainty estimate between 5% and 10% for the total sea-ice concentration based on observations of the same scene by different observers. To the best knowledge of the authors, papers about a better quantification of the accuracy of these observations have not been published since then.

In addition, ship observations were collected under different weather and daylight conditions as well as during ship transits with different ~~ship~~ speeds. The first two points influence the visibility and change the visual appearance of sea ice and openings, and can result in a larger spread of an observed sea-ice concentration value around the actual value. Different weather conditions also have an influence on the size of the area actually observed around the ship that is difficult to quantify. This observation area is supposed to be of one kilometre radius but it can be assumed that it is smaller in case of poor visibility than it is in case of clear-sky, good visibility conditions; visibility is not regularly reported along with the ice observations. A single observation of the sea-ice conditions takes a certain amount~~period~~ of time~~. The duration of this period,~~ which is a function of the experience of the observer. The observation area around the ship's~~²~~ track represented by a single observation is hence a function of the ships' speed and of the experience of the observer. As long as ice conditions do not change for a few kilometres this does not matter but in highly heterogeneous ice conditions, this can be important. Therefore, there is a variable representativity of the observed sea-ice conditions around and along the ship's~~²~~ track (see Sect. 6.1.4).

Ships often tend to avoid thick and deformed sea ice and ship-track forecasts are often optimized accordingly (e.g. [Pizzolato et al., 2016; Kuuliala et al., 2017]). Ship-based observations therefore often represent the thinner ice categories and/or conditions encountered in leads or openings. These are frozen over with sea ice in winter but are open water in summer. Therefore, particularly during summer or episodes of warmer weather, the sea-ice concentrations from the small scale ship-based observations are likely lower than from the larger scale satellite microwave radiometry. According to Ivanova et al. (2015), microwave radiometry tends to underestimate sea-ice concentrations over very thin (< 15 cm) ice. This suggests that during winter, sea-ice concentrations from ship-based observations could be, contrary to summer, slightly higher than from satellite microwave radiometry.

A systematic ~~investigation that allows~~ quantification of the uncertainty in ship-based sea-ice observations has not been carried out yet and is beyond our scope. Even though we do not use single ship-based observations but follow Beitsch et al. (2015) and average over all ship-based sea-ice observations along the ship's~~²~~ track of one day, discarding days with less than three observations (see Sect. 2.3), we cannot rule out~~exclude~~ that some of these daily average observations are biased because of the reasons discussed above.

5.1 Arctic

~~The first question to answer is how the two sorts of observational data (ship and satellite) are distributed over the sea-ice concentration range from 0% to 100%. This is illustrated in Fig. 14 in the form of histograms showing the number of sea-ice concentration data falling into bins as described in Sect. 2.3. We find relatively few observations, in total less than 60 daily~~

~~average along track mean sea ice concentration values, for bins < 55% sea ice concentration. This applies to both ship and satellite observations, with the exception of NT1 SSMI (Fig. 14 a) with ~130 sea ice concentration values in these lower concentration bins. Between 40 and 60 ship observations fall into each of the bins centred at 60% to 80%. The majority of the ship observations fall into the two bins with highest sea ice concentrations: 110 into bin 85 95% and 125 into bin 95 100%. The products NT1 SSMI, OSI 450, SICCI 25km, and SICCI 50km (Fig. 14 a, e, g and h) exhibit the largest number of observations in bin 85 95%. All other products exhibit the largest number of observations in bin 95 100% (Fig. 14 b, c, d, f, i and j). Differences in the occupation of the two high concentration bins are large for, e.g., NT2 AMSRE (Fig. 14 i): 95 and CBT SSMI (Fig. 14 b): 130 while for EUMETSAT OSISAF ESA CCI products and ASI SSMI, values distribute relatively evenly into the two high concentration bins.~~

Overall, for the Arctic, all ten products compare reasonably well to the ship-based observations (Fig. 15, Table 5). ~~However, the daily average along track mean sea ice concentrations scatter substantially around the diagonal.~~ At high concentrations (> ~80%), group I products~~EUMETSAT OSISAF ESA CCI~~ and ASI-SSMI ~~products~~ (Fig. 15 d to h) exhibit the most symmetric distributions around the identity line~~diagonal~~. NT1-SSMI (Fig. 15 a) ~~has~~shows an asymmetric distribution with a considerable fraction of satellite sea-ice concentrations even below~~<~~ 60%, translating into a difference between satellite- and ship-based sea-ice concentrations of up to 40%. Group II and IV~~Both other AMSRE~~ products~~: CBT and NT2~~ (Fig. 15 b, c, i, j)~~, and the two remaining SSM/I products: CBT SSMI and NOAA CDR (Fig. 15 b, e),~~ show an asymmetric distribution with more high satellite-based than high ship-based sea-ice concentrations. ~~For m~~Most products have~~, substantially~~ more data pairs ~~are situated~~ below the identity line~~diagonal~~, i.e.,~~suggesting that~~ satellite-based are smaller than ship-based sea-ice concentrations~~. This i~~as illustrated by a negative overall bias and regression lines located below the identity~~1 to 1 fit~~ line for six of the ten products (~~see~~ Table 5). Group II and IV~~CBT AMSRE, NT2 AMSRE, CBT SSMI, and NOAA CDR~~ products provide the smallest absolute overall bias of < 1%. Biases are larger for group I but at the same time the standard deviation of the difference (SDEV) is smallest for group I products. Highest correlations are obtained for CBT-AMSRE and group I products, except OSI-450. Best linear fits, i.e. slopes closest to the identity line, we find, however, for~~, but while~~ CBT-SSMI and NOAA-CDR ~~are the two products with slopes of the linear regression being closest to 1: 0.994 and 0.998, respectively, CBT AMSRE and NT2 AMSRE are the two products with such slopes deviating most from 1: 1.063 and 1.061, respectively. The three ESA CCI products provide together with CBT AMSRE the highest squared linear correlation: 0.775 (SICCI 50km) to 0.784 (SICCI 12km).~~

~~In Fig. 15, several of the products exhibit points along the y=0% sea ice concentration line, i.e. conditions where sea ice cover is reported by the ship based estimate while the satellite estimates exactly 0%. This applies most to CBT SSMI, NOAA CDR, ASI SSMI, and CBT AMSRE (Fig 15 b, e, d and j). These points with zero daily mean sea ice concentration are very likely the result of the weather filters applied (Sect. 2.1.3), which besides removing false sea ice caused by atmospheric effects, also removes true sea ice (Ivanova et al., 2015; Lavergne et al., 2019). The combination of explicit atmospheric correction and dynamic tuning of the weather filter in the EUMETSAT OSISAF ESA CCI products seems to reduce the occurrence of such cases (Fig. 15 e, f and g) notably. Also NT1 SSMI (Fig. 15 a) and NT2 AMSRE (Fig. 15 i) exhibit a comparably small number of satellite sea ice concentration at exactly 0% at non zero ship based concentrations. These observations agree well with the results shown in Fig. 1 except for ASI SSMI.~~

~~Now we briefly compare the results obtained for the~~ How do results of the entire year compare to~~with~~ those obtained separately for winter or summer months (see Fig. 5 for differences in the location of the ship-based observations)?~~.~~ ~~For winter (highest correlation is obtained for SICCI 50km: $R^2 = 0.606$) f~~For all products, the correlation~~R^2~~ is lower in winter than~~while for~~ summer and the entire year. ~~(highest correlation is obtained for SICCI 12km: $R^2 = 0.784$) R^2 is a little higher than for the entire year. For winter,~~ T~~t~~his can be explained by fewer observations during winter in general and by substantially ~~less~~fewer low sea-ice concentrations ~~values at lower concentrations~~; most observations during winter are > 75%. Except for ASI-SSMI, the differences in the bias between summer, winter and the entire year are small (~~The bias changes mostly by~~ mostly <~~less~~

than 1%). All products except SICCI-12km and ASI-SSMI provide a lower SDEV in winter than summer. Compared to the other groups, group I exhibits smallest SDEV in summer while group II does so in winter. between summer, winter and the entire year. ASI-SSMI provides the by far largest change in bias between winter and summer: 4.9%, while OSI-450 stands out with anthe smallest inter-seasonal bias change of only ~0.1% in bias and SDEV of only ~0.1% (Table 5, see also Sect. 6.1.4). Almost all products provide a lower standard deviation (SDEV) for winter than summer, except SICCI-12km and ASI-SSMI. For winter, CBT-SSMI has the smallest SDEV: 10.9% while NOAA-CDR, SICCI-25km and SICCI-50km are slightly higher: ~11.7%. For summer, EUMETSAT-OSISAF – ESA-CCI products provide the smallest SDEV: 11.7% to 12.9%. Again, OSI-450 stands out with an inter-seasonal SDEV change of only ~0.1%, followed by SICCI-25km and CBT-AMSRE with a value of 0.5%; CBT-SSMI provides the largest such change: 3.6%.

Binning the sea-ice concentrations of one data set, e.g. ship observations, into 10% wide bins and computing the mean sea-ice concentration of the other data set, e.g. here satellite observations, results in the red symbols in Fig. 15; doing the same but exchanging ship- and satellite observations in the blue symbols in Fig. 15. The motivation for such a step We want to better visualize the average distribution of the two data sets and investigate the partitioning of the data into sea-ice concentration bins of 10% width - comes from the notion in Sect. 2.3 that the average accuracy of the ship-based sea-ice concentration observations is 10%. For this purpose we bin sea-ice concentrations of one data set, e.g. ship observations, into 10% wide bins and compute the mean sea-ice concentration of the other data set (Fig. 15, red symbols) and vice versa (blue symbols). The binned values and associated regression lines illustrate even better the above-mentioned asymmetry in the distribution of the data pairs. For instance, NT1-SSMI (Fig. 15 a) sea-ice concentrations range between 60% and 100% over a ship-based observations range of 80 to 100%. Consequently, the average NT1-SSMI sea-ice concentration for ship-observation bin 95%-100% is ~85% (uppermost red triangle), while the average ship-based sea-ice concentration for NT1-SSMI bin 95%-100% is ~95% (uppermost blue square). For two equally well-distributed data sets, one would expect that red and blue symbols and regression lines are close to each other. This is not the case and we refer to Sect. 6.1.4 for more discussion of this issue.

From these binned values and associated regression lines we find: 1) Ship-based observations in the range 50% to 80% are under-estimated by the satellite-based ones, particularly by the EUMETSAT-OSISAF – ESA-CCI products as illustrated in Fig. 15 e to h): a mean satellite sea-ice concentration of 55% compares to a ship-based sea-ice concentration of 70%. The only product where this is even worse is NT1-SSMI (Fig. 15 a). 2) Red regression line slopes of ESA-CCI products are closer to 1 than the black ones. For most of the other products – except CBT-SSMI and NOAA-CDR – red regression line slopes deviate more from 1 than the black ones.

5.2 Antarctic

In the Antarctic, we have a larger relative fraction of ship observations at lower concentrations <50%: ~ 90 values. Between 25 and 55 values fall into bins 60% to 80%. Bin 85% to 95% is the bin with the highest count of ship observations: ~100 while bin 95% to 100% contains ~70 ship observations. We find a similar distribution over the different sea-ice concentration bins for all ESA-CCI products (Fig. 16 f, g and h), ASI-SSMI (Fig. 16 d) and OSI-450 (Fig. 16 e). All these products share a maximum count in bin 85% to 95% and agree with the ship observations count of most other bins within 10 counts. An exception is bin 45% to 55% with considerably more ship than satellite observations. All other products either have the highest count in bin 95% to 100%, especially NT2-AMSRE (Fig. 16 i), or have a similarly large count for bin 85% to 95% and bin 75% to 85%: ~80, but a count almost as low as 10 for bin 95% to 100% (NT1-SSMI, Fig. 16 a). We note that all products have larger counts at sea-ice concentrations < 25% than the ship observations.

The scatterplots of the daily average along-track mean sea-ice concentrations for the Antarctic (Fig. 167) reveal, for sea-ice concentrations > ~80%, mostly symmetric distributions for seven of the ten products.; only CBT-AMSRE, and particularly NT1-SSMI and NT2-AMSRE have asymmetric distributions here (Fig 17 j, and a, i). Like in the Arctic, NT1-SSMI has considerably more low than high sea-ice concentration values (compare Fig. 15 a). NT2-AMSRE haexhibits almost

no data points below the identity~~1-to-1 fit~~ line at > ~80% with data pairs concentrated at 100% satellite sea-ice concentration. ~~While the sea-ice concentrations distribute symmetric around the 1-to-1 line for most products until about 50%, there is a~~A considerable drop in the count of data values above the identity~~1-to-1~~ line at lower concentrations results in a highly ~~and the distribution becomes~~ asymmetric distribution at concentrations below ~50%. ~~This agrees with Fig. 16 showing a general lack of ship-based sea-ice concentrations < ~ 20%. Not surprisingly we find the lowest overall biases (see Table 6) for those products that exhibit more satellite- than ship-based high sea-ice concentrations and, at the same time, less satellite- than ship-based low sea-ice concentrations, i.e.~~ Group II products have the lowest overall biases (Table 6) but slopes of the linear regression are considerably steeper than the identity line (Fig. 16 b, c, j) in contrast to group III products (Fig. 16 a, d) and OSI-450 (Fig. 16 e)~~CBT-SSMI, CBT-AMSRE and NOAA-CDR with biases between -1.4% and -2.3%~~. We find the largest bias for NT1-SSMI: -11.0%. NT2-AMSRE shows~~is the only product with~~ a considerable positive bias: +4.5%. ~~NT1-SSMI, ASI-SSMI, and OSI-450 all provide slopes of the linear regression close to 1: 0.993, 0.993, and 1.010, respectively. Slopes for CBT-SSMI, NOAA-CDR and CBT-AMSRE increasingly deviate from 1: 1.057, 1.082, and 1.126, respectively.~~ Highest correlations between ship- and satellite-based observations we find for group I products and CBT-AMSRE, lowest SDEV values for group I products as well. ~~The highest overall linear correlation is obtained for SICCI-12km, followed by CBT-AMSRE and the other EUMETSAT-OSISAF – ESA-CCI products. These provide the lowest SDEV values ranging between 13.4% and 14.0% (Table 6), followed by NT1-SSMI and CBT-AMSRE with 14.8%. As is the case in the Arctic, all products but the EUMETSAT-OSISAF – ESA-CCI ones exhibit data pairs along the y=0% axis, associated with removal of true sea-ice concentration by a weather filter.~~

In contrast to the Arctic, correlations between ship- and satellite-based sea-ice concentrations are smaller in summer than winter when correlations are even higher than for the entire year for most products (Table 6) ~~A comparison between the results of the entire year with those obtained separately for winter and summer (see Fig. 5 for difference in locations) reveals differences to the Arctic. For winter (highest correlation is obtained for SICCI-12km and SICCI-25km: $R^2 = 0.771$) R^2 increases for most products compared to the entire year while for summer all products exhibit a smaller R^2 value (highest correlation is obtained for SICCI-12km: $R^2 = 0.698$).~~ For all products, except group III~~ASI-SSMI and NT1-SSMI~~, biases are smaller in winter than summer by mostly < 2%. NT2-AMRE is the only product with a positive bias in both seasons. The largest inter-seasonal bias change we find~~is obtained~~ for CBT-AMSRE: 2.7% and SICCI-25km: 2.9%, respectively, the smallest for CBT-SSMI: 0.4%. For all products, the SDEV is smaller by 3-5% (larger by 2-3%) compared to the entire year in winter (in summer)~~while for summer, SDEV values are larger by 2-3%~~. Inter-seasonal SDEV changes are hence considerably larger in the Antarctic than in~~for~~ the Arctic ~~with smallest values of 4.9% and 5.1% for NT1-SSMI and OSI-450, respectively, and largest value of 9.3% for NT2-AMSRE~~ (compare Tables 5 and 6).

Binning the sea-ice concentrations like described in Sect. 5.1 (red and blue symbols in Fig. 16~~7~~) leads to the following main observations. 1) All products – except NT1-SSMI and NT2-AMSRE – have the best agreement with ship-based observations in the sea-ice concentration range 60% to 80%. 2) All products under-estimate ship-based sea-ice concentrations for concentrations < ~50%. 3) The negative bias of ~10% observed for NT1-SSMI applies to the entire sea-ice concentration range. 4) NT2-AMSRE is the only product over-estimating ship-based sea-ice concentrations considerably; this over-estimation reaches 10% for the range 60% to 80%. Apart from that we find, like for the Arctic, that blue regression lines exhibit a considerably steeper slope than the red ones, suggesting that also in the Antarctic the distribution of the data over the range 0 to 100% is asymmetric (see Sect. 6.1.4).~~Regression lines based on these binned data (red lines in Fig. 17) have a similar or slightly steeper slope than those based on the un-binned data (black lines). Applying the binning to the satellite sea-ice concentration (blue symbols in Fig. 17) results in a distribution of the data pairs which without exception – as for the Arctic – yields substantially steeper regression lines, underpinning the over-estimation of the ship-based observations particularly at low concentrations.~~

5.3 Summary and discussion of comparison against ship-based observations

Group II products provide the smallest overall difference to the ship-based observations: around 0% (Arctic) and around -2% (Antarctic). Group I products provide differences around -7.5% (Arctic) and -3.5% (Antarctic). Group I and II products share similar average correlations (R^2) in the Arctic: 0.77 and 0.76, and in the Antarctic: 0.74 and 0.72, respectively. Standard deviations for group I products are smaller – by 1% in the Arctic and by 2% in the Antarctic – than for group II products. On average, these results are better than those obtained for group III and IV products. We refrain from giving a ranking or recommendation as to which product is the best when compared to ship-based observations.

We find the lowest correlation for ASI-SSMI (group III)~~ASI-SSMI provides the smallest values for R^2~~ in both hemispheres. However, it is the product with the largest~~ASI-SSMI reveals a substantially~~ improvement in the inter-comparison results between winter and summer in the Arctic: correlation increases, difference and standard deviation decrease. This could be attributed to the higher fraction of inter-mediate sea-ice concentrations during summer for which the comparably fine grid resolution of 12.5 km of the ASI-SSMI product could be of advantage. There is evidence that this behaviour is coupled to the usage of the near 90 GHz channels because we observed a similar, albeit less pronounced behaviour for SICCI-12km, which also employs near 90 GHz data and is provided at 12.5 km grid resolution (Table 2)~~While an increase of the correlation between winter and summer is observed also for all other products, such a notable decrease in difference and standard deviation is not – except for SICCI-12km. This product is also provided at 12.5 km grid resolution but in contrast to ASI-SSMI combines brightness temperatures at two different frequencies and hence different native resolutions (see Table 2)~~. Because in the Antarctic the sea-ice cover is more open year round~~also during winter~~ it is plausible that we did not find similar behaviour there for these two products~~uch an improvement in inter-comparison results between winter and summer is lacking there~~.

There are a few points to discuss. First of all, Fig.~~ure~~ 145 and Fig. 16~~through Fig. 17~~ reveal quite a high relative occurrence~~fraction~~ of sea-ice concentrations in the range 95% to 100%. This might have biased ~~the~~our results. We therefore repeated our comparison by discarding all data pairs with daily mean sea-ice concentrations > 95%. Main results (not shown) are an overall increase in the differences by about 2% and of the standard deviations by ~ 1% (group I) and 2-3% (group II) and a reduction of the correlation by ~0.08. Ranking between groups are otherwise not changed. ~~This results in R^2 of 0.68 versus 0.63 (Arctic) and 0.67 versus 0.63 (Antarctic) for group I and II, respectively, and in standard deviations of 13.8% versus 16.3% (Arctic) and 14.9% versus 18.0% (Antarctic). While group I exhibits larger differences than group II, inter-comparison results are better for group I than group II otherwise.~~ Secondly, the results obtained for group I products ~~The comparison to the ship based observations presented in Sect. 5 are~~is carried out using based on the truncated ~~EUMETSAT OSISAF – ESA CCI~~ sea-ice concentrations~~ data~~. Using the non-truncated ~~EUMETSAT OSISAF – ESA CCI products~~ data does not considerably change our findings (not shown). Differences~~Differences~~ between satellite-based and ship-based sea-ice concentrations ~~reduce~~decrease by between 0 and 0.3% with a concomitant increase in the standard deviation of up to 0.2% ~~(see Fig. 15 and Fig. 17, and Tables 5 and 6)~~; this applies primarily to winter when the fraction of near ~100% sea-ice concentrations is large. Thirdly, ~~While~~ application of the Gaussian-fit method (see Sect. 2.1.4 and Sect. 6.1.3) seems not appropriate given the ~~wide~~ sea-ice concentration range considered in this inter-comparison~~,~~. Even if it would be, we can~~it is reasonable to~~ assume that ~~it would change the~~ differences and ~~(~~standard deviations~~) found for all~~ obtained for the other products would change by less than one percent. ~~up to a few tenth of a percent (some tenths of a percent). However,~~ All these changes would be small compared to the accuracy of the ship-based sea-ice concentrations (see Sect. 2.3, ~~and~~ beginning of Sect. 5, and Sect. 6.1.4).

In Fig. 15 and Fig. 16, several of the products exhibit points along the y=0% sea-ice concentration line, i.e. conditions where sea- ice ~~cover~~ is reported by the ship~~-based estimate~~ while the satellite estimates exactly 0%. This applies most to group II products and~~CBT-SSMI, NOAA-CDR,~~ ASI-SSMI~~, and CBT-AMSRE~~ (Fig 15 b, c, d and j). These points with zero daily mean sea-ice concentration are very likely the result of the weather filters applied (Sect. 2.1.3), which besides removing false sea ice caused by atmospheric effects, also removes true sea ice (Ivanova et al., 2015; Lavergne et al., 2019). The combination

of explicit atmospheric correction and dynamic tuning of the weather filter in the group I EUMETSAT OSISAF – ESA CCI products seems to reduce the occurrence of such cases notable (Fig. 15 e, f and g); Fig. 16 e, f, and g) notably. Also NT1 SSMI (Fig. 15 a) and NT2 AMSRE (Fig. 15 i) exhibit a comparably small number of satellite sea ice concentration at exactly 0% at non zero ship based concentrations. These observations agree well with the results shown in Fig. 1 – except for ASI SSMI.

6 Discussion, Outlook and Conclusions

6.1 Discussion

In this paper, we assessed the quality of sea ice concentration of the EUMETSAT OSISAF – ESA CCI products against other sea-ice concentration products and independent data sets. These data sets are: 1) A near-100% reference sea-ice concentration data set based on the analysis of regions with convergent sea ice motion in high concentration sea ice during winter based on SAR imagery (Sect. 2.2 and Sect. 4), and 2) quality controlled compilations of about 15 000 individual visual ship based observations of the sea ice cover (Sect. 2.3 and Sect. 5). The first part of the assessment we carried out without additional data by showing and discussing time-series of sea-ice area (SIA) and extent (SIE) as well as difference between the sea ice concentrations of all ten products (Sect. 3).

6.1.1 Observed differences in sea-ice area and extent

Time series of SIA and SIE have since long been used to derive conclusions about the past development of the sea-ice cover and to even extrapolate its future development. In order to do so, such time series need to be sufficiently long, consistent and accurate. A long, consistent time-series is typically obtained using a fundamental climate data record of brightness temperatures as input for the retrieval, as is done, e.g., for group I product OSI-450, to ensure that inter-sensor differences are as small as possible. Our paper suggests that additional steps might be required, for instance, dynamic retrieval of tie points and dynamic adaptation of weather filters (see Sect. 6.1.2) to reach the goal of a long-term consistent sea-ice concentration data set to be used to compute long-term consistent time-series of SIA and SIE.

Recently, Meier and Steward (2019) suggested a method to obtain an estimate of SIE and NSIDC sea-ice index accuracy, which they found to be ~50 000 km² under certain circumstances for the Arctic. They also pointed out, however, that there is a clear bias (or spread) of 500 000 km² to 1 million km² between SIE estimates from different products (see also Ivanova et al., 2014). Therefore, as long as one does not know which product provides the best representation of the actual sea-ice cover, one is left alone with a relatively precise estimate of the SIE, which might likely be biased, however, by an amount an order of magnitude larger. Considerable spreads between products are also visible in our Fig 6 and Fig. 8, especially for SIA, which we think is the parameter suited better to describe state and variability of the polar sea ice covers. Notz (2014) found that the SIE and its trend provide a limited metric for the performance of numerical models. Petty et al. (2018) suggested that predictions of the September Arctic sea-ice minimum in area and extent would benefit from giving more weight to SIA. Niederdrenk and Notz (2018) concluded that observational uncertainty is the main source of uncertainty for estimating at which level of global warming the Arctic will lose its summer sea-ice cover. In the light of these findings, the inter-product differences in SIA and SIE resulting from our study provide useful information about which algorithm or group of algorithms is particularly well suited for investigations of SIA and SIE in both or just one hemispheres year-round or just a season. Because we were able to estimate the effect of the mis-match between true and grid resolution and of the pole-hole interpolation in the Arctic and could further rule out influences of different land-masks, we are confident that the inter-product differences observed are mostly originating from differences in how the algorithms can handle surface emissivity variations or variations in the atmospheric influence. we suggest putting emphasis on discussing inter product biases in SIE and especially SIA is warranted in the context of this paper about sea-ice concentration product evaluation.

The inter-annual variability of the ten products' SIA and SIE is very similar (Fig. 6 and Fig. 8) while differences in sea-ice concentration between the products can be substantial (Fig. 7, Fig. 9 through Fig. 11). Extensive filtering of potential coastal artifacts in the sea ice concentration can cause a particularly large difference in SIA and SIE between SICCI-50km, and the three other EUMETSAT OSISAF – ESA CCI products (see Fig. 7 and Fig. 10). A difference in SIA can often be explained with a difference in sea ice concentration retrieved by a particularly algorithm. A difference in SIE is, however, independent of the actual sea ice concentration as long as it is above 15%. The observed differences in SIE (Fig. 6 c, d) and Fig. 8 c, d) therefore potentially result from different sea ice concentrations in the marginal ice zone / along the ice edge, from differences in correction of the land spill-over effect (coastal correction henceforth), from differences in the weather filter, or from differences in the land cover fraction.

In the matrices showing the differences between SIA and SIE for all ten products for the AMSR-E period (Fig. 11, middle and right column), the influence of the different land cover fractions has been mitigated. We first discuss the Arctic. For SIA, EUMETSAT OSISAF – ESA CCI (group I) products agree with each other within ~ ±100 000 km² in March and September (Fig. 11 b, e). This is an important result taking into account that within this group data of different satellite sensors are used (SICCI-2: AMSR-E; OSI-450: SSM/I, SSMIS). The same applies to group II, i.e. CBT-SSMI, NOAA CDR, CBT-AMSRE, and NT2-AMSRE in September but not in March, when within group II SIA based on SSM/I-SSMIS data agrees to SIA based on AMSR-E data only within ~ ±300 000 km². In March, NT1-SSMI and ASI-SSMI (group III) stand out with a ~400 000 km² to ~800 000 km² smaller SIA than all other products. In September, only NT1-SSMI stands out with SIA differences to all other products similar to those in March. For SIE, the majority of all products agrees with each other within ~ ±200 000 km² (~ 4-5% of mean SIE) in September (Fig. 11 f); larger differences only occur between NT1-SSMI and OSI-450, CBT-SSMI or NOAA-CDR. In March, OSI-450, SICCI-12km, SICCI-25km, CBT-SSMI and NOAA-CDR exceed three to five of the other products by ≥ ~ 300 000 km², and only half of the products agree with each other within ~ ±200 000 km² (Fig. 11 e).

In the Antarctic (Fig. 11 h, i, k and l), EUMETSAT OSISAF – ESA CCI (group I) SIA values agree with each other within ~ ±200 000 km² in September and February (Fig. 11 h, i). For September (Fig. 11 h), NT1-SSMI and NT2-AMSRE stand out. NT1-SSMI SIA is smaller than all other products by between ~1.4 million km² (ASI-SSMI) and ~2.8 million km² (NT2-AMSRE). This confirms the documented under estimation of Antarctic sea ice concentration by the NASA Team algorithm during that time of the year (e.g., Comiso et al., 1997). In contrast, NT2-AMSRE SIA is larger than all other products by ~0.6 million km² (CBT-AMSRE) and ~2.8 million km² (NT1-SSMI). CBT-AMSRE SIA is larger than all other products (except NT2-AMSRE) while ASI-SSMI SIA is smaller than all other products (except NT2-AMSRE). For February (Fig. 11 k) inter-product SIA differences are overall small except for NT2-AMSRE, which exceeds all other products by ~300 000 km² (~15%) or more. For SIE, inter-product differences are much smaller than for SIA in September (Fig. 11 i) and comparable to those for SIA in February (Fig. 11 l). Most products agree with each other within ±200 000 km² in September and within ±300 000 km² in February. For September, we find largest differences for NT1-SSMI being by between 300 000 km² and 700 000 km² smaller than all other products, and for OSI-450 being larger than most other products by ~200 000 km². Note that, in contrast to SIA, NT2-AMSRE SIE differences are much smaller and compare to, e.g., CBT-AMSRE. In February, NT2-AMSRE SIE is larger than six other products by 300 000 km² (10%) or more, while SICCI-50km SIE is smaller than six other products by 300 000 km² or more. For SICCI-50km, we can attribute this smaller SIE in February to the already mentioned too aggressive filtering (see discussion of Fig. 7 and Fig. 10).

For Fig. 6 through Fig. 11 we used the truncated sea ice concentration values as far as it concerns the EUMETSAT OSISAF – ESA-CCI products. Repeating these computations with the non-truncated values, e.g. for September and March, does not change the results with respect to SIE because only the 15% sea-ice concentration threshold counts which is not changed by this action. With respect to SIA we find an increase by ~50 000 km² in the respective winter months and almost no impact for the summer months.

6.1.2 The role of weather filters

~~In Fig. 1 and Fig. 2 we~~ We illustrated that the weather filters implemented in each of the ten products, have quite different behaviour, despite the fact they all use the same gradient ratios of brightness temperature frequency channels. ~~The~~ pPotential users should be aware of this. We confirm that the dynamic open water filters designed for ~~the~~ group I ~~EUMETSAT-OSISAF - ESA-CCI~~ products (see Table 2) have a stable impact on the lower part of the sea-ice concentration, cutting through it at about 10% SIC. This is across the months, changes of sensors (and thus frequencies, calibration, etc…) and for both hemispheres. We refer to Lavergne et al. (2019) for discussions how this consistency could be improved further. The analysis sheds also light on how the other six products perform in terms of stability. ~~We are h~~Here, we are interested both in the temporal consistency of the weather filter effects (e.g. jumps across satellite series~~instruments~~, across months, across climate-induced trends) and the absolute level at which they cut through the sea-ice concentration distribution, especially with respect to the 15% threshold embedded in the SIE and SIA curves shown in Fig. 6 and Fig. 7~~8~~. Group II ~~CBT-SSMI, NOAA-CDR, and CBT-AMSRE~~ products all cut around 15%, sometimes below, sometimes above, but in general at higher sea-ice concentration than ~~the~~group I products ~~EUMETSAT-OSISAF – ESA-CCI ones~~ (Fig. 1 and Fig. 2). We observed evidence for an actual impact of weather-filter cut-off sea-ice concentrations variation over time in the SIE time series in winter in the Antarctic (Fig. 7 c).

~~CBT-SSMI exhibits jumps when transitioning from one sensor to the next, for example from 1987 to 1988 (SMMR to SSM/I) for both hemispheres in September (Fig. 1 g, Fig. 2 a) and in the Arctic in March (Fig. 1 a); see also NT1-SSMI in the Antarctic (Fig. 2 a). It is noteworthy that the 23.0 GHz channels of the SMMR instrument have been highly unstable since launch, and eventually ceased to function on 11 March 1985 (Njoku et al., 1998). Thus, the water vapour part of the "classic" weather filter is un reliable in the early decade of the satellite data record. This is solved in the OSI-450 product by relying on explicit atmospheric correction of the brightness temperatures using –among others– water vapour fields from atmosphere re-analysis (see Lavergne et al., 2019). This discontinuity seems to be apparent in the September Antarctic SIE (Fig. 7 c): OSI-450 and CBT-SSMI agree with each other for the SMMR period while after 1987 CBT-SSMI is below OSI-450 by ~ 150 000 km². This corresponds to the area of one quarter of all 25 km grid cells centred at 60°S, the approximate average location of the Antarctic September sea-ice edge. This change in SIE is concomitant with a jump in the weather-filter sea-ice concentration from 11% to 14% (Fig. 2 a).~~

~~The NOAA-CDR starts with SSM/I in 1987 and thus avoids the 1987/88 jump. However, compared to OSI-450 and SICCI-25km we find for NOAA-CDR: 1) The sea-ice concentration at which the weather filter applies varies seasonally. For instance, in the year 1996, the mean 5% percentile of sea-ice concentrations within the interval]0%, 30%] is 14% for March but 17% for September in the Arctic, and 16% for September but 18% for February in the Antarctic. OSI-450 cuts at 10%, SICCI-25km at 11% for these months, and in both hemispheres. 2) The inter-annual variation of the sea-ice concentration at which the filter applies is larger for NOAA-CDR than for OSI-450 and SICCI-25km. In addition, the curves for NOAA-CDR (and CBT-SSMI) in Fig. 1 a) (March) and Fig. 2 (September) exhibit a discontinuity in the transition from 2007 to 2008, which corresponds to when SSMIS (F17) is processed instead of SSM/I (F15). OSI-450 exhibits no discontinuity here. This discontinuity occurs in March (Arctic) and September (Antarctic), i.e. both at maximum sea-ice extent, and is concomitant with a shift between OSI-450 and NOAA-CDR SIE by 50 000 to 100 000 km² between 2007 and 2008 (not shown). Our conclusion from these observations is that because the weather filters of this class of products cut the sea-ice concentration distribution within ±5% to the sea-ice concentration threshold of 15% typically applied to compute SIA and SIE, they might have an influence on the observed differences in SIA and SIE between the products.~~

~~It appears as if for the remaining three products: NT2-AMSRE, NT1-SSMI and ASI-SSMI, considerations of the kind discussed above do not apply. NT2-AMSRE and ASI-SSMI provide a weather filter cut-off sea-ice concentration of ~ 1-2% according to our analysis (Fig. 1 and Fig. 2), well below 15%; little can be said about potential inconsistencies between SSM/I and SSMIS for ASI-SSMI and their impact for SIA or SIE estimates. NT1-SSMI exhibits a rather constant weather-filter cut-~~

~~off sea ice concentration of ~ 1% for the Arctic (Fig. 1) but shows much more variability of it for the Antarctic (Fig. 2). Weather filter cut off sea ice concentrations are ~ 5% for the SMMR period, decrease to ~ 2% for the SSM/I period, and then jump to ~ 6% for the SSMIS period; note that Fig. 2 d) is from the year 2004 and hence from the SSM/I period. Since these inconsistencies are, however, well below 15% we do not expect any impact on our results as far as it concerns the overall mean sea ice concentration, SIA and SIE.~~

~~In any case,~~ We believe Fig. 1 and Fig. 2 are a new illustration that data products can differ in many ways. Such time-series, adapted from Lavergne et al. (2019), are an effective tool for data-producers and users to assess the temporal consistency of sea-ice concentration data products.

6.1.3 The impact~~role~~ of truncating sea-ice concentrations at 100%

~~In near-100% sea ice concentration conditions, retrieval algorithms will naturally retrieve bell-shaped distribution of values, returning values both below and above 100% sea ice concentration. However, the above-100% values are almost never accessible to the user, and thus generally not accessible for validation. Here, we used the availability of these "off-range" estimates in the four EUMETSAT OSISAF – ESA-CCI products to demonstrate how the "off-range" distribution can effectively be reconstructed a-posteriori from the products with truncated sea ice concentration distributions (Fig. 3). This Gaussian fit methodology allows us to go deeper in the analysis of near-100% conditions. Indeed, if the analysis had been limited to the truncated distributions only (shown in Fig. 12), algorithms that over-estimate sea ice concentration (modal value of the non-truncated distribution larger than 100%) would obtain better validation statistics (smaller bias and RMSE) than products with no over-estimation (modal value of the non-truncated distribution exactly at 100%). The larger the over-estimation, the better the statistics would be. Using the Gaussian fit, we unveil a possible over estimation of several sea ice concentration products, including NT1-SSMI, CBT-SSMI, and NOAA-CDR in the Arctic, and NOAA-CDR (but only slightly) in Antarctic sea ice conditions. This Gaussian fit methodology also confirms that the EUMETSAT OSISAF – ESA-CCI products are slightly low biased in the Arctic (as already documented by Lavergne et al., 2019). The worst of these biases we find in the Arctic for SICCI-12km that was not openly distributed at the end of the ESA-CCI Sea Ice Phase 2 project, partly based on these results.~~

~~In Appendix H, we present the full set of Gaussian fits for all ten products for both Arctic and Antarctic in Fig. H1 and Fig. H2 (see also Fig. 3). Based on these additional results we can see that indeed the Gaussian fit matches the non-truncated sea ice concentration distribution of the EUMETSAT OSISAF – ESA-CCI products quite well by the good agreement in the shape of the distributions as well as the reasonably low RMSD of 0.0037 in six of the eight cases (0.0025 and 0.0050 otherwise). We can see also, however, that there are discrepancies and limitations. In the Arctic (App. H, Fig. H1) the Gaussian fit under estimates the probability in the left tail for SICCI-12km, SICCI-25km, and OSI-450; in the Antarctic we observe such an under estimation for SICCI-25km and OSI-450 (App. H, Fig. H2). At the same time, we find an over-estimation in the right tail, i.e. > 100% for SICCI-12km and SICCI-25km in the Arctic and for SICCI-50km in the Antarctic. Possible explanations for the quoted under estimation could be: i) Sea ice concentrations have actually been that low even at the locations of the RRDP2 near-100% references sea ice concentration data set. ii) The impact of tie points not matching with the actually present snow / sea ice surface conditions on the retrieved sea ice concentration is not symmetric around 100%. We also see that for SICCI-50km, our step to bin the sea ice concentrations to integer values before the inter-comparison with the other products, results in a distribution around 100%, which is almost too narrow to fit it properly.~~

~~For the other algorithms, in the Arctic, the Gaussian fit matches perfectly well for sea ice concentrations ≤ 99% for CBT-SSMI, NOAA-CDR, and CBT-AMSRE with RMSD values of 0.0017 and 0.0023 (this is even better than for the EUMETSAT OSISAF – ESA-CCI). The match is less good for NT1-SSMI and ASI-SSMI with RMSD values of 0.0050 and 0.0062 (App. H, Fig. H1); we discussed the latter already in the context of Fig. 3 and refer to Ivanova et al. (2015) who, because of the non-linearity of this algorithm, were forced to construct an artificial evaluation data set. By comparing the~~

~~fraction under the red curve for sea ice concentrations > 99% with the value for F_{99} of 0.806, we consider the Gaussian fit applicable. This can be confirmed for the Antarctic (App. H, Fig. H2 a)). For the Antarctic, the match between observed sea-ice concentrations ≤ 99% and Gaussian fit is less good than in the Arctic for, especially, CBT-SSMI and CBT-AMSRE; RMSD values are comparably large: 0.0050 and 0.0058, respectively, and the sea-ice concentration distributions is considerably less bell-shaped than in the Arctic. It is beyond the scope of this study to further fine tune the Gaussian fit so that the match with the observations improves. We note that the results with respect to Gaussian fits shown in Appendix H, Fig. H1 and Fig. H2 apply also to the longer RRDP2 near-100% reference sea ice concentration data set of winters 2007 through 2015, which contains considerable more data pairs.~~

~~Finally, t~~The analysis of the validation at 100% conditions (Sect. 4) raises a critical question to be discussed in the future among data producers and with the data users: "Given that sea-ice concentration products are used following application of~~after~~ a 100% sea-ice concentration threshold ~~is applied~~, is it better to have algorithms (slightly) overshoot the sea-ice concentration distribution or should data producers aim at an unbiased non-truncated distribution?" To let algorithms overshoot will return fewer below-100% estimates in the product files which might be positive for large areas of the inner sea-ice cover during winter~~,~~ ~~but will also automatically reduce the sensitivity of the product to actual small openings in the sea ice, which are so important for the ocean/atmosphere heat exchange in cold winter conditions.~~ However, one consequence of this (hypothetically) shifted sea-ice concentration distribution with modal values > 100% is that the sea-ice concentration in areas with a true < 100% sea ice concentration, i.e. 99% or even 98%, might be set to 100%. Such areas could contain leads. According to, e.g., Marcq and Weiss (2012) about 70% of the upward ocean-atmosphere heat exchange occurs through leads even though these cover only one to two percent of the Central Arctic ocean. Assuming a heat transfer through thick ice of 5 W/m² and through a lead of 400 W/m² (e.g. Marcq and Weiss, 2012, near-surface air-temperature difference of 30K) a heat flux calculation yields 5 W/m² for 100% and ~ 9 W/m² for 99% true sea-ice concentration, an increase by 80%. Using sea-ice concentrations of an algorithm with a modal value at 101% or higher might therefore result in a substantial under-estimation of the surface heat flux. Integrated over the sea-ice covered central Arctic Ocean (area ~ 7 million km²) this under-estimation could be as high as 2.4 * 10^12 MJ per day.

To aim at an unbiased algorithm might help with a better sensitivity to small openings (but note the RMSE of non-truncated retrievals ranges between 2% and 5% for the various algorithms studied here), however, the product grid will have more below-100% estimates. Our analysis, supported by the Gaussian-fit method, helps introducing the question and opening the discussion, but does not bring the answer.

6.1.4 ~~-~~Observed differences to ship-based observations

~~The comparison to the ship-based observations presented in Sect. 5 is carried out using truncated EUMETSAT-OSISAF – ESA-CCI sea ice concentration data. Using the non-truncated EUMETSAT-OSISAF – ESA-CCI products does not considerably change our findings. Differences between satellite- and ship-based sea-ice concentrations reduce by between 0 and 0.3% with a concomitant increase in the standard deviation of up to 0.2% (see Fig. 15 and Fig. 17, and Tables 5 and 6); this applies primarily to winter when the fraction of near-100% sea-ice concentrations is large. While application of the Gaussian-fit method (see Sect. 2.1.4 and Sect. 6.1.3) seems not appropriate given the wide sea-ice concentration range considered in this inter-comparison, it is reasonable to assume that it would change the differences (standard deviations) found for all other products by up to a few tenth of a percent (some tenths of a percent). However, these changes would be small compared to the accuracy of the ship-based sea-ice concentrations (see Sect. 2.3 and beginning of Sect. 5).~~

~~According to the summaries given in Tables 5 and 6, we can divide the ten products into three groups. Group I contains the EUMETSAT-OSISAF – ESA-CCI products, group II contains CBT-SSMI, NOAA-CDR, NT2-AMSRE and CBT-AMSRE, and group III consists of ASI-SSMI and NT1-SSMI. Note that this division into groups is similar to the one~~

~~introduced in the context of, e.g., Fig. 11. Products of group II provide the smallest overall difference to the ship based observations: around 0% (Arctic) and around -2% (Antarctic). An exception is NT2-AMSRE, which provides considerably more ice than the ship observations in the Antarctic: +4.5%. Products of group I provide differences around -7.5% (Arctic) and -3.5% (Antarctic); in both hemispheres the difference is largest for SICCI-25km. Groups I and II share similar average values for R^2 in the Arctic: 0.77 and 0.76 and in the Antarctic: 0.74 and 0.72, respectively. Standard deviations are a little smaller for group I than group II: 12.3% versus 13.2% (Arctic) and 13.7% versus 15.6% (Antarctic). NT1-SSMI provides by far the largest difference to ship observations in both hemispheres, paired with generally lower correlation and higher standard deviation.~~

~~ASI-SSMI provides the smallest values for R^2 in both hemispheres. ASI-SSMI reveals a substantially improvement in the inter-comparison results between winter and summer in the Arctic: correlation increases, difference and standard deviation decrease. This could be attributed to the higher fraction of inter-mediate sea-ice concentrations during summer for which the comparably fine grid resolution of 12.5 km of the ASI-SSMI product could be of advantage. While an increase of the correlation between winter and summer is observed also for all other products, such a notable decrease in difference and standard deviation is not – except for SICCI-12km. This product is also provided at 12.5 km grid resolution but in contrast to ASI-SSMI combines brightness temperatures at two different frequencies and hence different native resolutions (see Table 2). Because in the Antarctic the sea-ice cover is more open also during winter it is plausible that such an improvement in inter-comparison results between winter and summer is lacking there.~~

~~Figure 14 through Fig. 17 reveal quite a high fraction of sea-ice concentrations in the range 95% to 100%. This might have biased the results. We therefore repeated our comparison by discarding all data pairs with daily mean sea-ice concentrations ≥ 95%. Main results (not shown) are an overall increase in the differences by about 2% and of the standard deviations by ~ 1% (group I) and 2-3% (group II) and a reduction of the correlation by ~ 0.08. This results in R^2 of 0.68 versus 0.63 (Arctic) and 0.67 versus 0.63 (Antarctic) for group I and II, respectively, and in standard deviations of 13.8% versus 16.3% (Arctic) and 14.9% versus 18.0% (Antarctic). While group I exhibits larger differences than group II, inter-comparison results are better for group I than group II otherwise.~~

One of the innovations of the products of group I (see Table 2) is the self-optimizing capability of the algorithms to adopt to seasonally changing sea-ice conditions, i.e. the transition between winter and summer. If ship-based sea-ice observations are as reliable in summer as they are in winter then a comparison of the differences and standard deviations obtained in~~for~~ winter and summer could reveal how well an algorithm deals with the seasonally changing sea-ice conditions. If we focus on sea-ice concentrations < 95% to avoid the clustering of data pairs near 100% during winter, we find~~In the Arctic,~~ the CDRs of the group I products: SICCI-25km, SICCI-50km and OSI-450 to stand out with winter-to-summer changes in the difference between ship- and satellite-based sea-ice concentrations around 0.2%~~by 0.2%, 0.3% and 0.1%, respectively~~, compared to ~3.5% for group II products~~ of group II~~ in the Arctic. ~~Results are more diverse for the~~ Respective changes in the standard deviation range~~where products of group II exhibit winter-to-summer changes~~ between 0.1% ~~(CBT-SSMI)~~ and 5.2% for group II~~(CBT-AMSRE)~~ but are near ~2.7% for group I CDRs~~while SICCI-25km, SICCI-50km and OSI-450 exhibit values of 2.8%, 2.6% and 2.6%, respectively. Largest winter-to-summer changes are provided by ASI-SSMI: 6.7% (difference) and 6.1% (standard deviation)~~. In the Antarctic, smallest winter-to-summer differences of ~0.3% are obtained for group I products SICCI-12km and OSI-450~~: 0.2% and 0.4%, respectively~~, compared to ~2.5% for group II products~~ of group II~~. These provide a winter-to-summer change in standard deviation of ~6.5% while SICCI-12km and OSI-450 exhibit ~~smaller~~ values of ~~~3.7% and~~ 4.02%. These results~~, which have been obtained by, again, discarding mean sea-ice concentrations ≥ 95%,~~ suggest that most group I products~~EUMETSAT OSISAF – ESA CCI products~~ compare with the ship-based sea-ice observations more consistently across seasons than the other products.

It is noteworthy, however, to keep in mind the difference in scales and observational limitations between ship-based and satellite-based observations of the sea-ice concentration – as illustrated in Figure 17. For the pack ice / lead case (Fig. 17

a), Table 7 top), the variation of the ship-based observations depends strongly on the fraction of thin ice. For leads covered by open water, satellite sea-ice concentrations tend to exceed ship-based concentrations. This could explain the banana-shaped distribution of data pairs for the SH (Fig. 16). For leads covered by thin ice, it is the other way round. Ship-observations would reveal a total sea-ice concentration of 100%, while most of the tested algorithms underestimate the true sea-ice concentration in presence of thin ice [Cavalieri, 1994; Comiso and Steffen, 2001; Ivanova et al., 2015]. This could explain the larger fraction of ship-based sea-ice concentrations near 100% as is particularly pronounced, e.g., for NT1-SSMI (Fig. 15 a) and, in general, the larger range of satellite versus ship-based sea-ice concentrations at comparably high concentrations. For the marginal ice zone (Fig. 17 b), Table 7 bottom), it is more likely that most products provide smaller sea-ice concentrations than observed from a ship. During winter, a considerable fraction of the sea ice might be thin ice – causing under-estimation as stated above. During summer, a considerable fraction of the sea ice might be too wet to be recognized as ice by satellite microwave radiometry – causing an under-estimation as well (see e.g. Worby and Comiso, 2004; Ozsoy-Cicek et al., 2009). In addition, low ice concentrations are often filtered by the weather filters applied (see Sect. 2.1.3). This results in a substantially larger range of ship-based sea-ice concentrations at comparably low satellite sea-ice concentrations. Furthermore, this also results in a larger fraction of low ice-concentration values for the satellite-based than the ship-based observations. This explains why mean ship-based sea-ice concentrations per binned satellite sea-ice concentration (blue symbols in Fig. 15 and 16) are shifted so much to the right compared to the red symbols; this is also evident from the larger fraction of data pairs below than above the identity line for sea-ice concentrations below 60 to 80%.

We note that another data set of a different kind of ship-based observations of Arctic sea-ice conditions is available at the Arctic and Antarctic Research Institute (AARI) and has recently been used for a sea-ice concentration algorithm inter-comparison study using an approach different to the one used in our paper (Alekseeva et al., 2019). We might extent our inter-comparison studies to their data set in the future.

~~6.2 Outlook~~

~~The algorithms implemented in the EUMETSAT OSISAF – ESA CCI products are continuously under development, and several improvements are planned in the course of the next phase of the ESA CCI sea ice project (so called CCI+), and the running phase of the EUMETSAT OSISAF project. Some of the research and development items planned are directly triggered by the findings in this paper. In particular, CCI+ will focus on improving upon the SICCI 12km data record that combines the ~19 GHz and ~90 GHz channels of AMSR-E and AMSR2 missions. The version of SICCI 12km evaluated in this paper was not performing well enough (especially bias in NH) and has not been released. Algorithms using ~90 GHz channels will be studied in more depth during CCI+, since these channels have the potential to bring higher spatial resolution and thus bridging the gap towards the WMO GCOS requirements. Another relative weakness of the EUMETSAT OSISAF – ESA CCI data products seems to be the correction of the land spill-over contamination, which showed most in the SIE and SIA time series for SICCI 50km. A dedicated effort to improve on this is starting in the context of the EUMETSAT OSISAF project. Finally, the small (but significant) low bias of the OSI 450 and SICCI 25km at near 100% conditions will be addressed towards the next version of the EUMETSAT OSISAF – ESA CCI data products, scheduled for 2021. The sea ice concentration uncertainty estimates will be analysed during the next phase of the ESA CCI sea ice project (CCI+). In particular, an end to end uncertainty analysis will be done with the aim of identifying individual uncertainty contributions and for possibly splitting the SIC uncertainty budget into more components.~~

~~6.3~~6.2 Conclusions

Recently, three new global sea-ice concentration (SIC) climate data records (CDRs) have been released. They are described in Lavergne et al. (2019). These ~~so called EUMETSAT OSISAF – ESA CCI~~ products: SICCI-25km, SICCI-50km, and OSI-450, utilize a dynamic, self-optimizing hybrid sea-ice concentration algorithm, which is applied to satellite microwave

brightness temperature measurements of the SMMR, SSM/I and SSMIS instruments (OSI-450) or the AMSR-E and AMSR2 instruments (SICCI-25km and SICCI-50km); see Table 1 for instruments and frequencies. Within this paper, these newEUMETSAT OSISAF – ESA CCI products are evaluated by means of an inter-comparison to products of seven other sea-ice concentration productsalgorithms (see Table 2 for acronyms, and satellite sensors and frequencies used, and assignment to groups of algorithms I to IV) and with independent sea-ice cover data. These independent sea-ice cover data are a global winter-time near-100% reference sea-ice concentration data set (Sect. 2.2) and a global year-round data set of ship-based visual observations of the sea ice cover (Sect. 2.3). Because five of the products are based on AMSR-E data, our core evaluation period is the AMSR-E measurement period, i.e. June 2002 through September 2011.

We find a very good and consistent agreement in inter-annual variation of the monthly mean SIA and SIE time series for both hemispheres for the overlap periods of the respective products used at their native grid resolution. We can explain Uunexpected low SIE of SICCI-50km during Arctic winter and Antarctic summer we can explain by the coarse resolution of the 6.9 GHz frequency observations combined with a too aggressive filtering of near-coastal and potentially weather-influenced grid cells near coastlines, which removed a substantial number of grid cells with ice. We note that SIE differences are to be expected simply from the different grid resolutions. When inter-comparing products on the same grid (50km) applying the same land masktaking this issue into account, the EUMETSAT OSISAF – ESA CCI products of group I provide quite similar values ofor SIC, SIA and SIE for both hemispheres, during times of both maximum and minimum sea-ice cover. Overall differences are < 1.0% for SIC, and < 100 000 km² (Arctic) and < 200 000 km² (Antarctic) for both SIA and SIE. A similarly good agreement in SIC, SIA and SIE for both hemispheres is observed we find for the products pair CBT-SSMI and – NOAA-CDR of group II (see Table 2), as can be expected from the design of NOAA-CDR (see Appendix F and Peng et al., 2013). Between the remaining four products, i.e., ASI-SSMI, NT1-SSMI, CBT-AMSRE, and NT2-AMSRE (Table 2), and between these and the above-quoted six products, we find considerably larger differences between SIC, SIA, and SIE – which vary with algorithm, season, and hemisphere. Largest differences we findare found for NT1-SSMI and NT2-AMSRE: NT1-SSMI provides less sea ice than other products particularly infor summer in the Arctic and winter in the Antarctic;, and NT2-AMSRE: provides more sea ice than other products in the Antarctic. Lowest spread among all ten products is achieved for the Arctic SIE in September; here the maximum inter-product difference is < 400 000 km², i.e. ~ 10% of the total Arctic September SIE. We therefore can confirm Based on our results we state that it matters which algorithm and/or product is used for monitoring the polar sea-ice cover as long as one is interested in absolute values; similarity of trends has been shown elsewhere (e.g. Ivanova et al., 2014; Comiso et al., 2017a).

Results quoted in the previous paragraph rely on computations applying the often-used 15% SIC threshold (e.g. Gloersen et al., 1992). Our investigations suggest that it might be worth to start reconsideringre-thinking about this threshold because, as we illustrated in our paper in Fig. 1 and Fig. 2, the weather filters applied might have inter-sensor jumps and fail to cut at a constant sea-ice concentration remaining constant across the different satellite sensors used. . WhileFor example, sea-ice concentrations from sensor A might be cut by the weather filter at 14% while these might be cut at 17% for a subsequent sensor B. As a result, more sealess ice is removed for sensor Bleft and the sea-ice extent computed from sea-ice concentration data of sensor B is systematically smaller than the one computed from sensor A. We observefound evidence for this in our results. A more thorough analysis of trends over sub-periods observed by the ten products could reveal other such impacts. and remark that the This impact of these inconsistencies is likely to be particularly pronounced in the peripheral seas with a comparably large fraction of the marginal ice zone, such as the Bering Sea or the Barents Sea. Note that the OSI-450 algorithm provides a particularly stable weather-filter induced sea-ice concentration cut-off at ~10% across the sensors used.

Sea-ice concentrations are retrieved from satellite microwave brightness temperatures using an empirical geophysical physical algorithmmodel, which usually involves a limited set of tie points. However, These are brightness temperatures, or parameters derived from these, which are typical for the encountered surface types, which in the simplest of our cases are open water: 0% SIC and close pack ice: 100% SIC. Because of tthe natural variability of those surface properties of 100% sea ice

relevant for ~~its~~ microwave remote sensing of sea ice is large and these tie points~~, one fixed tie point value for 100% sea ice, even if retrieved daily,~~ can only be an average signature associated with a significant spread~~representation of these properties. In other words, ten different kinds of 100% sea ice can cause ten different brightness temperatures~~. As a result, ~~a retrieved~~ sea-ice concentrations retrieved by such algorithms naturally vary~~ies~~ *around* (below and above) 100%~~. This means~~ even though the actual sea-ice concentration is exactly 100%~~ the retrieved one could be, for example, 97% or 100% or 103%~~. The natural variability of the sea-ice surface properties and the linearity of most algorithms suggest~~s~~ that the spread of retrieved sea-ice concentrations around 100% follows a Gaussian distribution. However, ~~A~~all ten products examined here either truncate sea-ice concentrations at 100%, i.e. fold retrieved values > 100% to exactly 100%, or do simply not allow retrieval of SIC > 100% (NT2-AMSRE) and the natural variability cannot be assessed. We develop a Gaussian-fit method to re-construct the full distribution of sea-ice concentrations around 100%. We demonstrate its performance on the group I~~EUMETSAT-OSISAF – ESA-CCI~~ products (as these~~y~~ provide, for the first time, both the non-truncated and truncated values) and subsequently use it to re-construct non-truncated sea-ice concentration distributions for the remaining six products (Fig. 3, and Appendix H, Fig. H1 and Fig. H2). Based on our results we conclude that it is worthwhile to re-think the concept of truncation at 100% (but also at 0% SIC) and critically re-assess evaluation results at the two ends of the sea-ice concentration distribution. Indeed, we argue that direct evaluation of truncated data sets give a misleading information on the accuracy of the sea-ice concentration data, and favour those data sets that overestimate sea-ice concentrations. Such overestimation has direct implications on the ability of a given sea-ice concentration data set to e.g. observe small openings in an otherwise complete sea-ice cover. We invite the sea-ice concentration data producers and users to take this into consideration and discuss the implications towards future versions of such data products.

Data availability. All sea-ice concentration products except SICCI-12km are publicly available from the sources provided in the respective sections of the supplementary material and the reference list. The SICCI-12km product is available upon request from T. Lavergne. The standardized ship-based observations are available from the Integrated Climate Data Center (ICDC): http://icdc.cen.uni-hamburg.de/1/daten/cryosphere/seaiceparameter-shipobs/. The RRDP2 data set is publicly available from the source specified in the reference list.

7 Appendices

7.1 Appendix A. The EUMETSAT-OSISAF – ESA-CCI algorithm suite

The four products OSI-450, SICCI-12km, SICCI-25km, and SICCI-50km have in common that they are based on a hybrid, self-tuning, self-optimizing sea-ice concentration algorithm (Lavergne et al., 2019). This algorithm is applied to brightness temperature (TB) observations of the SMMR, SSM/I and SSMIS instruments for OSI-450, providing a fully revised version of the OSI-409 CDR (Tonboe et al., 2016). This algorithm is applied to brightness temperatures measured by the AMSR-E and AMSR2 instruments for the SICCI CDRs. Apart from the input satellite data the processing chains are the same for these four products. The algorithm is a generalization of the Comiso Bootstrap frequency mode algorithm (App. C) and of the Bristol algorithm (Smith and Barret, 1994; Smith 1996) and is described in detail in Lavergne et al. (2019). Two algorithms that each combine three frequency channels (e.g. ~19 GHz at vertical polarization, and ~37 GHz at both horizontal and vertical polarizations) are respectively optimized to provide best accuracy in Open Water (the B_{OW} algorithm) and Consolidated Ice (the B_{CI} algorithm) conditions. The sea-ice concentrations obtained with each of the two optimized algorithms are merged linearly into a hybrid sea-ice concentration SIC_{hybrid} according to the general formula:

$$\begin{cases} w_{OW} = 1; \text{for } B_{OW} < 0.7 \\ w_{OW} = 0; \text{for } B_{OW} > 0.9 \\ w_{OW} = 1 - \frac{B_{OW} - 0.7}{0.2}; \text{for } B_{OW} \in [0.7; 0.9] \end{cases} ; \quad SIC_{hybrid} = w_{OW} \times B_{OW} + (1 - w_{OW}) \times B_{CI} , \tag{A1}$$

For sea-ice concentrations below 70%, SIC_{hybrid} relies completely on B_{OW} and for sea-ice concentrations above 90% it relies entirely on B_{ICE}. The B_{OW} and B_{ICE} algorithms can be regarded as a generalized version of the Comiso Bootstrap and Bristol algorithms, in that sense that they combine the three different brightness temperature channels used by the two algorithms in a 3-dimensional TB space, and optimize their data projection plane for best accuracy.

In this paper, we use the sea-ice concentration CDR derived from SMMR, SSM/I and SSMIS data: OSI-450 [https://doi.org/10.15770/EUM_SAF_OSI_0008], and two sea-ice concentration CDRs derived from AMSR-E and AMSR2 data: SICCI-25km [https://doi.org/10.5285/f17f146a31b14dfd960cde0874236ee5] and SICCI-50km [https://doi.org/10.5285/5f75fcb0c58740d99b07953797bc041e]. While SICCI-25km is based on brightness temperatures measured at ~19 GHz and ~37 GHz, similar to OSI-450, SICCI-50km is based on brightness temperatures measured at ~7 GHz and ~37 GHz. OSI-450 and SICCI-25km come at 25 km grid resolution while SICCI-50km has 50 km grid resolution. In addition, we use a fourth product, SICCI-12km, which is provided at 12.5 km grid resolution and is based on brightness temperatures measured by AMSR-E and AMSR2 at ~19 GHz and ~90 GHz. Here, we use a prototype of SICCI-12km, which was produced during the ESA CCI Sea Ice project, but was not released publicly (partly based on the results presented in this manuscript). All these data sets have daily temporal resolution and are provided on polar EASE grids version 2.0 (Brodzik et al. 2012, 2014).

7.2 Appendix B. The ARTIST sea-ice (ASI) algorithm

The ARTIST Sea Ice (ASI) algorithm (Kaleschke et al., 2001; Spreen et al., 2008) is a modified hybrid of the Near 90 GHz algorithm (Svendsen et al., 1987) and the NASA Team algorithm (see App. D). Water and ice are distinguished at high resolution by the TB polarization difference (P) at ~90 GHz:

$$P = TB_{90}^{V} - TB_{90}^{H}$$

The basic equations for the ASI algorithm are based on the Near 90 GHz algorithm of Svendsen et al. (1987):

$$P = a \times (C \times \Delta\epsilon_{ice} \times T_{ice} + (1 - C) \times \Delta\epsilon_{water} \times T_{water}) \quad \text{(B1)}$$

with the atmospheric influence $a = (1.1 \times e^{-\tau} - 0.11) \times e^{-\tau}$

C is the total sea-ice concentration, T is the temperature, $\Delta\epsilon$ is the difference in surface emissivity between vertical and horizontal polarization for the ice or water surface fraction, and τ is the total atmospheric optical depth for Arctic conditions at this frequency and viewing conditions. For ice free (C = 0) and totally ice covered (C = 1) conditions, Eq. (B1) yields the tie-points for open water $P_{water} = a_{water} \times \Delta\epsilon_{water} \times T_{water}$ and sea ice $P_{ice} = a_{ice} \times \Delta\epsilon_{ice} \times T_{ice}$. Taylor expansions of Eq. (B1) around C=0 and C=1 lead to a pair of equations for P, in which the atmospheric influences a_{water} and a_{ice} can be substituted with the aid of the tie point equations – provided that the variation of the atmospheric influence is small over water or ice (see Spreen et al., 2008). After substitution one obtains

$$C = \left(\frac{P}{P_{water}} - 1\right) \times \left(\frac{\Delta\epsilon_{water} \times T_{water}}{\Delta\epsilon_{ice} \times T_{ice} - \Delta\epsilon_{water} \times T_{water}}\right) \text{ for C} \rightarrow 0 \quad \text{(B2)}$$

$$C = \frac{P}{P_{ice}} + \left(\frac{P}{P_{ice}} - 1\right) \times \left(\frac{\Delta\epsilon_{water} \times T_{water}}{\Delta\epsilon_{ice} \times T_{ice} - \Delta\epsilon_{water} \times T_{water}}\right) \text{ for C} \rightarrow 1 \quad \text{(B3)}$$

According to Svendsen et al. (1987) the ratio of the surface emissivity differences can be set to a constant value (-1.14). With this simplification and by assuming that the atmospheric influence inherent in P is a smooth function of the sea-ice concentration one can use a third order polynomial function to interpolate between the solutions of Eq. (B2) and Eq. (B3) to obtain sea-ice concentrations between 0 and 1 as a function of P:

$$C(P) = d_3 \times P^3 + d_2 \times P^2 + d_1 \times P + d_0 \quad \text{(B4)}$$

The coefficients d_i are derived with a linear equation system based on Eq. (B2) and Eq. (B3) and their first derivatives (Spreen et al., 2008).

The larger, compared to the lower frequencies used in most products (see Table 2), weather influence at ~90 GHz frequencies by atmospheric water content and surface wind speed can cause substantial over-estimation of the sea-ice concentration over open water and within the ice edge (Kern, 2004; Andersen et al., 2006). Over open water, the weather influence is reduced by combining sea-ice concentrations obtained with Eq. (B4) with NASA-Team algorithm (NTA, see also App. D) sea-ice concentrations following:

$$C = C_{ASI} \text{ for } C_{NTA} > 5\%; C = 0\% \text{ for } C_{NTA} \leq 5\% \quad \text{(B5)}$$

Hence, the ASI algorithm is a hybrid of the near-90GHz algorithm (Eq. (B1) through Eq. (B4)) and the NTA (Kaleschke et al., 2001; Ezraty et al., 2007; Girard-Ardhuin, personal communication, June 3 2019).

We use the ASI algorithm sea-ice concentration product provided via the Integrated Climate Data Center: https://icdc.cen.uni-hamburg.de [last access date: 27/2/2019]. This product is processed at the French Institute for Exploitation of the Sea (IFREMER) from SSM/I and SSMIS data, and provided via ICDC after application of a running 5-day-median filter, further reducing spurious weather-influence induced sea-ice concentration in the open water (Kern et al., 2010), on a polar-stereographic grid with 12.5 km grid resolution (at 70 degrees latitude). We abbreviate this data with ASI-SSMI.

7.3 Appendix C. The Comiso-Bootstrap algorithm

The Comiso-Bootstrap algorithm (Comiso, 1986; Comiso et al, 1997; Comiso et al., 2003; Comiso and Nishio, 2008) combines TB observations at either two different frequencies (frequency mode, 37 GHz and 19 GHz, vertical polarization) or at two different polarizations (polarization mode, 37GHz, vertical and horizontal polarization). It is bas~~root~~ed on the observation that brightness temperatures measured at these frequencies / polarizations over closed sea ice tend to cluster along a line (ice line) while those over open water tend to cluster around a single point in the respective two-dimensional brightness temperature space. The total sea-ice concentration is computed using

$$C = \frac{TB_f^V - TB_{f,OW}^V}{TB_{f,I}^P - TB_{f,OW}^V} \quad \text{(C1)}$$

with the brightness temperature measured at vertical polarization and frequency f = 37 GHz (polarization mode) or f = 19 GHz (frequency mode): TB_f^V, the open water tie point $TB_{f,OW}^V$ at vertical polarization and the same frequency as TB_f^V, and the intersection of the ice line with a line from the open water tie point through the observed brightness temperature: $TB_{f,I}^P = A \times \frac{B-W}{Q-A} + B$. Scalars A and B are functions of the ice tie points for first-year ice (FYI) and multiyear ice (MYI) at 37 GHz at vertical and horizontal polarization (polarization mode) or at 19 GHz and 37 GHz, both vertical polarization (frequency mode). Q and W are functions of the actually observed brightness temperature and the water tie point at the respective frequencies / polarizations. The two algorithms (frequency and polarization mode) are combined so that only the polarization mode is used in high concentration conditions and the frequency mode otherwise.

We use daily gridded sea-ice concentrations derived with the Comiso-Bootstrap (CBT) algorithm from SMMR, SSM/I and SSMIS instruments, as processed at NASA Goddard Space Flight Center (GSFC), and made available at https://nsidc.org/data/nsidc-0079. They are on a polar-stereographic grid with 25 km grid resolution (at 70 degrees latitude). We abbreviate this data with CBT-SSMI. For practical reasons, we access these GSFC CBT-SSMI fields from the NOAA sea-ice concentration CDR (App. F) files, where they are provided as additional data (Meier and Windnagel, 2018). The GSFC CBT-SSMI sea-ice concentration data set involves manual filtering, especially at the beginning of the record (SMMR period).

In addition, we use daily gridded sea-ice concentrations derived with this algorithm from AMSR-E data (Comiso et al., 2003; Comiso and Nishio, 2008) as provided by NSIDC (AE_SI25.003, Cavalieri et al., 2014, https://nsidc.org/data/ae_si25/versions/3, last access date: 26/4/2018) on the same polar-stereographic grid. The AMSR-E Comiso Bootstrap algorithm sea-ice concentration is referred with CBT-AMSRE throughout this paper. Note that the NSIDC product AE_SI25.003 does not contain CBT-AMSRE sea-ice concentrations itself. It contains the NT2 sea-ice concentration

and the difference "Comiso Bootstrap minus NT2 sea-ice concentration". Therefore, we needed to compute the CBT-AMSRE sea-ice concentration by adding the NT2 sea-ice concentration to that difference.

7.4 Appendix D. The NASA-Team algorithm

The NASA-Team algorithm (Cavalieri et al., 1984, 1992, 1999) combines the large difference of the normalized brightness temperature polarization difference at 19 GHz, $PR = \frac{TB_{19}^{V} - TB_{19}^{H}}{TB_{19}^{V} + TB_{19}^{H}}$, between water and ice, with the observation, that the normalized brightness temperature frequency difference between 37 and 19 GHz at vertical polarization, $GR = \frac{TB_{37}^{V} - TB_{19}^{V}}{TB_{37}^{V} + TB_{19}^{V}}$, is negative for MYI and close to zero or slightly positive for FYI and open water. The total sea-ice concentration is derived as the sum of the fractions of MYI and FYI, which is constrained to a maximum of 1:

$$C_{FYI} = \frac{F_0 + F_1 \, x \, PR + F_2 \times GR + F_3 \times PR \times GR}{D}, \; C_{MYI} = \frac{M_0 + M_1 \, x \, PR + M_2 \, x \, GR + M_3 \, x \, PR \, x \, GR}{D},$$

$$\text{with } D = D_0 + D_1 \times PR + D_2 \times GR + D_3 \times PR \times GR \qquad \text{(D1)}$$

Where coefficients F_i, M_i and D_i include the tie point information.

We use daily gridded sea-ice concentrations derived with the NASA-Team (NT1) algorithm from SMMR, SSM/I and SSMIS instruments, as processed at NASA Goddard Space Flight Center (GSFC), and made available at https://nsidc.org/data/nsidc-0051. They are on a polar-stereographic grid with 25 km grid resolution (at 70 degrees latitude). We abbreviate this data with NT1-SSMI. For practical reasons, we access these GSFC NT1-SSMI fields from the NOAA sea-ice concentration CDR (App. F) files, where they are provided as additional data (Meier et al., 2017; Meier and Windnagel, 2018). The GSFC NT1-SSMI sea-ice concentration data set involves manual filtering, especially at the beginning of the record (SMMR period).

7.5 Appendix E. The enhanced NASA-Team algorithm (NT2)

Inter-comparison studies such as those of Comiso and Steffen (2001) and Comiso et al. (1997) led to the development of the enhanced NASA-Team algorithm (NT2) (Markus and Cavalieri, 2000; Comiso et al., 2003) to mitigate effects such as layering in snow on sea ice on the accuracy of the sea-ice concentrations obtained with ~~the~~ NT1. ~~The~~ NT2 is conceptually different from the other algorithms presented here. The three relevant parameters (see below) are modelled as a function of sea-ice concentration in steps of 1% for 12 different atmospheric states using a radiative transfer model. The sea-ice concentration resulting in the minimum cost function between modelled and observed values of these parameters is taken as the retrieved total sea-ice concentration. The three parameters used are selected such that the influence of layering in snow on sea ice is mitigated:

$$\Delta GR = \frac{TB_{90}^{H} - TB_{19}^{H}}{TB_{90}^{H} + TB_{19}^{H}} - \frac{TB_{90}^{V} - TB_{19}^{V}}{TB_{90}^{V} + TB_{19}^{V}}$$

$$PR_{19}^{rotated} = -\frac{TB_{37}^{V} - TB_{19}^{V}}{TB_{37}^{V} + TB_{19}^{V}} \times sin\,\theta_{19} + \frac{TB_{19}^{V} - TB_{19}^{H}}{TB_{19}^{V} + TB_{19}^{H}} \times cos\,\theta_{19}$$

$$PR_{90}^{rotated} = -\frac{TB_{37}^{V} - TB_{19}^{V}}{TB_{37}^{V} + TB_{19}^{V}} \times sin\,\theta_{90} + \frac{TB_{90}^{V} - TB_{90}^{H}}{TB_{90}^{V} + TB_{90}^{H}} \times cos\,\theta_{90} \qquad \text{(E1)}$$

The rotation is done in the space given by PR_{19} and GR (see App. D) or by PR_{90} and GR for $PR_{19}^{rotated}$ and $PR_{90}^{rotated}$, respectively, at an angle Θ chosen such that the ice lines in the respective space are parallel to the GR axis.

We use daily gridded NT2 sea-ice concentrations derived from AMSR-E data as provided by NSIDC: AE_SI25.003 (Cavalieri et al., 2014, https://nsidc.org/data/ae_si25/versions/3, last access date: 26/4/2018) on polar-stereographic grid with 25 km grid resolution. We abbreviate this data with NT2-AMSRE.

7.6 Appendix F. The NOAA/NSIDC sea-ice concentration CDR

The NOAA/NSIDC sea-ice concentration CDR combines sea-ice concentrations computed with the NT1 algorithm (App. D) with those computed with the CBT algorithm (App. C), via

$$C = \max(C_{NT1}, C_{CBT}) \quad \text{(F1)}$$

within the ice edge. The ice edge is defined by the CBT sea-ice concentration of 10%. The generation and characteristics of the NOAA/NSIDC CDR as well as details about filters (see also Sect. 2.1) and about the statistical uncertainty estimate provided with the product are described in Peng et al. (2013) and Meier and Windnagel (2018). We use the daily gridded sea-ice concentration data of NOAA/NSIDC CDR version 3, named NOAA-CDR in this manuscript, provided by NSIDC on polar-stereographic grid with 25 km grid resolution (Meier et al., 2017, https://nsidc.org/data/g02202/versions/3, last access date: 7/2/2019).

It is important to note that the data sets NT1-SSMI (App. D) and CBT-SSMI (App. C), both from GSFC are not used as input in the NOAA/NSIDC CDR. Instead, sea-ice concentrations are computed at NSIDC using re-implementations of the two algorithms, which allow for a fully-automated and transparent processing as required for a CDR, and combined with Eq. (F1). One of the key difference between the NSIDC and GSFC versions is that the NSIDC ones do not involve manual editing, and start with SSM/I in July 1987.

7.7 Appendix G. Matrices of sea-ice concentration, area, and extent differences

This subsection contains the full set of matrices of differences between all ten products of the overall hemispheric average monthly mean sea-ice concentration of the AMSR-E measurement period and of the respective overall monthly mean sea-ice area (SIA) and extent (SIE) in Fig. G1 through Fig. G6.

7.8 Appendix H. Gaussian fits for all ten products

This subsection contains the two sets of Gaussian fits obtained for the Arctic (Fig. H1) and Antarctic (Fig. H2) based on the methodology described in Sect. 2.1.4; see also Fig. 3). These are the fits obtained from data of the overlap period between the AMSR-E measurement period and the RRDP2 near-100% reference sea-ice concentration data set period, that is in~~for~~ winter of years 2007 through 2011.

Author contributions. SK led the writing in most sections, with contributions by TL (Sect. 2.1, Sect. 6.1, Sect. 6.2), LTP (Sect. 1, Sect. 2.1), DN (Sect. 1, Sect. 3), and RTT (Sect. 2.1, Sect. 6.2). AMS and TL contributed to concept and work of Sect. 2.1.3. TL contributed to concept and work of Sect. 2.1.4. RS and LTP produced and provided the RRDP2 data set and consulted its usage (Sect. 2.2). DN and TL contributed to concept and work as well as design of figures of Sect. 3. SK performed the data analysis and inter-comparison with contributions in the interpretation of the results from all co-authors.

Competing interests. The authors declare that they have no conflict of interest.

Acknowledgements. The work presented here was funded by EUMETSAT (through the 2nd Continuous Developments and Operation Phase of OSI SAF) and ESA (through the Climate Change Initiative Sea_Ice_cci project), and the German Research Foundation (DFG) Excellence Initiative CLISAP under Grant EXC 177/2. The publication itself is funded by the Deutsche Forschungsgemeinschaft (DFG, German Research Foundation) under Germany's Excellence Strategy – EXC 2037 'CLICCS

– Climate, Climatic Change, and Society' – Project Number: 390683824, contribution to the Center for Earth System Research and Sustainability (CEN) of the University of Hamburg.

8 References

Alekseeva, T. Tikhonov, V., Frolov, S., Repina, I., Raev, M., Sokolova, J., Sharkov, E., Afanasieva, E., and Serovetnikov, S.: Comparison of Arctic sea ice concentration from the NASA Team, ASI, and VASIA2 algorithms with summer and winter ship data, Rem. Sens., 11(21), 2481, https://doi.org/10.3390/rs11212481, 2019.

Andersen, S., Tonboe, R. T., Kern, S., and Schyberg, H.: Improved retrieval of sea ice total concentration from spaceborne passive microwave observations using Numerical Weather Prediction model fields: An intercomparison of nine algorithms, Rem. Sens. Environ., 104(4), 374-392, 2006.

Andersen, S., Pedersen, L. T., Heygster, G., Tonboe, R. T., and Kaleschke, L.: Intercomparison of passive microwave sea ice concentration retrievals over the high concentration Arctic sea ice, J. Geophys. Res., 112, C08004, https://doi.org/10.1029/2006JC003543, 2007.

Beitsch, A., Kern, S., and Kaleschke, L.: Comparison of SSM/I and AMSR-E sea ice concentrations with ASPeCt ship observations around Antarctica, IEEE Trans. Geosci. Rem. Sens., 53(4), 1985-1996, https://doi.org/10.1109/TGRS.2014.2351497, 2015.

Brodzik, M. J., Billingsley, B., Haran, T., Raup, B., and Savoie, M. H.: EASE-Grid 2.0: Incremental but Significant Improvements for Earth-Gridded Data Sets, ISPRS Int. Geo-Inf., 1(1), 32-45, https://doi.org/10.3390/ijgi1010032, http://www.mdpi.com/2220-9964/1/1/32., 2012.

Brodzik, M. J., Billingsley, B., Haran, T., Raup, B., and Savoie, M. H.: Correction: Brodzik, M. J. et al. EASE-Grid 2.0: Incremental but Significant Improvements for Earth-Gridded Data Sets, ISPRS Int. Geo-Inf., 1(1), 32-45, 2012. ISPRS Int. Geo-Inf., 3(3), 1154-1156, https://doi.org/10.3390/ijgi3031154, http://www.mdpi.com/2220-9964/3/3/1154, 2014.

Brucker, L., Cavalieri, D. J., Markus, T., and Ivanoff, A.: NASA Team 2 sea ice concentration algorithm retrieval uncertainty, IEEE Trans. Geosci. Rem. Sens., 52(11), 7336-7352, https://doi.org/10.1109/TGRS.2014.2311376, 2014.

Cavalieri, D. J.: A microwave technique for mapping thin sea ice, J. Geophys. Res., 99(C6), 12561-12572, 1994.

Cavalieri D. J., Gloersen, P., and Campbell, W. J.: Determination of Sea Ice Parameters With the NIMBUS 7 SMMR, J. Geophys. Res., 89(D4), 5355-5369, 1984.

Cavalieri, D. J., Crawford, J., Drinkwater, M., Emery, W. J., Eppler, D. T., Farmer, L. D., Goodberlet, M., Jentz, R., Milman, A., Morris, C., Onstott, R., Schweiger, A., Shuchman, R., Steffen, K., Swift, C. T., Wackerman, C., and Weaver, R. L.: NASA sea ice validation program for the DMSP SSM/I: final report. NASA Technical Memorandum 104559. National Aeronautics and Space Administration, Washington, D.C., 126 pp., 1992.

Cavalieri, D. J., St. Germain, K. M., and Swift, C. T.: Reduction of weather effects in the calculation of sea ice concentration with the DMSP SSM/I, J. Glaciol., 41(139), 455-464, 1995.

Cavalieri, D. J., Parkinson, C. L., Gloersen, P., Comiso, J. C., and Zwally, H. J.: Deriving long-term time series of sea ice cover from satellite passive-microwave multisensor data sets, J. Geophys. Res., 104(C7), 15803–15814, https://doi.org/10.1029/1999JC900081, 1999.

Cavalieri, D. J., Markus, T., Hall, D. K., Gasiewski, A. J., Klein, M., and Ivanoff, A.: Assessment of EOS Aqua AMSR-E Arctic sea ice concentrations using Landsat-7 and airborne microwave imagery, IEEE Trans. Geosci. Rem. Sens., 44(11), 3057-3069, https://doi.org/10.1109/TGRS.2006.878445, 2006.

Cavalieri, D. J., Markus, T., Hall, D. K., Ivanoff, A., and Glick, E.: Assessment of AMSR-E Antarctic winter sea-ice concentrations using Aqua MODIS, IEEE Trans. Geosci. Rem. Sens., 48(9), 3331-3340, https://doi.org/10.1109/TGRS.2010.2046495, 2010.

Cavalieri, D. J., Markus, T., and Comiso, J. C.: AMSR-E/Aqua daily L3 25km brightness temperature and sea ice concentration polar grids, version 3, Boulder, Colorado USA, NASA National Snow and Ice Data Center Distributed Arctive Archive Center, https://doi.org/10.5067/AMSR-E/AE_SI25.003, [date accessed: 2018-04-26], 2014.

Cho, K., Sasaki, N., Shimoda, H., Sakata, T., and Nishio, F.: Evaluation and improvement of SSM/I sea ice concentration algorithms for the Sea of Okhotsk, J. Rem. Sens. of Japan, 16(2), 47-58, 1996.

Comiso J. C.: Characteristics of arctic winter sea ice from satellite multispectral microwave observations, J. Geophys. Res., 91(C1), 975-994, 1986.

Comiso, J. C.: Large Decadal Decline of the Arctic Multiyear Ice Cover. J. Climate, 25(4), 1176–1193, https://doi.org/10.1175/JCLI-D-11-00113.1, 2012.

Comiso, J. C., and Nishio, F.: Trends in the sea ice cover using enhanced and compatible AMSR-E, SSM/I, and SMMR data, J. Geophys. Res., 113, C02S07, https://doi.org/10.1029/2007JC004257, 2008.

Comiso, J. C., and Steffen, K.: Studies of Antarctic sea ice concentrations from satellite data and their applications, J. Geophys. Res., 106(C12), 31361-31385, 2001.

Comiso, J. C., Cavalieri, D. J., Parkinson, C. L., and Gloersen, P.: Passive microwave algorithms for sea ice concentration: A comparison of two techniques, Rem. Sens. Environ., 60(3), 357-384, 1997.

Comiso, J. C., Cavalieri, D. J., and Markus, T.: Sea ice concentration, ice temperature, and snow depth, using AMSR-E data, IEEE Trans. Geosci. Rem. Sens., 41(2), 243-252, https://doi.org/10.1109/TGRS.2002.808317, 2003.

Comiso, J. C., Meier, W. N., and Gersten, R. A.: Variability and trends in the Arctic Sea ice cover: Results from different techniques, J. Geophys. Res. - Oceans, 122(8), 6883–6900, https://doi.org/10.1002/2017JC012768, 2017a.

Comiso, J. C., Gersten, R. A., Stock, L.V., Turner, J., Perez, G. J., and Cho, K.: Positive trends in the Antarctic sea ice cover and associated changes in surface temperature, J. Climate, 30(6), 2251–2267, https://doi.org/10.1175/JCLI-D-16-0408.1, 2017b.

Ezraty, R., Girard-Ardhuin, F., Piollé, J.-F., Kaleschke, L., and Heygster, G.: Arctic and Antarctic sea ice concentration and Arctic sea ice drift estimated from special sensor microwave data – Users's Manual, Version 2.1, IFREMER, Brest, France, February 2007.

Gloersen, P., Campbell, W., Cavalieri, D. J., Comiso, J. C., Parkinson, C. L., and Zwally, H. J.: Arctic and Antarctic sea ice, 1978-1987: satellite passive-microwave observations and analysis, Scientific and technical information program, vol. NASA SP-511, National Aeronautics and Space Administration (NASA), Washington D.C., 1992.

Ivanova, D. P., Gleckler, P. J., Taylor, K. E., Durack, P. J., and Marvel, K. D.: Moving beyond the total sea ice extent in gauging model biases. J. Clim., 29(24), 8965-8987, https://doi.org/10.1175/JCLI-D-16-0026.1, 2017.

Ivanova, N., Johannessen, O. M., Pedersen, R. T., and Tonboe, R. T.: Retrieval of Arctic sea ice parameters by satellite passive microwave sensors: A comparison of eleven sea ice concentration algorithms, IEEE Trans. Geosci. Rem. Sens., 52(11), 7233-7246, https://doi.org/10.1109/TGRS.2014.2310136, 2014.

Ivanova, N., Pedersen, L. T., Tonboe, R. T., Kern, S., Heygster, G., Lavergne, T., Sørensen, A., Saldo, R., Dybkjær, G., Brucker, L., and Shokr, M.: Inter-comparison and evaluation of sea ice algorithms: towards further identification of challenges and optimal approach using passive microwave observations, The Cryosphere, 9, 1797-1817, https://doi.org/10.5194/tc-9-1797-2015, 2015.

Kaleschke, L., Lüpkes, C., Vihma, T., Haarpaintner, J., Bochert, A., Hartmann, J., and Heygster, G.: SSM/I sea ice remote sensing for mesoscale ocean-atmosphere interaction analysis, Can. J. Rem. Sens., 27(5), 526-537, 2001.

Kern, S.: A new method for medium-resolution sea ice analysis using weather-influence corrected Special Sensor Microwave/Imager 85 GHz data, Int. J. Rem. Sens., 25(21), 4555-4582, https://doi.org/10.1080/01431160410001698898, 2004.

Kern, S., Kaleschke, L., and Clausi, D. A.: A comparison of two 85-GHz SSM/I ice concentration algorithms with AVHRR and ERS-2 SAR imagery, IEEE Trans. Geosci. Rem. Sens., 41(10), 2294-2306, https://doi.org/10.1109/TGRS.2003.817181, 2003.

Kern, S., Kaleschke, L., and Spreen, G.: Climatology of the Nordic (Irminger, Greenland, Barents, Kara and White/Pechora) Seas ice cover based on 85 GHz satellite microwave radiometry: 1992-2008, Tellus, 62A(4), 411-434, https://doi.org/10.1111/j.1600-0870.2010.00457.x, 2010.

Kuuliala, L., Kujala, P., Suominen, M., and Montewka, J.: Estimating operability of ships in ridged ice fields, Cold Reg. Sci. Technol., 135, 51-61, https://doi.org/10.1016/j.coldregions.2016.12.003, 2017.

Kwok, R.: Sea ice concentration estimates from satellite passive microwave radiometry and openings from SAR ice motion, Geophys. Res. Lett., 29(9), 1311, https://doi.org/10.1029/2002GL014787, 2002.

Lavergne, T., Sørensen, A. M., Kern, S., Tonboe, R., Notz, D., Aaboe, S., Bell, L., Dybkjær, G., Eastwood, S., Gabarro, C., Heygster, G., Killie M. A., Brandt Kreiner, M., Lavelle, J., Saldo, R., Sandven, S., and Pedersen, L. T.: Version 2 of the EUMETSAT OSI SAF and ESA CCI sea-ice concentration climate data records, The Cryosphere, 13(1), 49-78, https://doi.org/10.5194/tc-13-49-2019, 2019.

Maass, N., and Kaleschke, L.: Improving passive microwave sea ice concentration algorithms for coastal areas: applications to the Baltic Sea, Tellus, 62A(4), 393-410, https://doi.org/10.1111/j.1600-0870.2010.00452.x, 2010.

Markus, T., and Burns, B. A.: A method to estimate subpixel-scale coastal polynyas with satellite passive microwave data, J. Geophys. Res., 100(C3), 4473-4487, 1995.

Markus, T., and Cavalieri, D. J.: An enhancement of the NASA Team sea ice algorithm, IEEE Trans. Geosci. Rem. Sens., 38(3), 1387-1398, 2000.

Markus, T., and Dokken, S. T.: Evaluation of late summer passive microwave Arctic sea ice retrievals, IEEE Trans. Geosci. Rem. Sens., 40(2), 348-356, 2002.

Meier, W. N.: Comparison of passive microwave ice concentration algorithm retrievals with AVHRR imagery in Arctic peripheral seas, IEEE Trans. Geosci. Rem. Sens., 43(6), 1324-1337, https://doi.org/10.1109/TGRS.2005.846151, 2005.

Meier, W. N., and Steward, J. S.: Assessing uncertainties in sea ice extent climate indicators, Environ. Res. Lett., 14, 035005, https://doi.org/10.1088/1748-9326/aaf52c, 2019.

Meier, W. N., and Windnagel, A.: Sea ice concentration – climate algorithm theoretical basis document, NOAA Climate Data Record Program CDRP-ATBD-0107 Rev. 7 (03/062018), available at https://www.ncdc.noaa.gov/cdr/oceanic/sea-ice-concentration, 2018.

Meier, W. N., Hovelsrud, G. K., van Oort, B. E. H., Key, J. R., Kovacs, K. M., Michel, C., Haas, C., Granskog, M. A., Gerland, S., Perovich, D. K., Makshtas, A., and Reist, J. D.: Arctic sea ice in transformation: A review of recent observed changes and impacts on biology and human activity, Rev. Geophys., 51, 185-217, https://doi.org/10.1002/2013RG000431, 2014.

Meier, W. N., Fetterer, F., Savoie, M., Mallory, S., Duerr, R., and Stroeve, J.: *NOAA/NSIDC Climate Data Record of Passive Microwave Sea Ice Concentration, Version 3*. Boulder, Colorado USA. NSIDC: National Snow and Ice Data Center, https://doi.org/10.7265/N59P2ZTG, [Date accessed: 2019-02-07], 2017.

Melia, N., Haines, K., Hawkins, E., and Day, J. J.: Towards seasonal Arctic shipping route predictons, Environ. Res. Lett., 12(8), 084005, https://doi.org/10.1088/1748-9326/aa7a60, 2017.

Niederdrenk, A. L., and Notz, D.: Arctic sea ice in a 1.5°C warmer world, Geophys. Res. Lett., 45(4), 1963-1971, https://doi.org/10.1002/2017GL076159, 2018.

Notz, D.: Sea-ice extent and its trend provide limited metrics of model performance, The Cryosphere, 8(1), 229-243, https://doi.org/10.5194/tc-8-229-2014, 2014.

Njoku, E. G., Rague, B., and Fleming, K.: The Nimbus-7 SMMR Pathfinder Brightness Temperature Data Set, Jet Propulsion Laboratory Publication, Pasadena, USA, 98-4, 1998.

Ozsoy-Cicek, B., Xie, H., Ackley, S. F., Ye, K.: Antarctic summer sea ice concentration and extent: comparison of ODEN 2006 ship observations, satellite passive microwave and NICsea ice charts, The Cryosphere, 3, 1-9, https://doi.org/10.5194/tc-3-1-2009, 2009.

Pedersen, L. T., Saldo, R., Ivanova, N., Kern, S., Heygster, G., Tonboe, R. T., Huntemann, M., Ozsoy, B., Girard-Ardhuin, F., and Kaleschke, L.: Reference dataset for sea ice concentration, https://doi.org/10.6084/m9.figshare.6626549.v6, https://figshare.com/articles/Reference_dataset_for_sea_ice_concentration/6626549, 2019.

Peng, G., Meier, W. N., Scott, D., and Savoie, M.: A long-term and reproducible passive microwave sea ice concentration data record for climate studies and monitoring, Earth Syst. Sci. Data, 5, 311-318, https://doi.org/10.5194/essd-5-311-2013, 2013.

Petty, A. A., Stroeve, J. C., Holland, P. R., Boisvert, L. N., Bliss, A. C., Kimura, N., and Meier, W. N.: The Arctic sea ice cover of 2016: a year of record-low highs and higher-than-expected lows, The Cryosphere, 12(2), 433-452, https://doi.org/10.5194/tc-12-433-2018, 2018.

Pizzolato, L., Howell, S. E. L., Dawson, J., Laliberte, F., and Copland, L.: The influence of declining sea ice on shipping activity in the Canasian Arctic, Geophys. Res. Lett., 43(23), 12146-12154, https://doi.org/10.1002/2016GL071489, 2016.

Reid, P., Stammerjohn, S., Massom, R., Scambos, T., and Lieser, J. L.: The record 2013 Southern Hemisphere sea-ice extent maximum, Ann. Glaciol., 56(69), 99-106, https://doi.org/10.3189/2015AoG69A892, 2015.

Schlosser, E., Haumann, F. A., and Raphael, M. N.: Atmospheric influences on the anomalous 2016 Antarctic sea ice decay, The Cryosphere, 12(3), 1103-1119, https://doi.org/10.5194/tc-12-1103-2018, 2018.

Smith, D. M.: Extraction of winter total sea ice concentration in the Greenland and Barents Seas from SSM/I data, Int. J. Rem. Sens., 17(13), 2625-2646, 1996.

Smith D. M., and Barrett, E. C.: Satellite mapping and monitoring of sea ice, CB/RAE/9/2/4/2034/113/ARE, RSU, University of Bristol, Bristol, UK, 1994.

Spreen, G., Kaleschke, L., and Heygster, G., Sea ice remote sensing using AMSR-E 89-GHz channels, J. Geophys. Res., 113, C02S03, https://doi.org/10.1029/2005JC003384, 2008.

Svendsen, E., Mätzler, C., and Grenfell, T. C.: A model for retrieving total sea ice concentration from a spaceborne dual-polarized passive microwave instrument operating near 90 GHz, Int. J. Rem. Sens., 8(10), 1479-1487, 1987.

Stuecker, M. F., Bitz, C. M., and Armour, K. C.: Conditions leading to the unprecedented low Antarctic sea ice extent during the 2016 austral spring season, Geophys. Res. Lett., 44, 9008-9019, https://doi.org/10.1002/2017GL074691, 2017.

Tonboe, R. T., Eastwood, S., Lavergne, T., Sørensen, A. M., Rathmann, N., Dybkjær, G., Pedersen, L. T., Høyer, J. L., and Kern, S.: The EUMETSAT sea ice concentration climate data record, The Cryosphere, 10, 2275-2290, https://doi.org/10.5194/tc-10-2275-2016, 2016.

Turner, J., Hosking, J. S., Phillips, T., and Marshall, G. J.: Temporal and spatial evolution of the Antarctic sea ice prior to the September 2012 record maximum extent, Geophys. Res. Lett., 40, 5894-5898, https://doi.org/10.1002/2013GL058371, 2013.

Turner, J., Phillips, T., Marshall, G. J., Hosking, J. S., Pope, J. O., Bracegirdle, T. J., and Deb, P.: Unprecedented springtime retreat of Antarctic sea ice in 2016, Geophys. Res. Lett., 44, 6868-6875, https://doi.org/10.1002/2017GL073656, 2017.

Wayand, N. E., Bitz, C. M., and Blanchard-Wrigglesworth, E.: A year-round subseasonal-to-seasonal sea ice prediction portal, Geophys. Res. Lett., 46(6), 3298-3307, https://doi.org/10.1029/2018GL0816565, 2019.

Wiebe, H., Heygster, G., and Markus, T.: Comparison of the ASI ice concentration algorithm with Landsat-7 ETM+ and SAR imagery, IEEE Trans. Geosci. Rem. Sens., 47(9), 3008-3015, https://doi.org/10.1109/TGRS.2009.2026367, 2009.

Worby, A. P., and Allison, I. A.: Ship-Based Technique for Observing Antarctic Sea Ice: Part I: Observational Techniques and Results, Research Report No. 14, Antarctic Cooperative Research Centre, Hobart, TAS, Australia, 1999.

Worby, A. P., and Comiso, J. C.: Studies of the Antarctic sea ice edge and ice extent from satellite and ship observations, Rem. Sens. Environ., 92, 98-111, 2004.

Worby, A. P., and Dirita, V.: A technique for making ship-based observations of Antarctic sea-ice thickness and characteristics - Part II: User Operating Manual, Research Report No. 14, Antarctic Cooperative Research Centre, Hobart, TAS, Australia, 1999.

Worby, A. P., Geiger, C. A., Paget, M. J., Van Woert, M. L., Ackley, S. F., and DeLiberty, T. L.: The thickness distribution of Antarctic sea ice. J. Geophys. Res., 2008, 113, https://doi.org/10.1029/2007JC004254, 2008.

Tables

Table 1. Overview of relevant multi-channel satellite microwave sensors.

sensor	relevant frequencies [GHz]	operation periods
Scanning Multichannel Microwave Radiometer (SMMR)	6.6, 10.7, 18.0, 21.0, 37.0	1978-10-25 – 1987-08-20
Special Sensor Microwave/Imager (SSM/I)	19.4, 22.2, 37.0, 85.5	1987-07-09 – today
Special Sensor Microwave Imager and Sounder (SSMIS)	19.4, 22.2, 37.0, 91.7	2003-10-18 – today
Advanced Microwave Scanning Radiometer on EOS (AMSR-E)	6.9, 10.7, 18.7, 23.8, 36.5, 89.0	2002-05-05 – 2011-10-04
Advanced Microwave Scanning Radiometer 2 (AMSR2)	6.9, 7.3, 10.7, 18.7, 23.8, 36.5, 89.0	2012-05-18 – today

Table 2. Overview of the investigated sea-ice concentration products. Column "ID (Algorithm)" holds the identifier we use henceforth to refer to the data record, and which algorithm it uses. Group is an identifier for the retrieval concept used. Column "Input data" refers to the input satellite data for the data set. Column "Open water filter" refers to whether weather-related spurious sea-ice concentrations in open water and low concentration areas are filtered. Weather filters do not remove weather related noise over areas with near 100% sea-ice concentration. Column "Atmospheric correction" refers to correcting the input TBs for a potential inherent weather influence using additional independent weather information. Column "ErrorUncertainties" refers to provision of sea-ice concentration uncertainties, and "Period" is the time period for which we use the data set, given as StartYearStartMonth-EndYearEndMonth.

ID (algorithm)	Group	Input data & frequencies	Grid resolution & type	Open water filter	Atmospheric correction	ErrorUncertainties	Period
OSI-450 (SICCI2)	I	SMMR, SSM/I, SSMIS 19.35 & 37.0 GHz	25 km x 25 km EASE2.0	Yes	Yes	Yes	197901-201512
SICCI-12km (SICCI2)	I	AMSR-E, AMSR2 18.7 & 89.0 GHz	12.5 km x 12.5 km EASE2.0	Yes	Yes	Yes	200205-201705
SICCI-25km (SICCI2)	I	AMSR-E, AMSR2 18.7 & 36.5 GHz	25 km x 25 km EASE2.0	Yes	Yes	Yes	200205-201705
SICCI-50km (SICCI2)	I	AMSR-E, AMSR2 6.9 & 36.5 GHz	50 km x 50 km EASE2.0	Yes	Yes	Yes	200205-201705
ASI-SSMI (ASI)	III	SSM/I, SSMIS 85.5 GHz	12.5 km x 12.5 km PolarStereo	Yes	No	No	199201-201812
CBT-AMSRE (Comiso-Bootstrap)	II	AMSR-E 18.7 & 36.5 GHz	25 km x 25 km PolarStereo	Yes	No	No	200205-201109
CBT-SSMI (Comiso-Bootstrap)	II	SMMR, SSM/I, SSMIS 19.35 & 37.0 GHz	25 km x 25 km PolarStereo	Yes	No	No	197810-201712
NT1-SSMI (NASA-Team)	III	SMMR, SSM/I, SSMIS 19.35 & 37.0 GHz	25 km x 25 km PolarStereo	No	No	No	197810-201712
NOAA-CDR (Comiso-Bootstrap & NASA-Team)	II	SSM/I, SSMIS 19.35 & 37.0 GHz	25 km x 25 km PolarStereo	Yes	No	Yes	198708-201712
NT2-AMSRE (NASA-Team-2)	IV	AMSR-E 18.7, 36.5 & 89.0 GHz	25 km x 25 km PolarStereo	Yes	Yes	No	200205-201109

Table 3. Inter-comparison results to near-100% SIC (RRDP2) for the Arctic (see Fig. 14 a). Rows "Gaussian": Mean difference of modal value of Gaussian fit to satellite SIC ≤ 99% (compare Fig. 3) minus near-100% reference SIC (RRDP2 SIC) ± one sigma of the Gaussian fit (see Fig. 14 a). Rows "'Non-truncated": Mean difference satellite SIC minus RRDP2 SIC ± one standard deviation of the difference for SICCI and OSI-450 products. Rows "Truncated": Mean difference of satellite SIC constrained to a maximum value of 100% minus RRDP2 SIC ± one standard deviation of the difference. All values in these rows are given in percent sea-ice concentration. Values in rows denoting the periods 2007-2015 and 2007-2011, contain the number of valid data pairs. See text for meaning of * in column "NT2-AMSRE".

Group	I				III		II			IV
NH	SICCI-12km	SICCI-25km	SICCI-50km	OSI-450	ASI-SSMI	NT1-SSMI	CBT-SSMI	NOAA-CDR	CBT-AMSRE	NT2-AMSRE
2007-2015	23262	23262	23262	23343	23343	23343	23343	23037	--	--
Gaussian	-2.4±5.2	-1.2±3.1	-0.5±1.9	-1.0±3.0	-4.1±3.6	+0.1±5.2	+1.4±4.5	+2.7±4.6	--	--
Non-truncated	-4.2±5.9	-2.2±3.7	-0.5±2.1	-1.9±3.6	--	--	--	--	--	--
Truncated	-4.8±5.2	-2.7±3.1	-1.1±1.5	-2.4±3.0	-4.5±3.5	-2.6±4.5	-1.1±1.9	-0.7±1.6	--	--
2007-2011	13351	13351	13351	13432	13432	13432	13432	13126	13344	13344
Gaussian	-2.4±5.0	-1.0±2.9	-0.4±1.9	-0.8±2.8	-3.7±3.7	+0.9±4.6	+1.3±3.6	+3.5±5.0	+1.0±3.9	-0.7±1.7*
Non-truncated	-4.2±5.4	-2.0±3.5	-0.6±2.0	-1.7±3.3	--	--	--	--	--	--
Truncated	-5.0±5.0	-2.8±3.1	-1.4±1.6	-2.2±2.7	-3.9±3.1	-1.9±3.7	-0.9±1.7	-0.6±1.4	-1.1±1.8	-0.9±1.0

Table 4. As Table 3 but for the Antarctic (see Fig. 14 b).

Group	I				III		II			IV
SH	SICCI-12km	SICCI-25km	SICCI-50km	OSI-450	ASI-SSMI	NT1-SSMI	CBT-SSMI	NOAA-CDR	CBT-AMSRE	NT2-AMSRE
2007-2015	6397	6397	6397	6449	6449	6449	6449	6430	--	--
Gaussian	-0.7±3.7	-1.1±3.0	-0.3±2.5	-1.1±3.1	-6.2±3.9	-5.1±5.9	+0.2±4.5	+0.8±4.4		
Non-truncated	-0.7±4.0	-1.4±4.0	-0.7±2.4	-1.5±3.8	--	--	--	--	--	--
Truncated	-1.9±2.9	-2.3±3.0	-1.3±1.7	-2.3±2.9	-6.5±4.0	-6.0±5.5	-1.7±2.4	-1.3±2.1	--	--
2007-2011	5896	5896	5896	5896	5896	5896	5896	5877	5896	5896
Gaussian	-0.6±4.2	-1.1±3.0	-0.3±2.5	-1.1±3.1	-5.6±4.0	-5.4±6.5	-0.2±4.6	+0.9±4.5	+0.2±5.4	-0.2±3.2*
Non-truncated	-0.7±3.9	-1.5±3.8	-0.8±2.4	-1.5±3.7	--	--	--	--	--	--
Truncated	-2.1±2.9	-2.6±3.1	-1.6±1.9	-2.2±2.8	-6.4±4.0	-5.8±5.5	-1.7±2.4	-1.3±2.1	-1.8±2.5	-0.3±0.5

Table 5. Summary of the statistics of the comparison between daily mean ship-based and satellite SIC data (see Fig. 15, black symbols) for – from top to bottom - the entire year, only winter and only summer. DIFF is the mean difference satellite minus ship-based SIC, SDEV is the respective standard deviation; R^2 is the squared linear correlation coefficient. All concentration values are given in percent.

Group	I				III		II			IV
All year	SICCI-12km	SICCI-25km	SICCI-50km	OSI-450	ASI-SSMI	NT1-SSMI	CBT-SSMI	NOAA-CDR	CBT-AMSRE	NT2-AMSRE
DIFF	-6.9	-7.8	-7.3	-7.3	-5.4	-13.8	+0.4	+0.6	-0.7	-0.7
SDEV	12.0	12.1	12.4	12.9	16.1	14.5	13.4	13.3	12.9	13.3
R^2	0.784	0.781	0.775	0.734	0.647	0.693	0.737	0.745	0.778	0.767
Winter										
DIFF	-7.4	-7.4	-6.2	-7.4	-8.6	-14.2	<|0.1|	-0.2	-1.5	-0.3
SDEV	12.6	11.8	11.8	12.8	17.4	13.8	10.9	11.6	12.6	11.5
R^2	0.558	0.594	0.606	0.591	0.429	0.507	0.595	0.587	0.551	0.595
Summer										
DIFF	-6.7	-8.0	-7.9	-7.3	-3.7	-13.6	+0.7	+0.9	-0.3	-0.9
SDEV	11.7	12.3	12.7	12.9	15.1	14.9	14.5	14.0	13.1	14.1
R^2	0.814	0.793	0.780	0.754	0.722	0.702	0.734	0.750	0.806	0.771

Table 6. As Table 5 but for the Antarctic (see Fig. 16, black symbols).

Group	I				III		II			IV
All year	SICCI-12km	SICCI-25km	SICCI-50km	OSI-450	ASI-SSMI	NT1-SSMI	CBT-SSMI	NOAA-CDR	CBT-AMSRE	NT2-AMSRE
DIFF	-3.0	-4.4	-3.1	-3.8	-3.3	-11.0	-1.8	-2.3	-1.4	+4.5
SDEV	13.4	13.8	14.0	13.7	15.7	14.8	15.2	15.5	14.8	16.9
R^2	0.763	0.745	0.737	0.733	0.671	0.698	0.711	0.716	0.755	0.679
Winter										
DIFF	-1.6	-2.7	-2.6	-3.2	-3.6	-11.6	-1.6	-2.0	+0.2	+3.8
SDEV	9.8	9.6	10.5	10.5	10.6	11.7	10.7	11.0	9.5	10.7
R^2	0.771	0.771	0.741	0.731	0.659	0.700	0.748	0.751	0.753	0.732
Summer										
DIFF	-3.9	-5.6	-3.4	-4.2	-3.1	-10.6	-2.0	-2.5	-2.5	+5.0
SDEV	15.3	16.1	16.0	15.6	18.4	16.6	17.7	17.9	17.4	20.0
R^2	0.698	0.666	0.675	0.667	0.614	0.640	0.643	0.651	0.693	0.621

Table 7. Summary of hypothetic daily average sea-ice concentrations from Figure 17 for top: the pack ice case (a) and bottom the marginal ice zone (MIZ) (b). Left two columns: sea-ice concentrations as shown in Figure 17; middle two columns: illustration of the effect of sea-ice concentration under-estimation for thin ice; right two columns: illustration of the effect of sea-ice concentration over-estimation, e.g. thick ice with a wet snow cover (top), or of sea-ice concentration under-estimation, e.g. MIZ during end of summer (bottom).

Pack ice, a)	Lead is open water		Lead is thin ice; Satellite underestimates by 20%		Lead is open water; ice surface properties cause 5% over-estimation on 50% of the ice	
	Ship	Satellite	Ship	Satellite	Ship	Satellite
Day 1	48	92	100	98	48	96
Day 2	100	95	100	99	100	98
Day 3	68	90	100	97	68	95
MIZ, b)			50% of sea ice is thin ice; Satellite underestimates by 20%		50% of sea ice is soaked wet; Satellite fails to see this as ice	
	Ship	Sat	Ship	Satellite	Ship	Satellite
Day 1	35	40	35	36	35	20
Day 2	67	38	67	35	67	19
Day 3	63	63	63	57	63	44

Figures

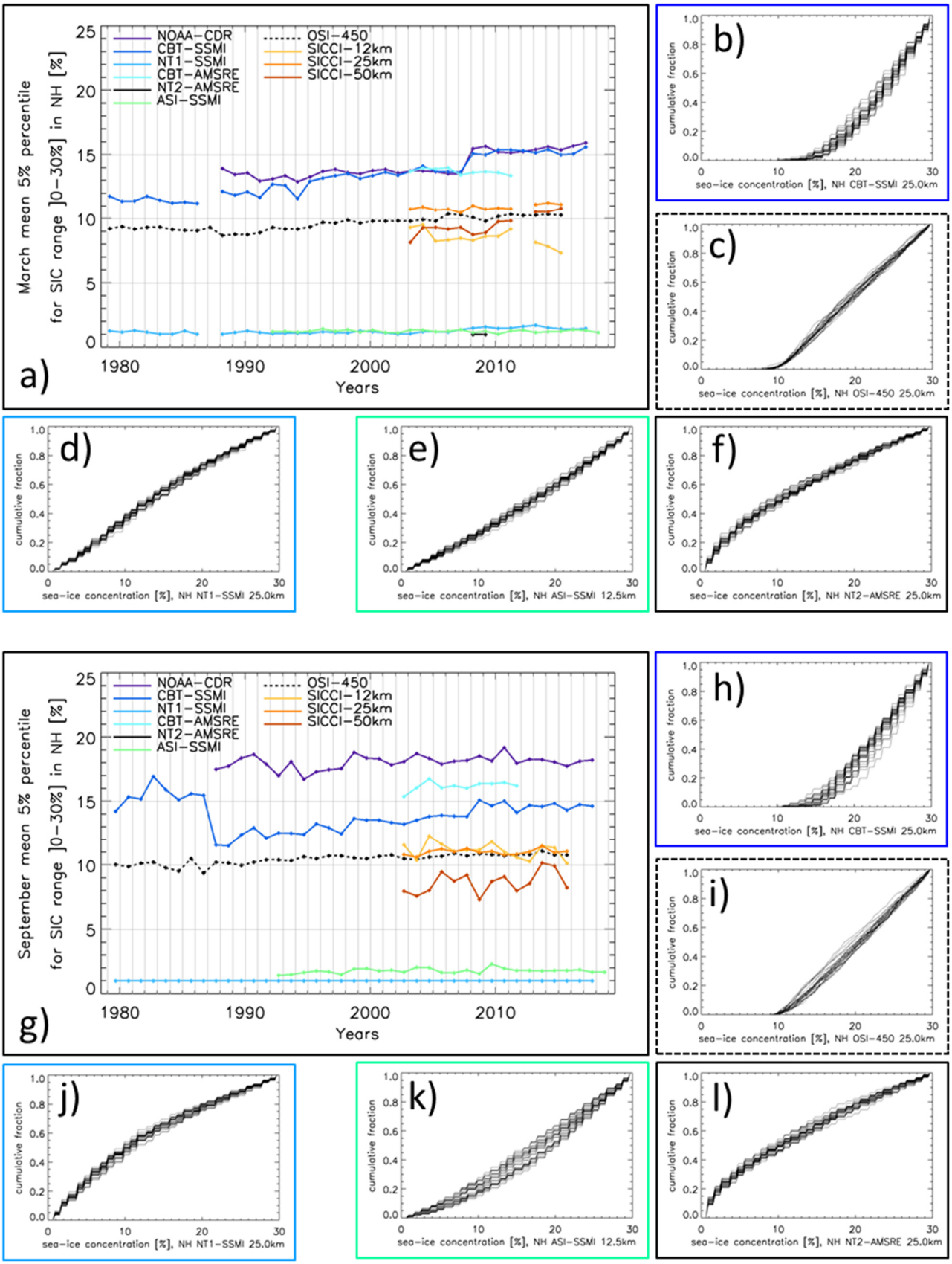

Figure 1. Time series of the monthly mean 5%-percentile sea-ice concentration of the range]0.0% to 30.0%] for the Arctic in~~for~~ **(a)** March and **(g)** September for all ten products. **(b)** to **(f)** and **(h)** to **(l)** Daily cumulative sea-ice concentration distributions of five selected products in~~for~~ these two months, respectively, in~~for~~ a sample year: 2004. See Table 2 for the time periods with data from the respective products.

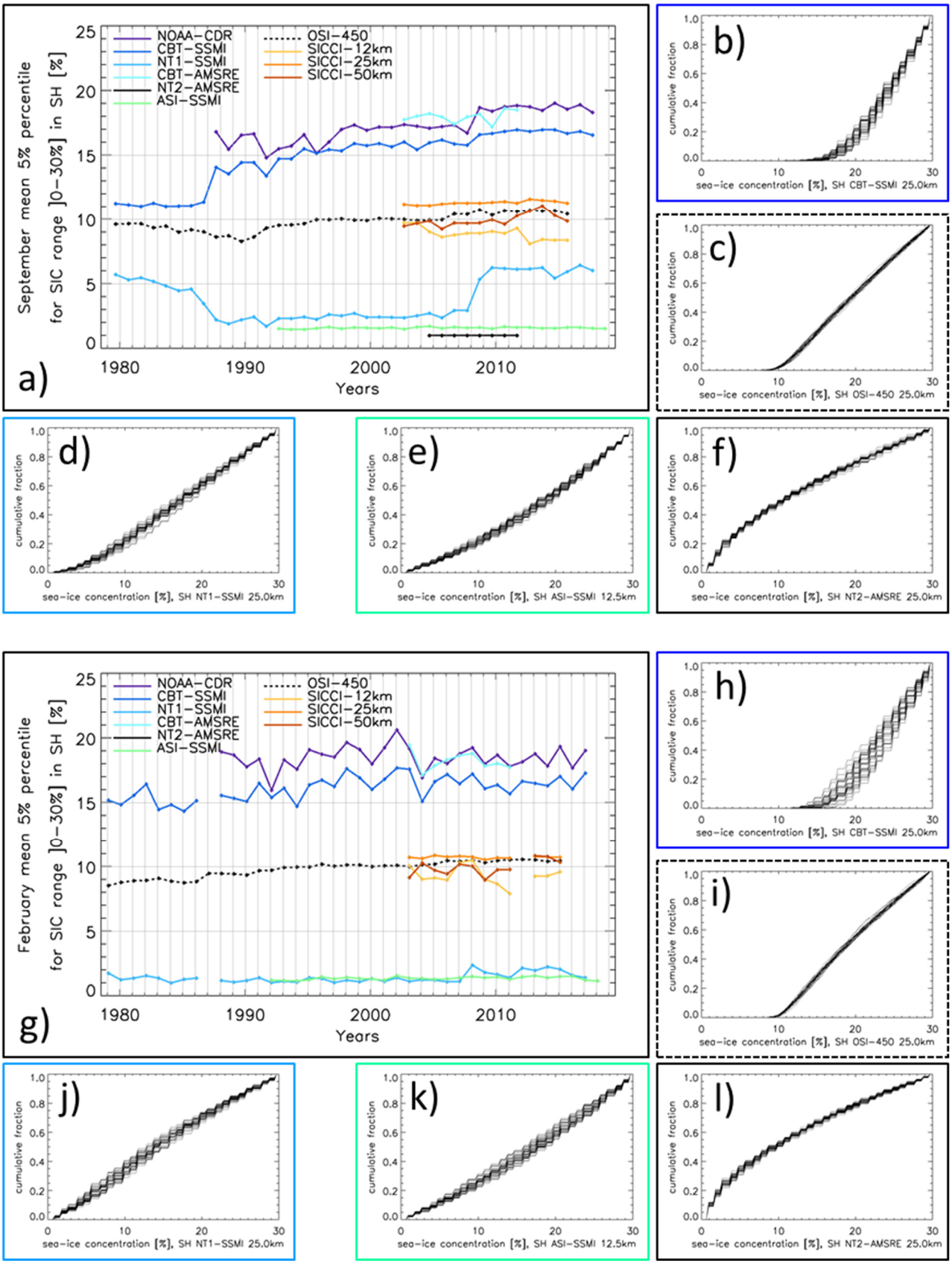

Figure 2. Time series of the monthly mean 5%-percentile sea-ice concentration of the range]0.0% to 30.0%] for the Antarctic in~~for~~ **(a)** September and **(g)** February for all ten products. **(b)** to **(f) and (h)** to **(l)** Daily cumulative sea-ice concentration distributions of five selected products ~~for~~in these two months, respectively, in~~for~~ a sample year: 2004. See Table 2 for the time periods with data from the respective products.

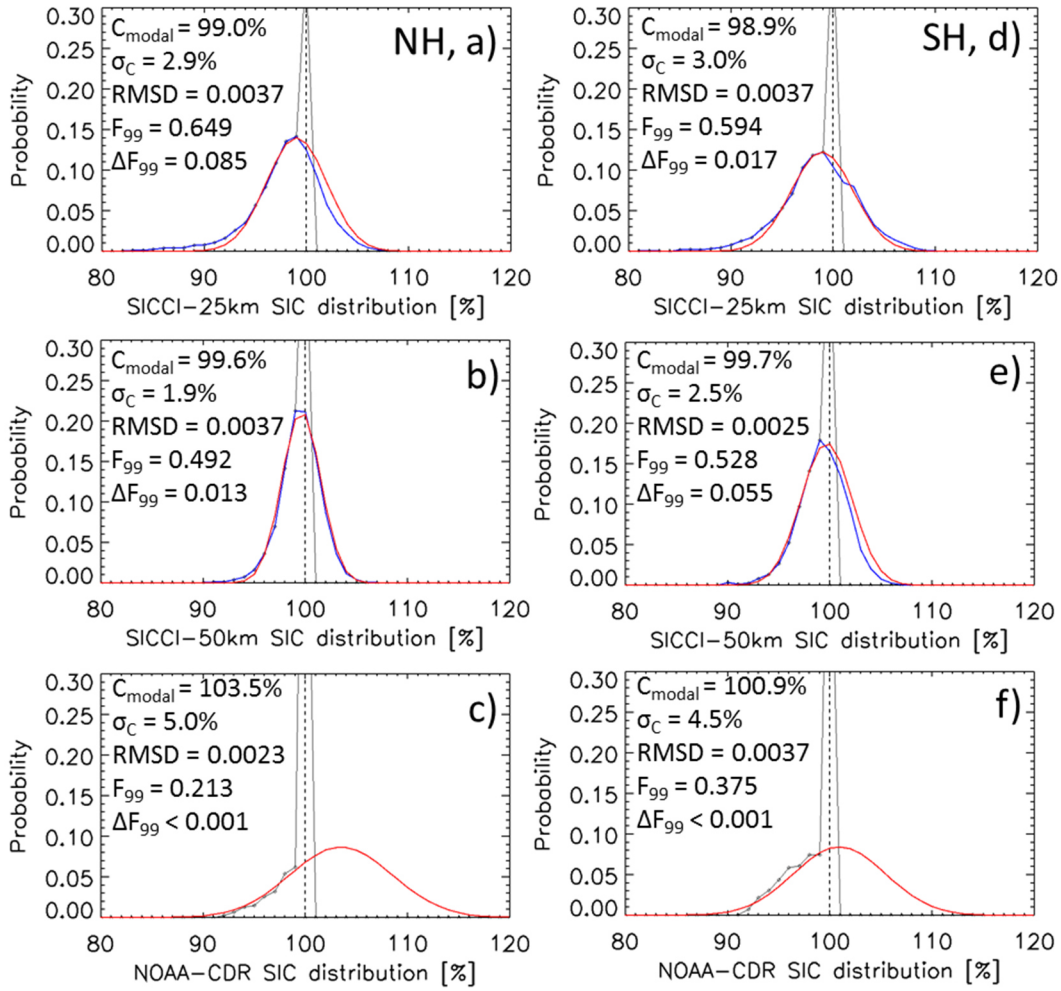

Figure 3. Examples of the sea-ice concentration distribution at near-100% reference sea-ice concentration locations. Black symbols and lines show values cut off at 100%; blue lines denote the original distribution (for SICCI-25km and SICCI-50km only); red lines denote the distribution resulting from the Gaussian fit to values of the distribution ≤ 99%. In each panel, ~~image~~ the modal sea-ice concentration (= center of the Gaussian fit: C_{modal}), the standard deviation of the fit σ_C and fit parameters with respect to the fraction of the distribution ≤ 99% (F_{99}, ΔF_{99}, see text for more explanation) and the root-mean-squared difference (RMSD) between original and fitted probability are given. **(a)** to **(c)** Arctic, **(d)** to **(f)** Antarctic. See Appendix H for Fig. H1 and Fig. H2 containing plots of this kind for all ten products.

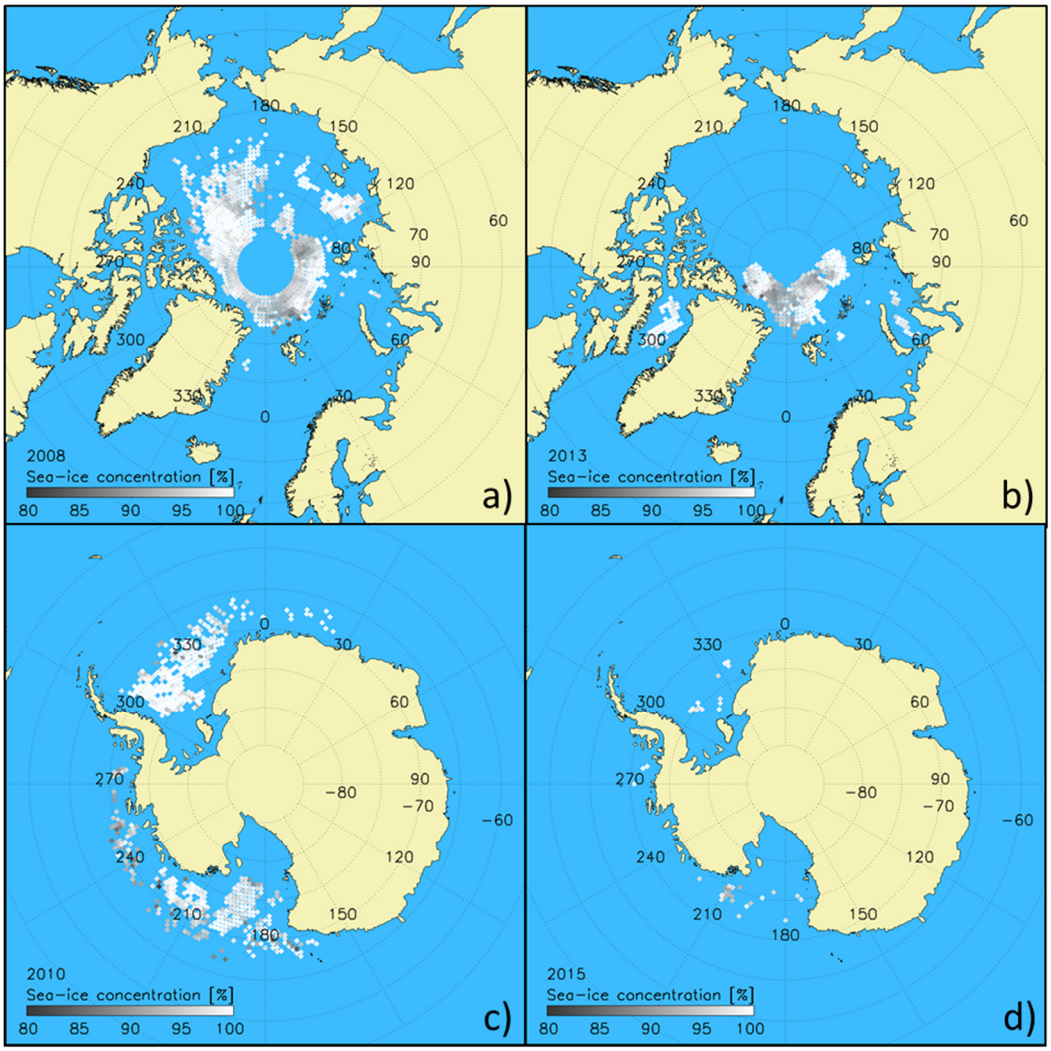

Figure 4. Illustration of the typical distribution of near-100% SIC reference data by means of the co-located OSI-450 sea-ice concentration for~~in~~ **(a,b)** the Arctic and **(c,d)** the Antarctic for~~in~~ a year with good (left) and poor (right) data coverage.

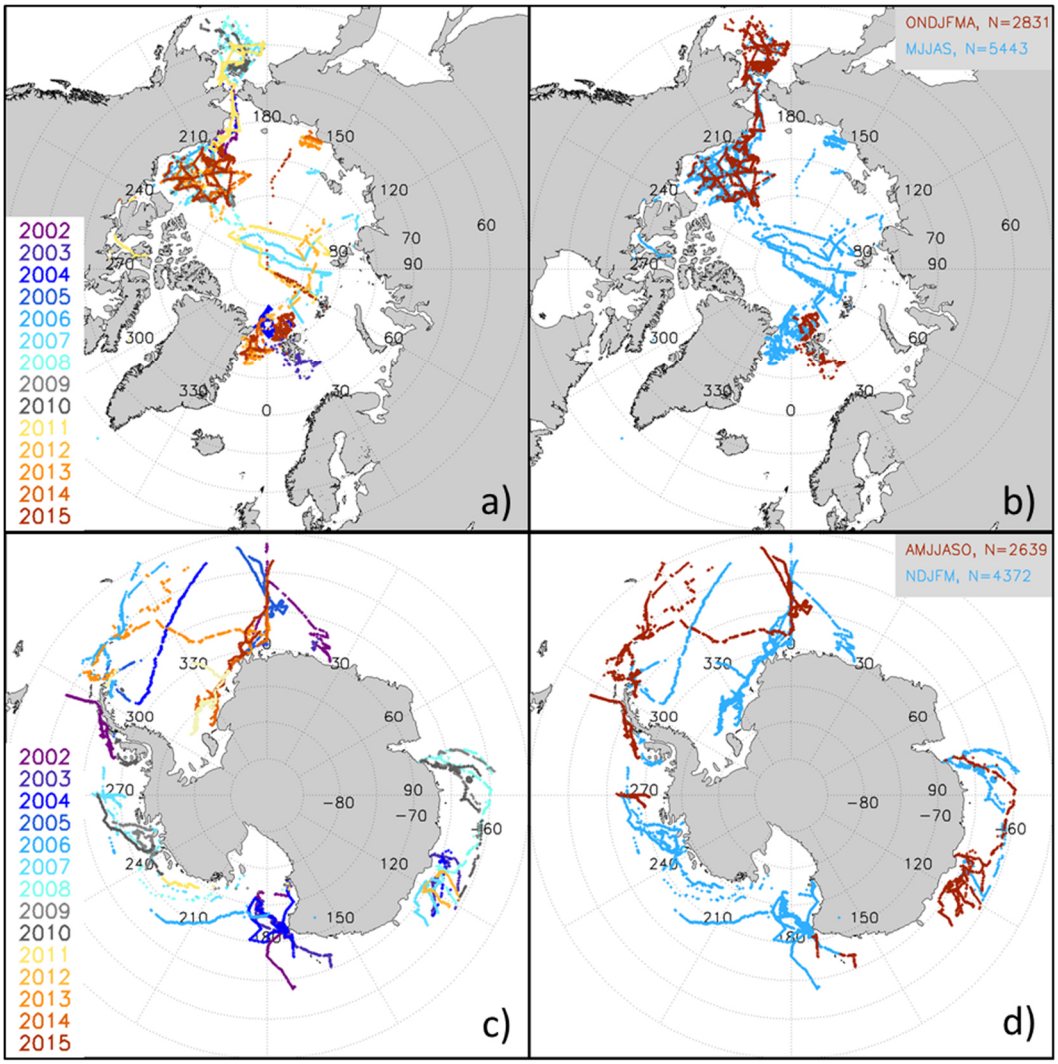

Figure 5. Spatiotemporal distribution of the ship tracks ~~in~~for **(a,b)** the Arctic and **(c,d)** the Antarctic from which ship-based visual observations of the sea-ice cover were used. Maps on the left illustrate the years, maps on the right distinguish between winter (red) and summer (cyan) months.

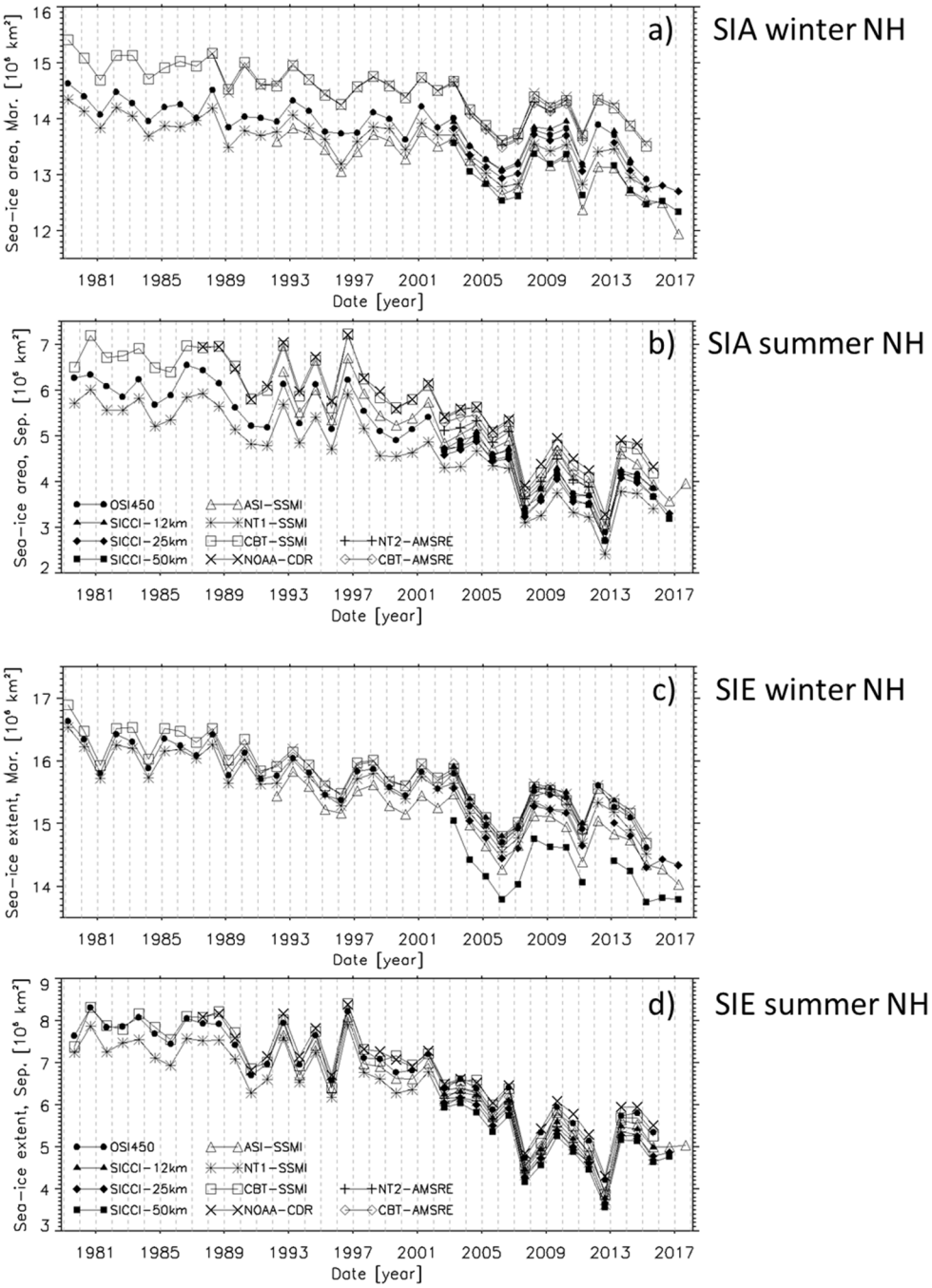

Figure 6. Arctic sea-ice area **(a,b)** and extent **(c,d)** computed ~~for~~in **(a,c)** winter (March) and **(b,d)** summer (September) from the sea-ice concentration data sets used. See Table 2 for start and end month of the respective time series.

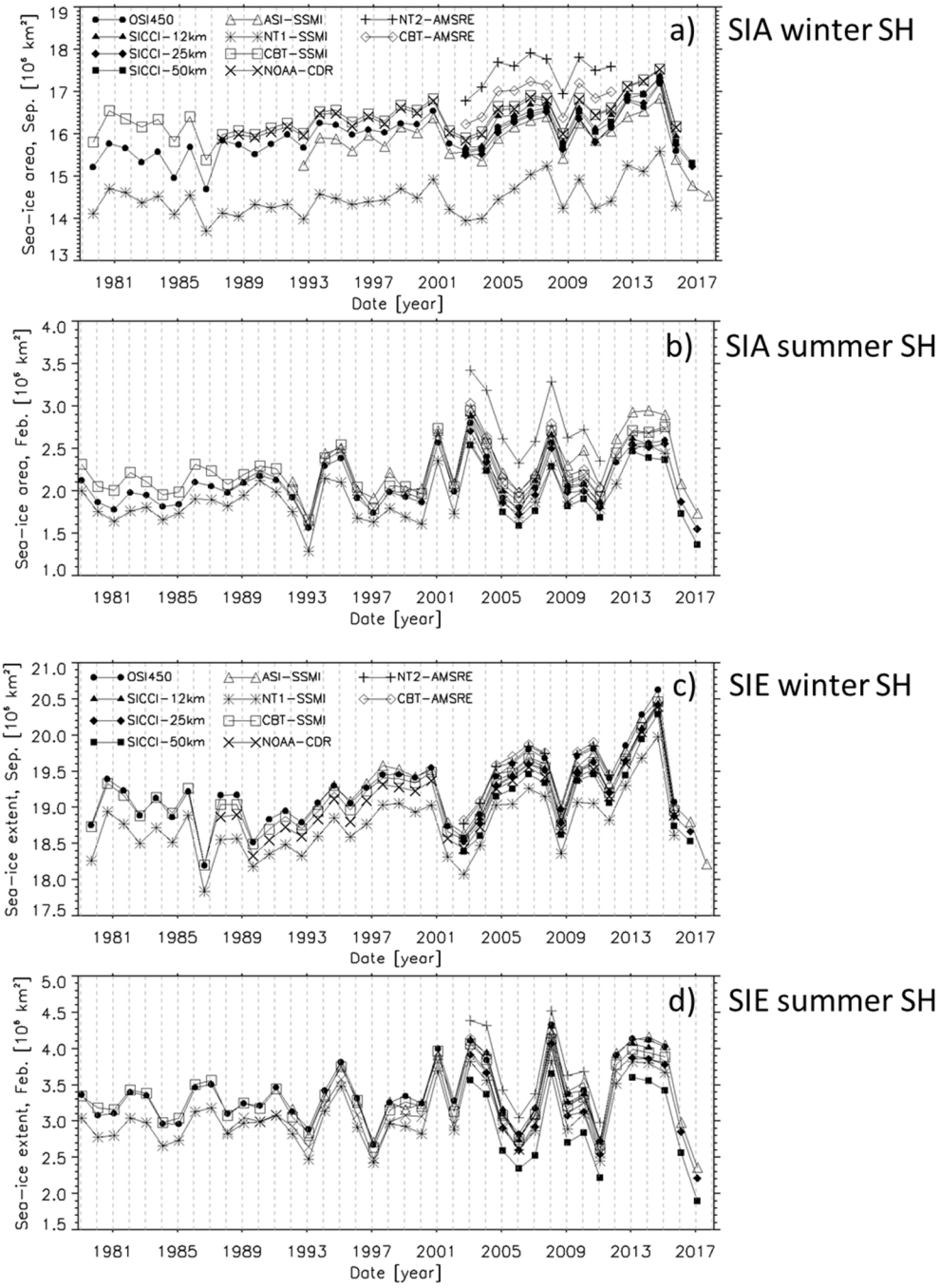

Figure 7. As Fig. 6 but for the Antarctic.

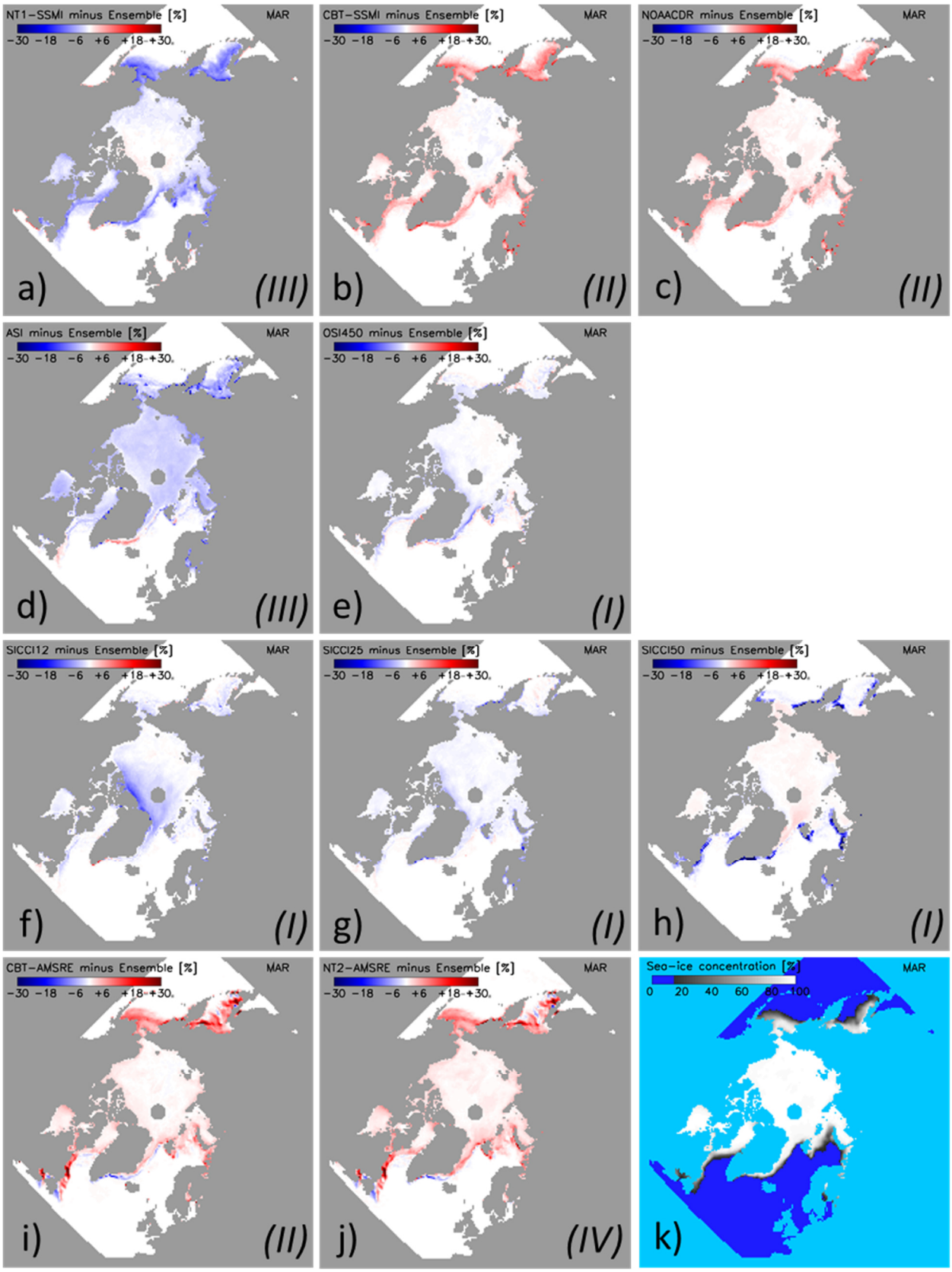

Figure 8. (a) to **(j)** Maps of the difference between the multi-annual average monthly SIC of the individual algorithms and the 10-algorithm ensemble median multi-annual average monthly SIC **(k)** for the Arctic in winter~~for~~ (March) 2003-2011. Differences are only computed for sea-ice concentration of both data sets > 15%. Roman numbers I to IV denote the group assigned to the respective algorithm (see text for details).

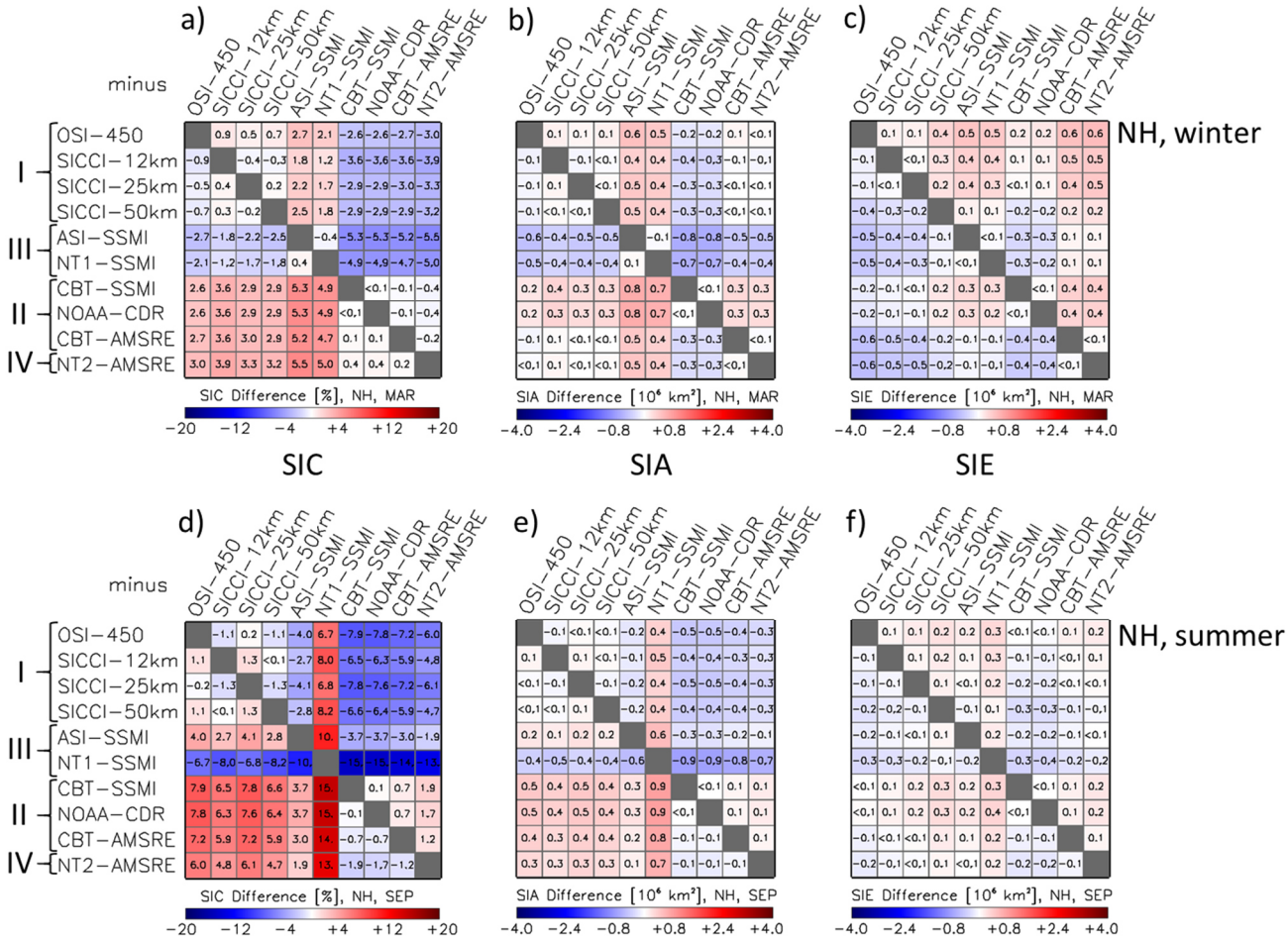

Figure 9. Differences (row minus column) between all ten products of, from left to right, the average sea-ice concentration SIC, average SIA, and average SIE for the Arctic (NH) ~~for~~in winter **(a)** through **(c)** and summer **(d)** through **(f)**. The averages are computed from monthly mean values of the respective months (MARch, SEPtember) of the AMSR-E period 06/2002 to 09/2011. All data are on EASE 2.0 grid with 50 km grid resolution. The land-mask of the SICCI-50km product is applied to all products. Roman numbers I to IV denote groups according to Table 2. For matrices of all remaining months we refer to Fig. G1 through Fig. G3 in Appendix G.

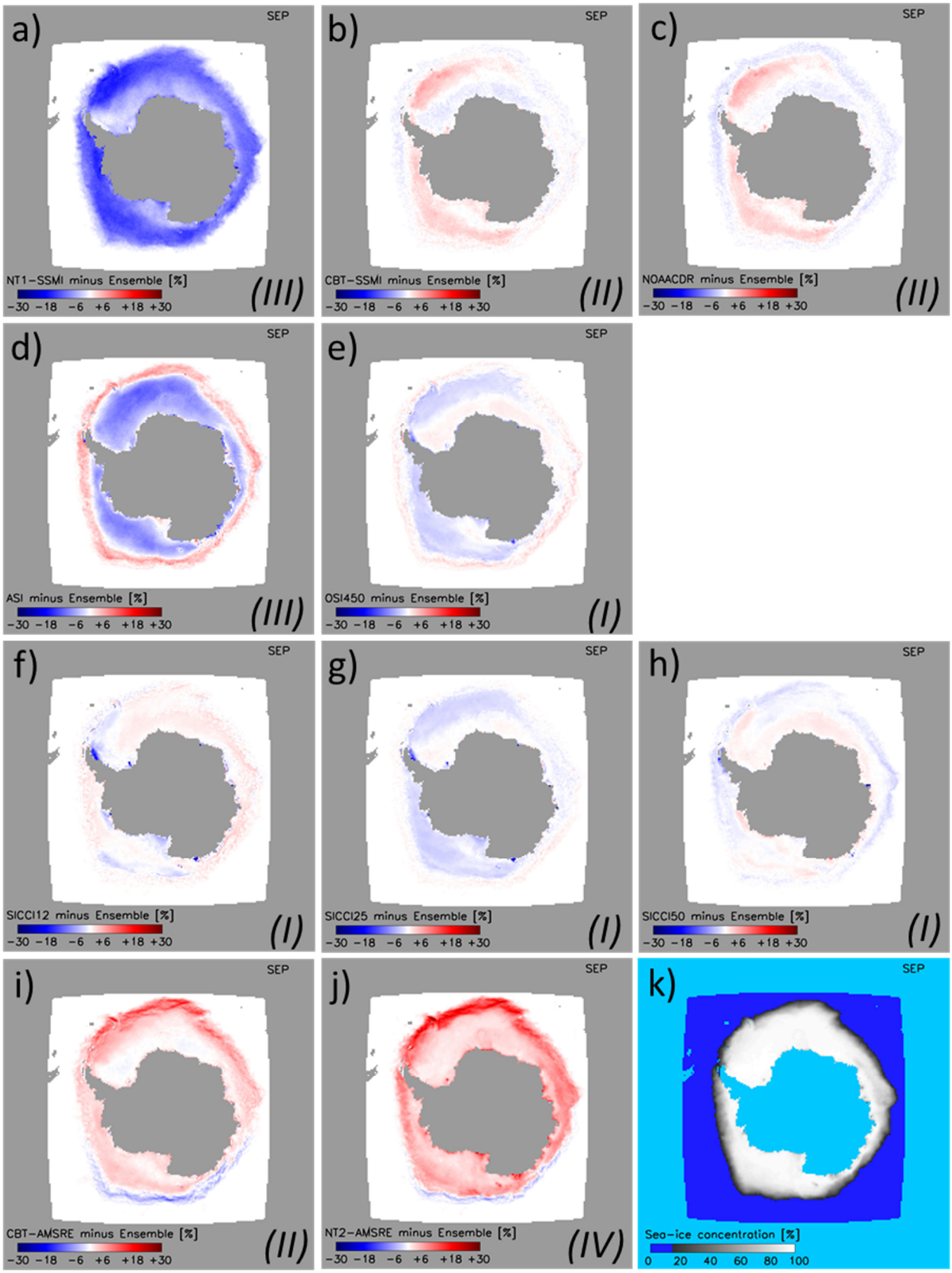

Figure 10. (a) to **(j)** Maps of the difference between the multi-annual average monthly SIC of the individual algorithms and the 10-algorithm ensemble median multi-annual average monthly SIC **(k)** for the Antarctic in winter~~for~~ (September) 2002-2011. Differences are only computed for sea-ice concentration of both data sets > 15%. Roman numbers I to IV denote the group assigned to the respective algorithm (see text for details).

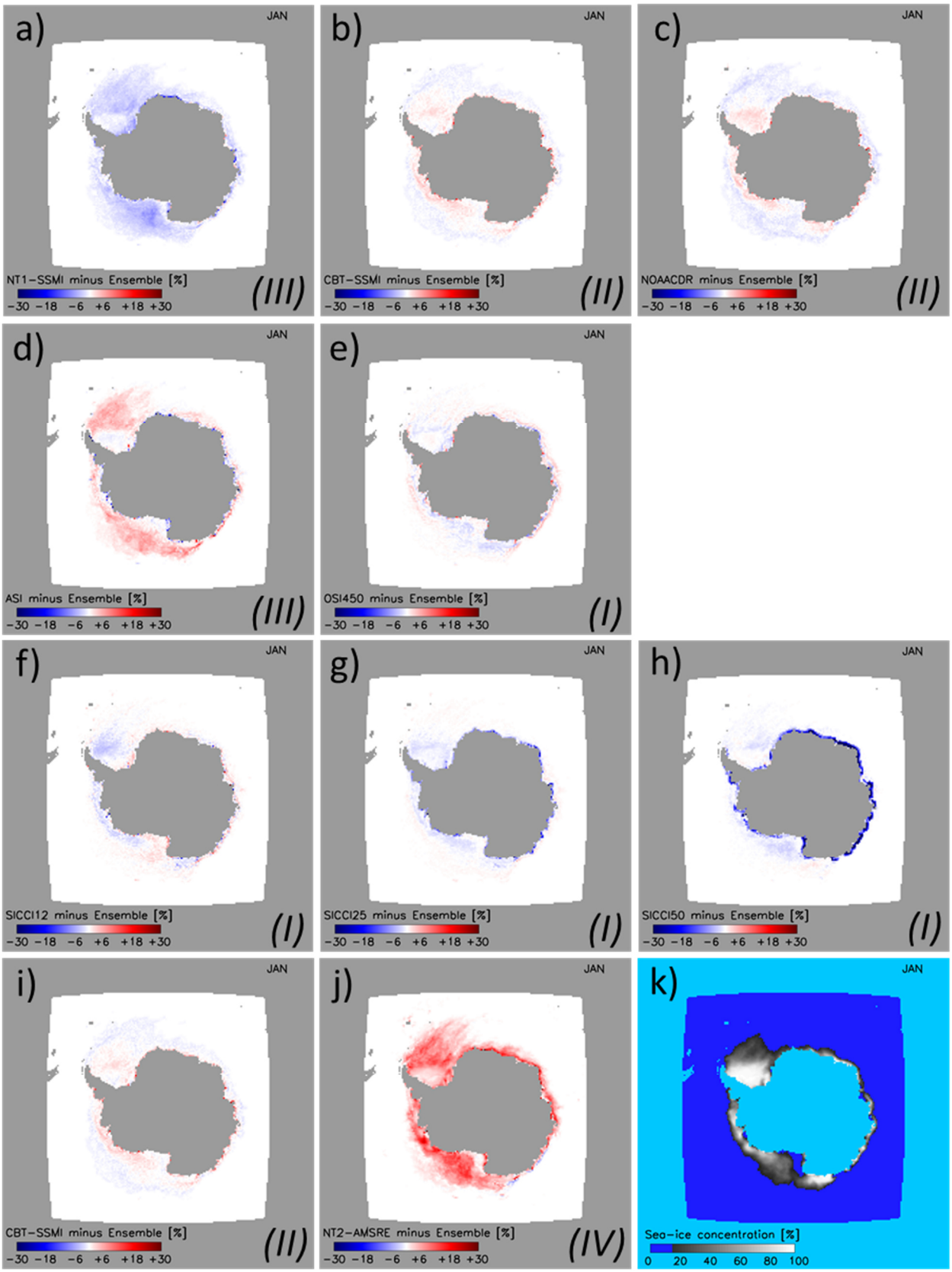

Figure 11. As Fig. 10 but in summer~~for~~ (January) 2003-2011.

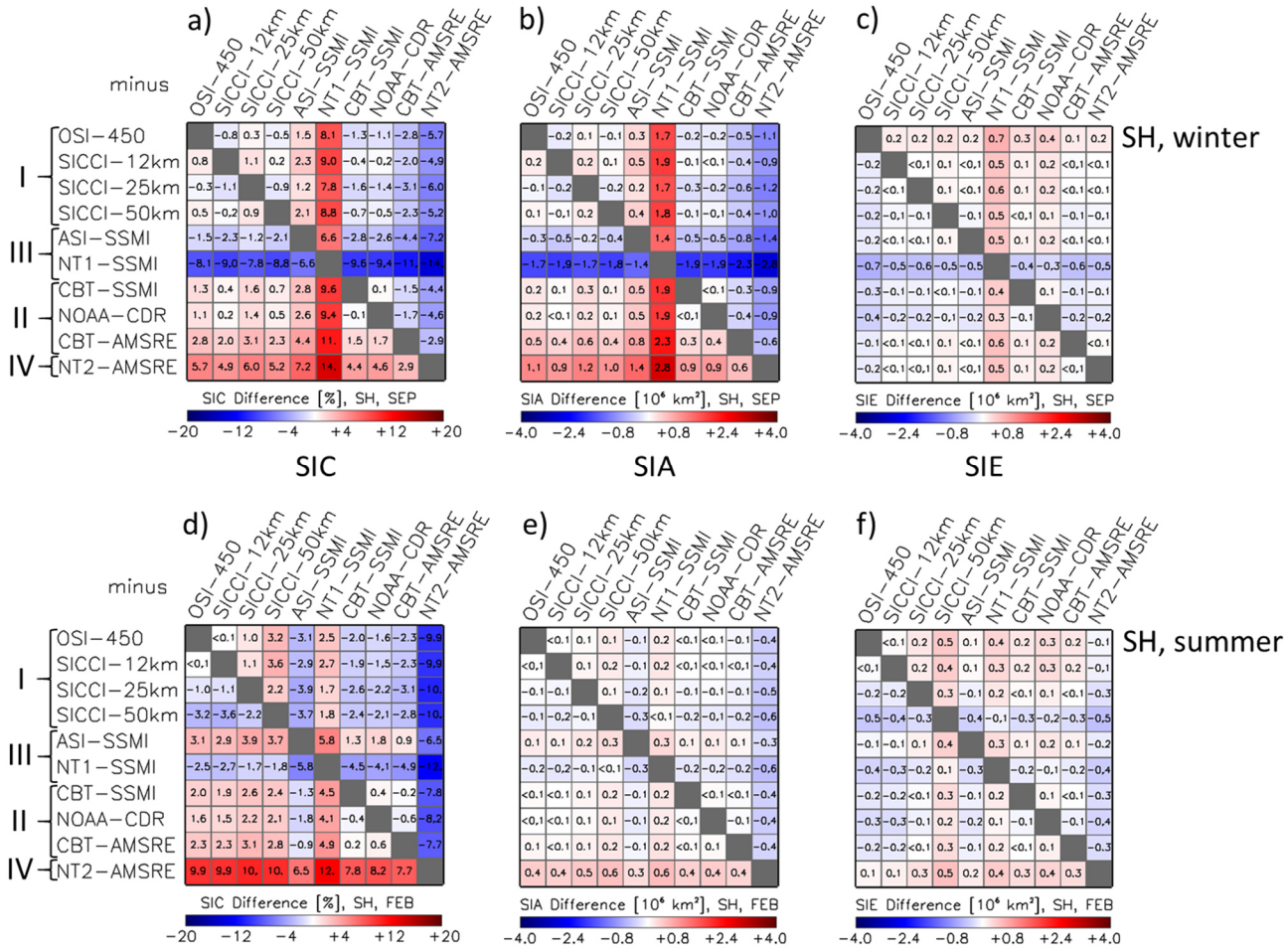

Figure 12. Differences (row minus column) between all ten products of, from left to right, the average sea-ice concentration SIC, average SIA, and average SIE for the Antarctic (SH) ~~for~~in winter **(a)** through **(c)** and summer **(d)** through **(f)**. The averages are computed from monthly mean values of the respective months (SEPtember, FEBruary) of the AMSR-E period 06/2002 to 09/2011. All data are on EASE 2.0 grid with 50 km grid resolution. The land-mask of the SICCI-50km product is applied to all products. Roman numbers I to IV denote groups according to Table 2. For matrices of all remaining months we refer to Fig. G4 through Fig. G6 in Appendix G.

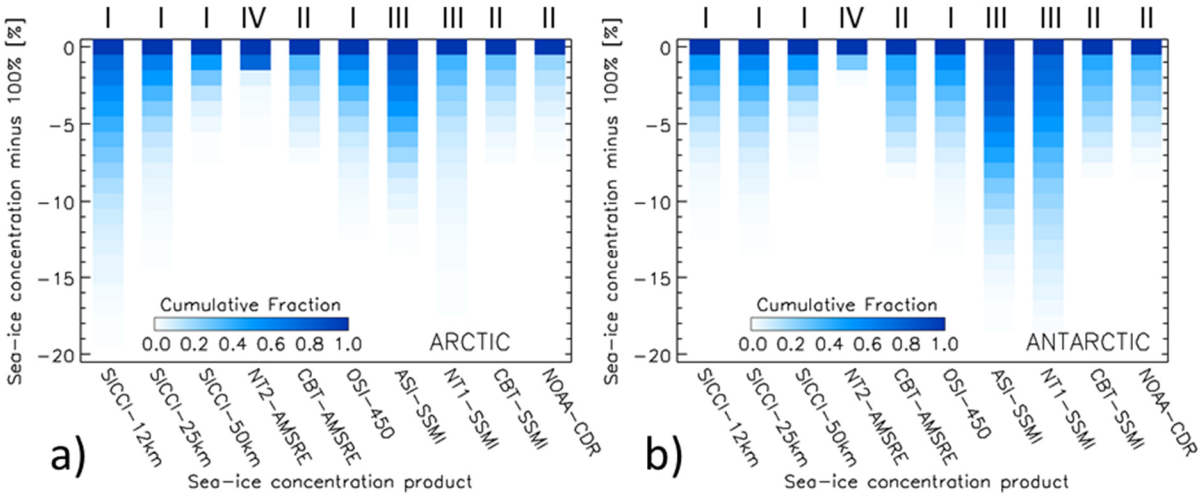

Figure 13. Cumulative distribution of the SIC difference to 100% at the near-100% reference SIC locations for all ten algorithms based on data ~~for~~of years 2007 through 2011 for **(a)** the Arctic, and **(b)** the Antarctic. Roman numbers at the top denote product groups (see Table 2).

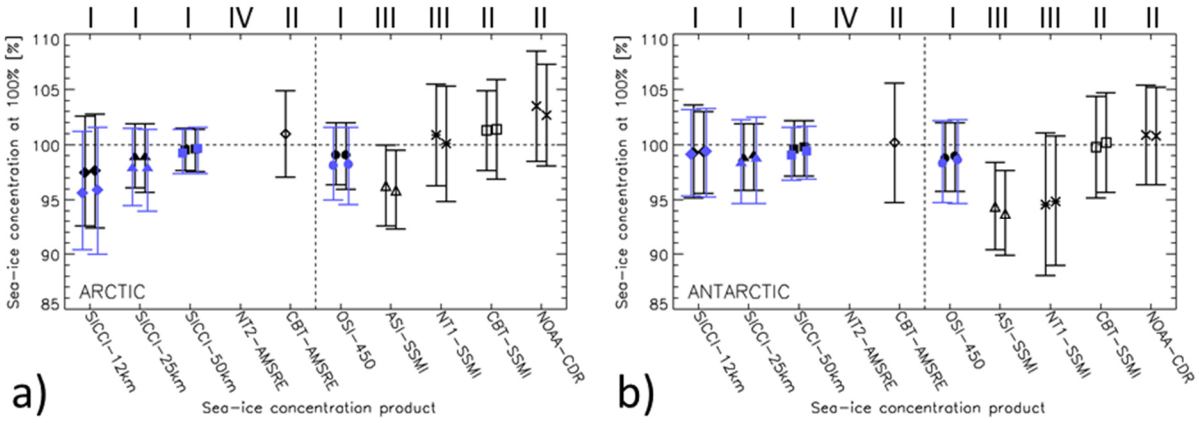

Figure 14. Summary of the results of the inter-comparison to the near-100% reference SIC (RRDP2) for **(a)** the Arctic and **(b)** the Antarctic. Shown for each sea-ice concentration product in black is the center of the Gaussian fit of the sea-ice concentration ≤ 99% at the respective RRDP2 locations (see Fig. 43). Bars denote ± one standard deviation of the Gaussian fit. For symbol pairs (all products but CBT-AMSRE and NT2-AMSRE) the left symbol is based on data of ~~denotes results for~~ years 2007-2011, the right one on data of ~~for~~ years 2007-2015. Blue symbols denote the mean non-truncated sea-ice concentration at the near-100% reference SIC for OSI-450 and SICCI products; blue bars denote the respective sea-ice concentration standard deviation. Roman numbers at the top denote product groups (see Table 2). No values are shown for NT2-AMSRE, because a Gaussian fit could not be adequately applied.

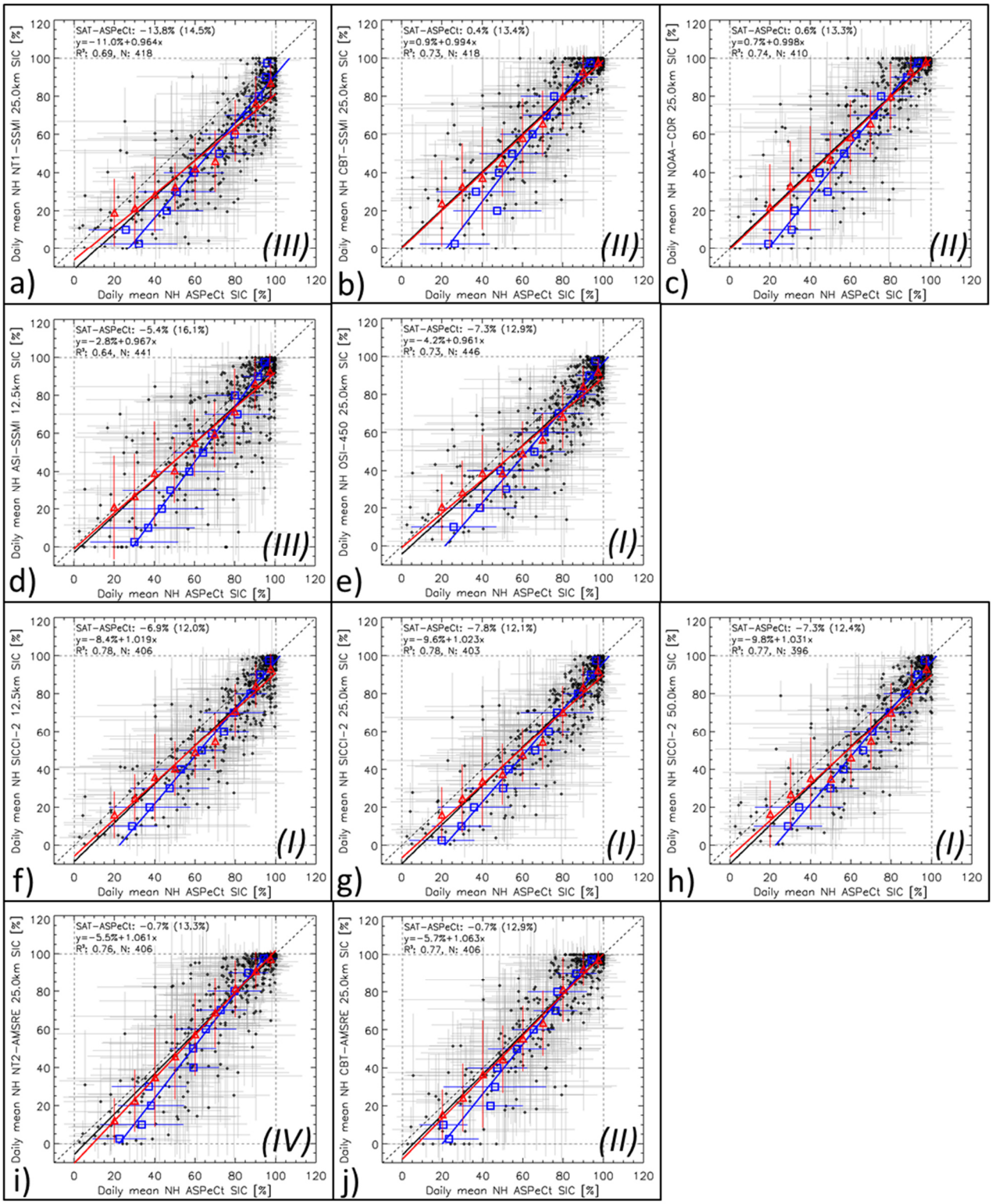

Figure 15. Scatterplots of co-located daily average SIC from visual ship-based observations (ASPeCt, x-axis, note that these are ASSIST/IceWatch for the Arctic) and the ten satellite SIC algorithm products (SAT, y-axes) for the Arctic during~~for~~ years 2002-2011. Red symbols denote the average satellite SIC binned into 10% ASPeCt SIC intervals (except 0 … 5% and 95% … 100%, where 5% bins are used). Blue symbols denote the average ASPeCt SIC binned into 10% satellite SIC intervals, respectively. Error bars denote one standard deviation of the average. Dotted lines denote the identity line~~1-to-1 fit~~. Solid lines denote the linear regression of the respective value pairs. The mean difference and the standard deviation, the linear regression equation, the number of valid data pairs (N), and the squared linear correlation coefficient (R^2) is given in the top left or every image for the daily SIC values. Roman numbers I to IV denote the group assigned to the respective algorithm (see text for details).

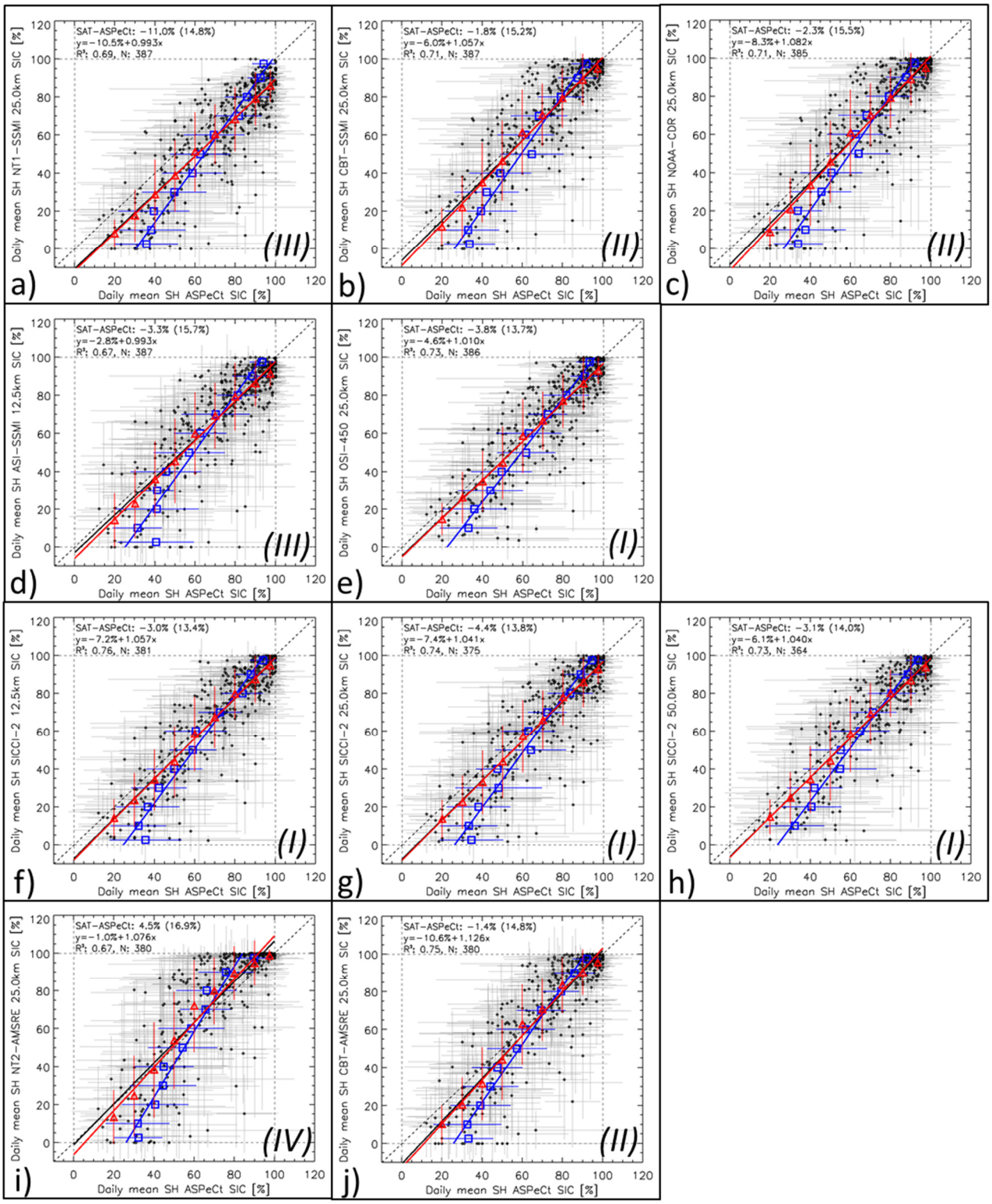

Figure 16. As Fig. 15 but for the Antarctic.

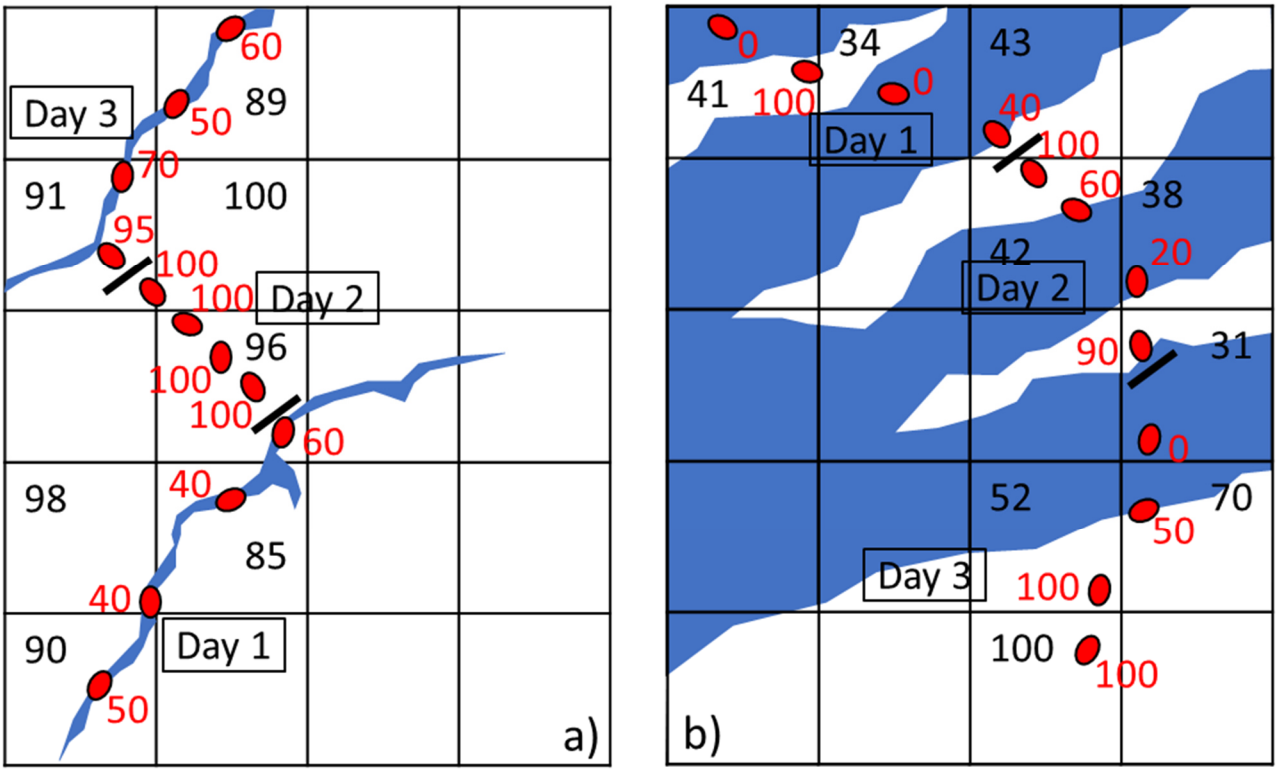

Figure 17. Illustration of the representativity of ship-based observations (red ellipses and numbers) compared to gridded satellite observations (black grid and numbers) for a) close pack ice with leads and b) an open sea-ice cover in the marginal ice zone. Size of ellipses is in scale with the grid-cell size of 25 km by 25 km. Short black bars denote transitions between days. See also Table 7.

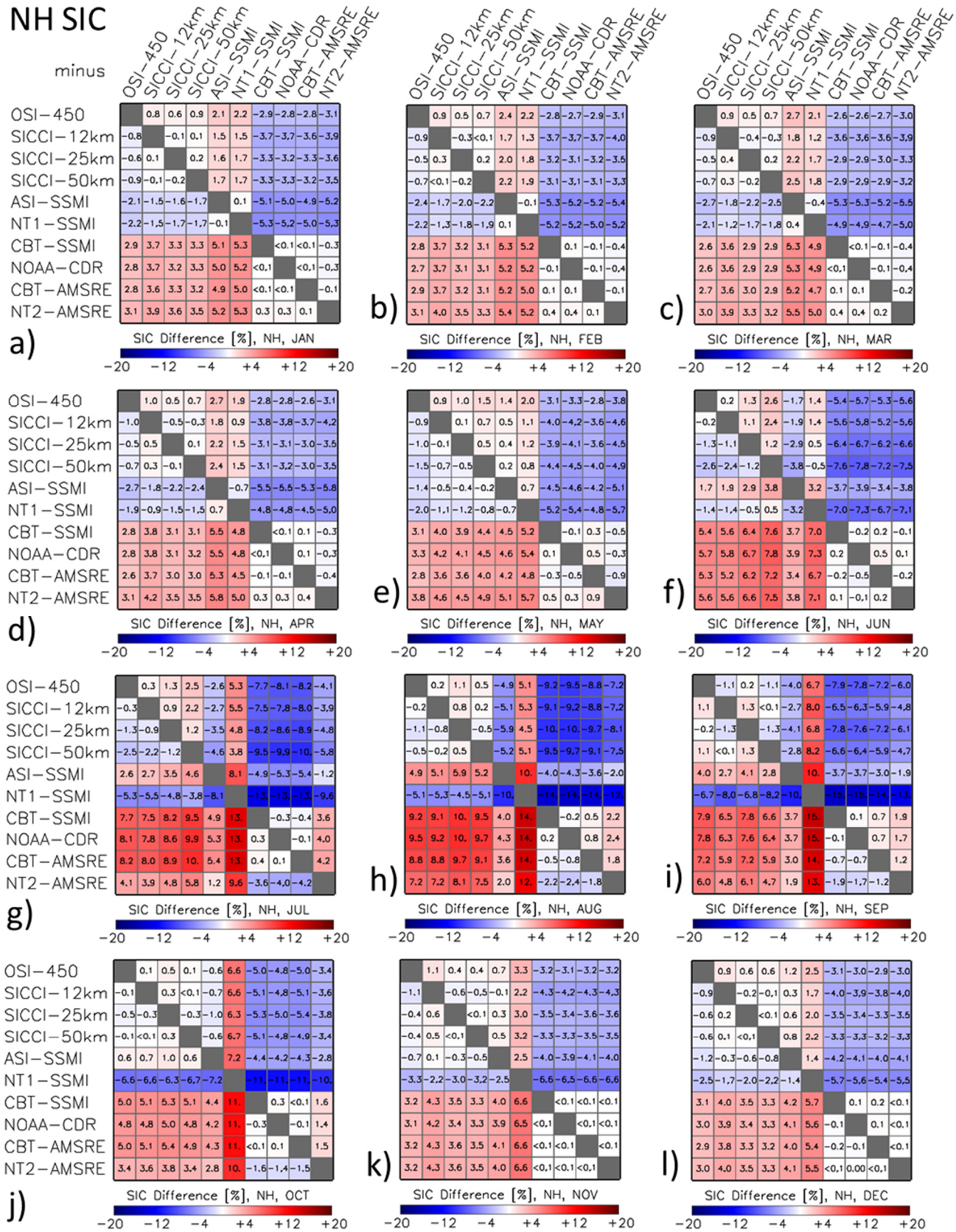

Figure G1. Differences between all ten products of the average sea-ice concentration for the Arctic. The averages are computed from monthly mean values of the respective months of the AMSR-E period 06/2002 to 09/2011. All data are on EASE 2.0 grid with 50 km grid resolution. The land-mask of the SICCI-50km product is applied to all products.

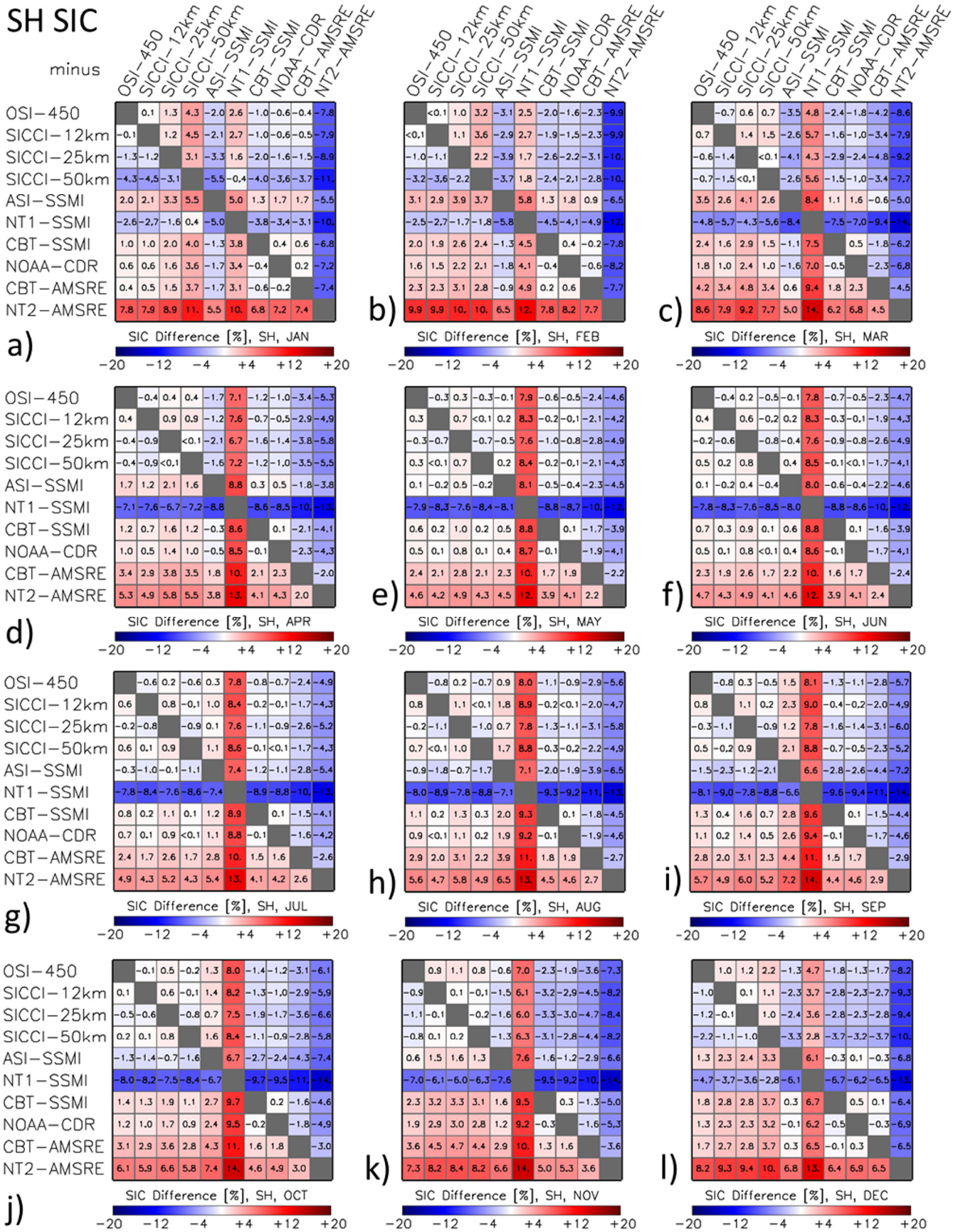

Figure G4. As Fig. G1 but for the Antarctic.

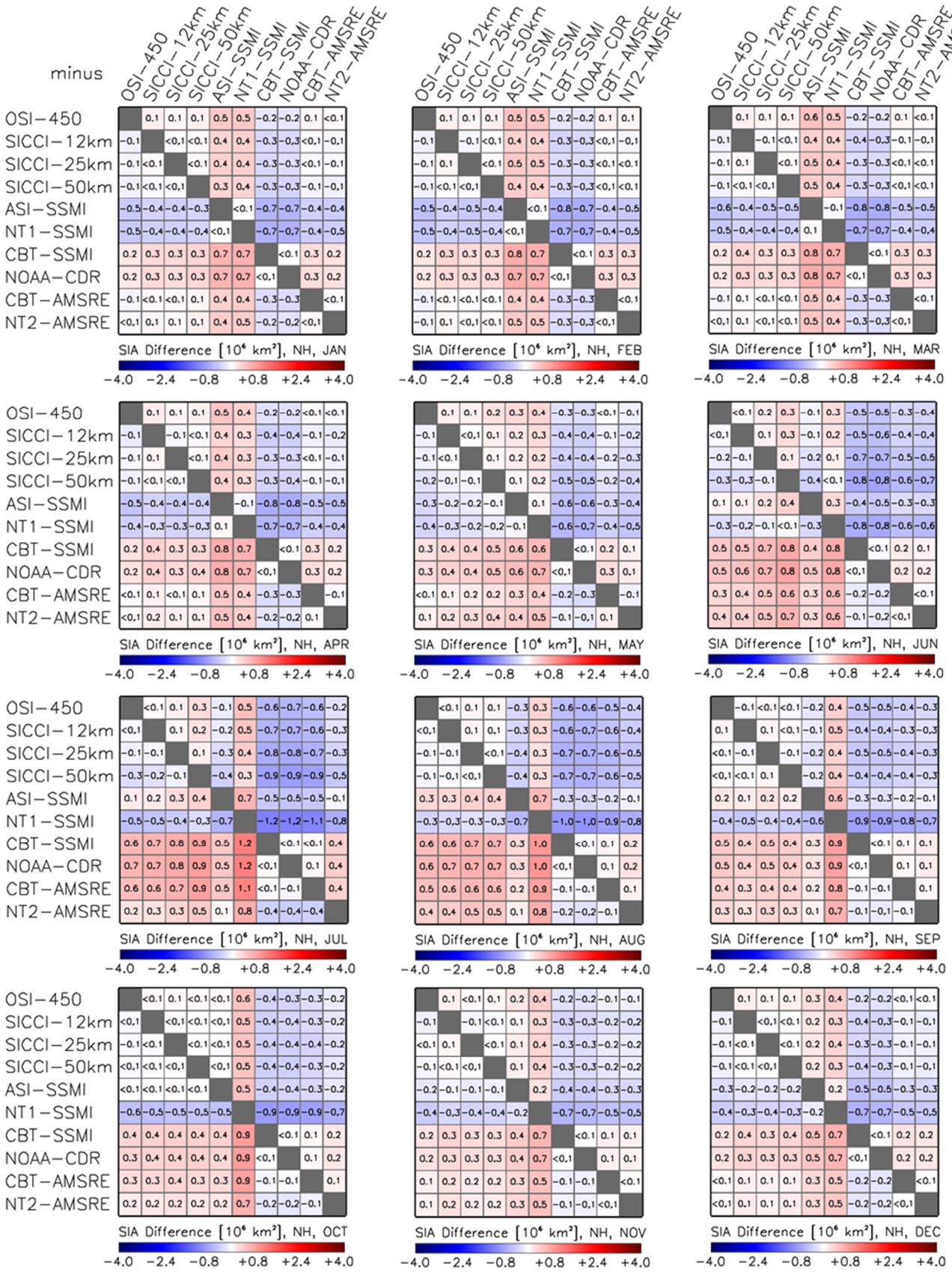

Figure G2. Differences between all ten products of the average sea-ice area (SIA) for the Arctic. The differences are computed from monthly mean SIA of the respective months of the AMSR-E period 06/2002 to 09/2011. All data are on EASE 2.0 grid with 50 km grid resolution. The land-mask of the SICCI-50km product is applied to all products.

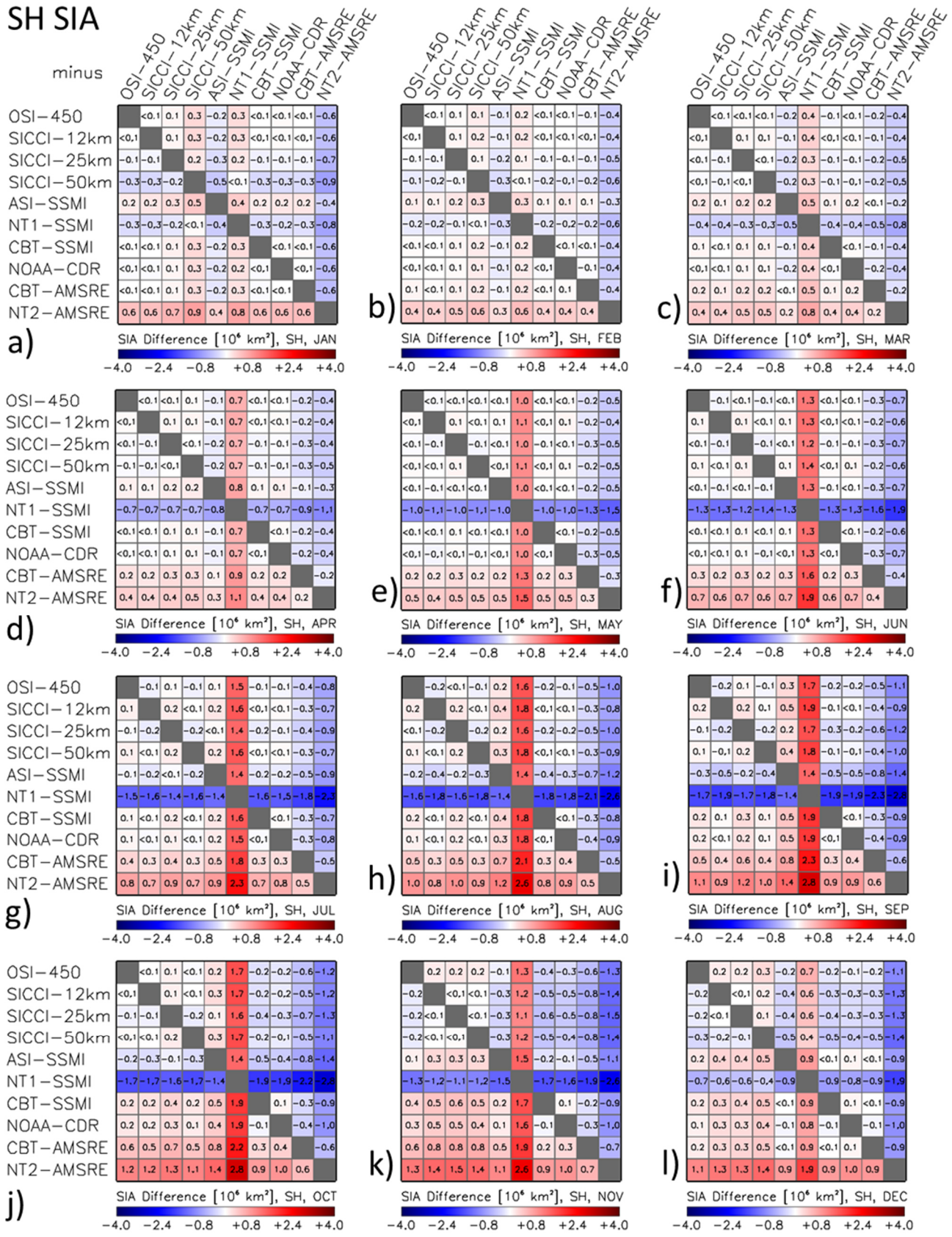

Figure G5. As Fig. G2 but for the Antarctic. Note the larger range of the SIA differences compared to the Arctic.

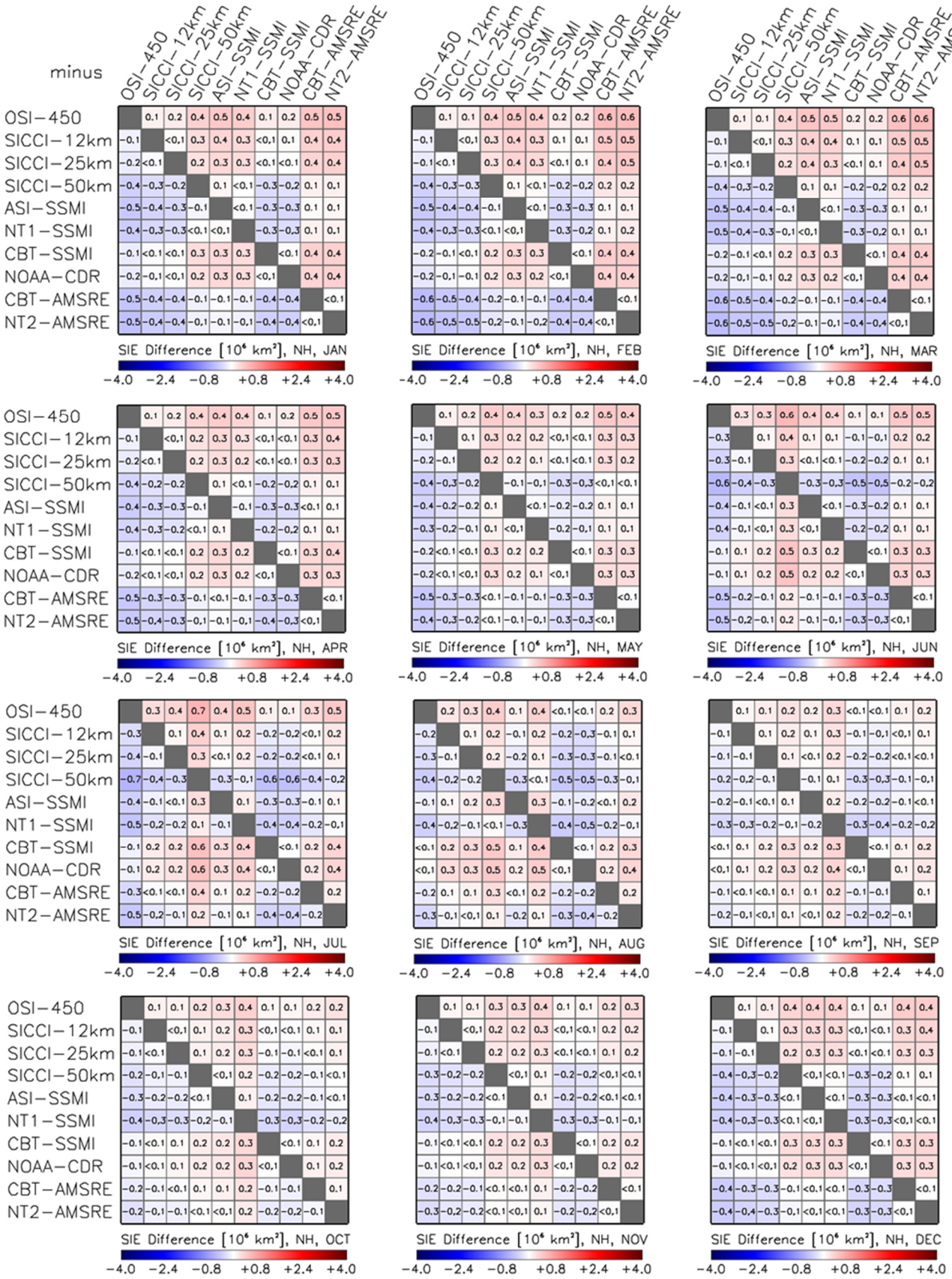

Figure G3. Differences between all ten products of the average sea-ice extent (SIE) for the Arctic. The differences are computed from monthly mean SIE of the respective months of the AMSR-E period 06/2002 to 09/2011. All data are on EASE 2.0 grid with 50 km grid resolution. The land-mask of the SICCI-50km product is applied to all products.

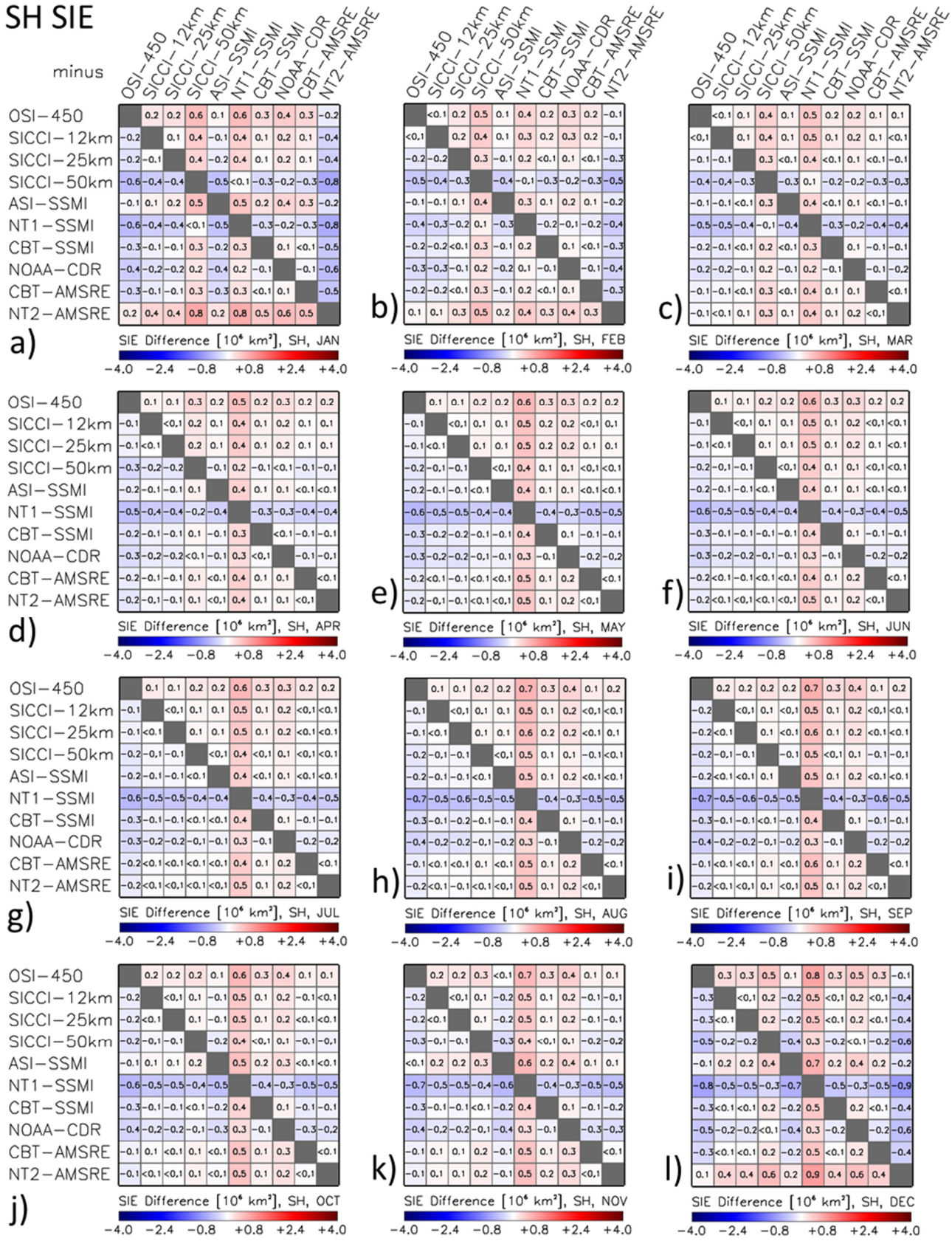

Figure G6. As Fig. G3 but for the Antarctic. Note the larger range of the SIE differences compared to the Arctic.

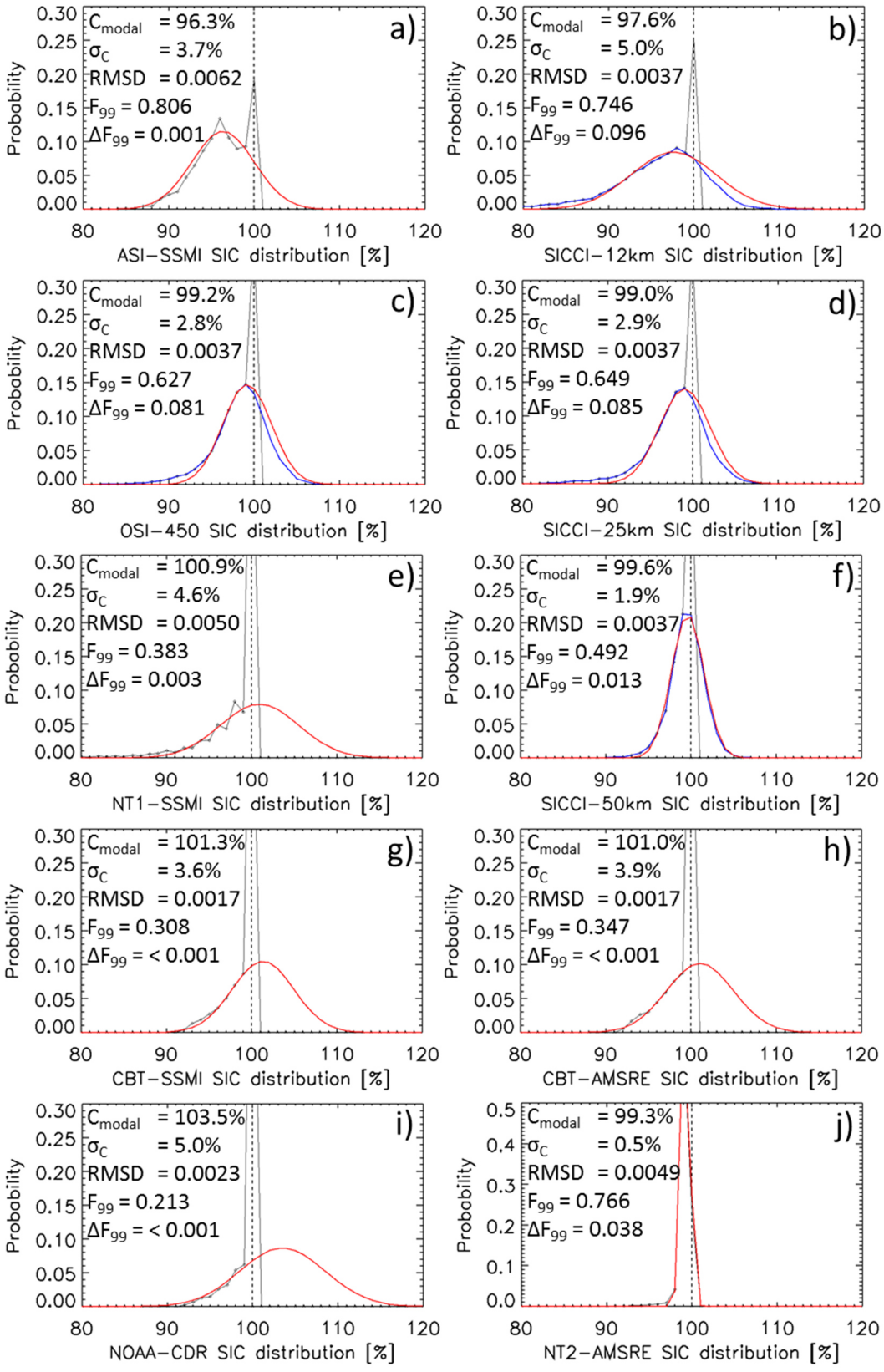

Figure H1. Sea-ice concentration distribution at RRDP2 near-100% reference sea-ice concentration locations in the Arctic during winter for 2007-2011. Black symbols and lines show values cut off at 100%; blue lines denote the original distribution (for OSI-450, SICCI-12km, SICCI-25km and SICCI-50km); red lines denote the distribution resulting from the Gaussian fit to values of the distribution ≤ 99%. In each image the modal sea-ice concentration (= center of the Gaussian fit: C_{modal}), the standard deviation of the fit σ_C and fit parameters with respect to the fraction of the distribution ≤ 99% (F_{99}, ΔF_{99}, see text in Sect. 2.1.4 for more explanation) and the root-mean-squared difference (RMSD) between original and fitted probability are given.

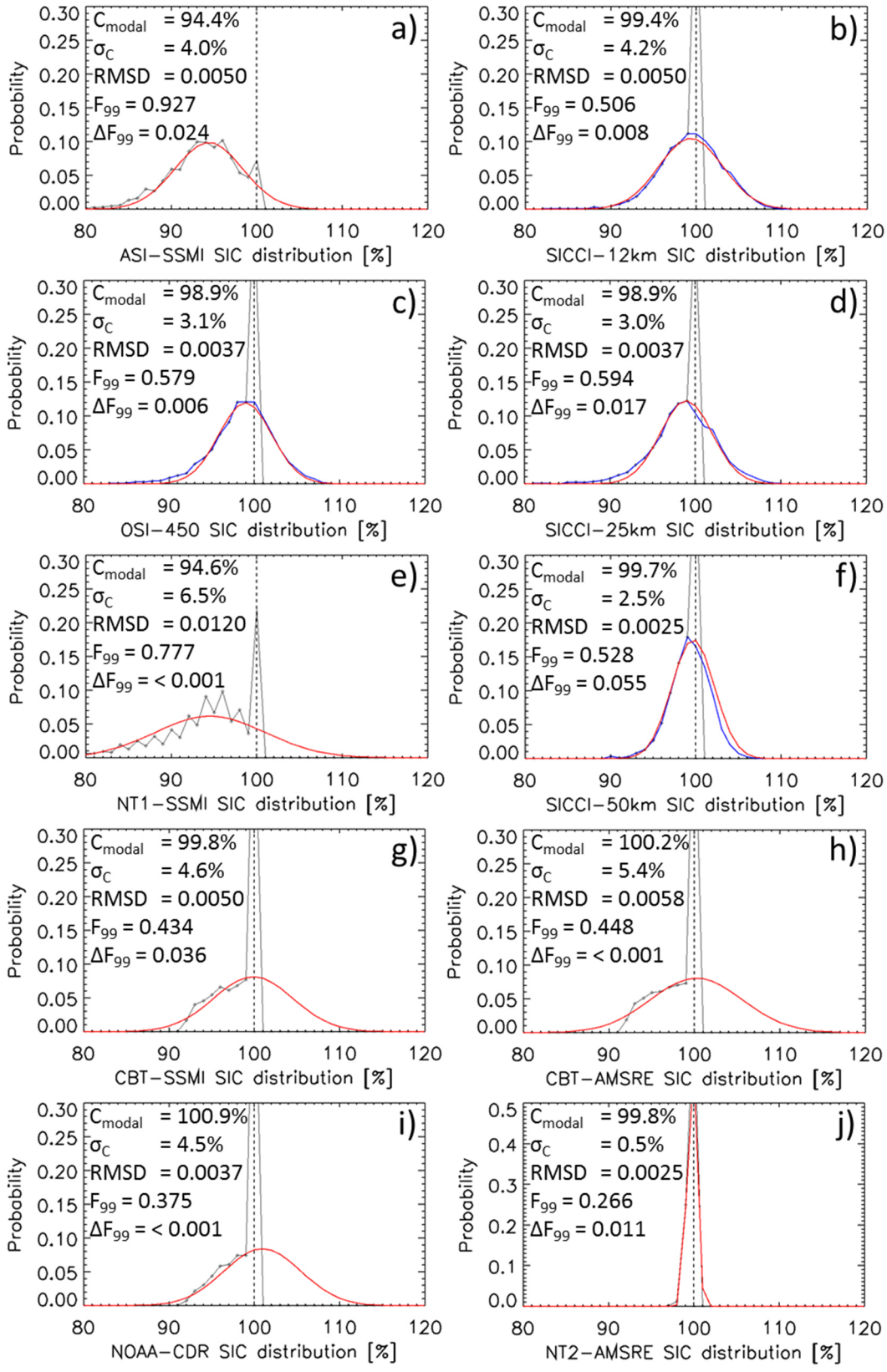

Figure H2. As Fig. H1 but for the Antarctic.